Wellhead Fatigue Response Affected by Seabed Interaction

by

© Etido Gideon Akpan

A Thesis submitted to the

School of Graduate Studies

In partial fulfillment of the requirements for the degree of

Masters in Engineering

Faculty of Engineering and Applied Science

Memorial University of Newfoundland

October, 2018

St. John's Newfoundland Canada

Abstract

Subsea wellhead system assessment is a vital aspect of well integrity assurance. This thesis focuses on the fatigue damage of the wellhead which has become an important design consideration in the design of offshore structures. Subsea wellheads are generally exposed to fatigue, due to environmental loads such as waves, winds and currents, which implies cyclic loading to the wellhead. The conductor-soil interaction may have significant impact on stress range variation in wellhead system and consequently on accumulative fatigue damage. In practice, the seabed soil is usually replaced with linear elastic springs to define lateral force-displacement curves. There are several models proposed in the literature to simulate the lateral response of soil to force applied by the conductor. However, the selection of an appropriate model depending on seabed soil condition and the nature of soil-structure interaction may have significant influence on fatigue performance of wellhead system. In this thesis, the influences of a range of different lateral force-displacement models were examined through implementation into global riser analysis. Finite element analysis software, OrcaFlex, was used to model the riser configuration and global load analysis. Both static and dynamic analyses of the drilling riser system were conducted. The loads of particular interest with contribution to the accumulated wellhead fatigue damage were investigated with focus on assessment of the impact of conductor-soil interaction and soil properties. The result showed that the selection of lateral P-y curve and the soil properties governing the soil stiffness may have significant influence on fatigue damage. It was observed that, the stiffer soil models will greatly reduce the bending moment at the wellhead datum leading to decrease in fatigue damage and increase fatigue life of the wellhead, whereas, the softer soil model leads to more damage and decrease fatigue life of the wellhead. This implied the significance of developing new models to incorporate the cyclic soil stiffness degradation for fatigue analysis of the drilling risers.

Acknowledgments

This research was completed at Memorial University of Newfoundland through funding provided by the Research and Development Corporation (RDC) (now Innovate NL) and Memorial University of Newfoundland through VP start-up funding support.

My immense thanks go to my amiable supervisor, Dr. Hodjat Shiri, for his keen supervision, unalloyed support and indispensable suggestions throughout the course of this research. He has a lot of experience in the oil and gas industry as a pipeline and subsea engineer and has given me very thoughtful input which has helped to make this thesis a success.

I also want to express my heartfelt appreciation to School of Graduate Studies (SGS), Memorial University for their financial support and I am really grateful for this superb assistance.

Last but not least, many thanks to my late parents, Mr. & Mrs. Gideon Charles Akpan who laid the foundation for me to be where I am today, and also to my siblings for their prayers, support and affectionate encouragement which helped and inspired me throughout my studies.

Table of Contents

Abstract…… i

Acknowledgements…….. ii

Tables of Contents…… iii

List of Tables……... viii

List of Figures……... ix

List of Abbreviations…… xiii

Chapter 1

Introduction…….. 1

1.1 Background…….. 1

1.2 Objective…….. 3

1.3 Outline of Thesis ……. 3

1.4 Contribution in Subsea Wellhead Analysis ……. 4

Chapter 2

Literature review ……. 5

2.1 Overview of Offshore Drilling …… 5

2.1.1 Drilling Riser ……..... 6

2.1.2 System Description ……... 8

2.1.3 Subsea Wellhead System ……... 9

2.2 Marine Riser Mechanics …….. 11

2.2.1 Effective Tension and Apparent Weight ……... 11

2.2.2 Stresses …….. 14

2.2.3 Strains …… 16

2.2.4 Finite Element Formulation ……... 17

2.3 Basic Concepts of Fatigue …… 20

2.3.1 Fatigue Damage of Wellhead ……. 21

2.3.2 S-N Curves ……. 22

2.3.3 Cumulative Damage Assessment ……... 23

2.3.4 Stress Concentration Factor …… 26

2.4 Fatigue as a Challenge in Soil-Structure Interaction ……. 27

2.5 Overview of Soil Modelling Approach …….. 27

Chapter 3

Analysis of Drilling Riser and Conductor for Deepwater Drilling ……. 31

3.1 Vibration Equation of Marine Risers ……..... 31

3.2 Analysis of Dynamic Response of Riser ……... 39

3.3 Lateral Load-Bearing Capacity of Conductor and Surface Casing ……... 44

3.4 Analysis Model of Lateral Load-Bearing Capacity for Conductor ……... 44

3.4.1 Force Analysis ……..... 44

3.4.2 Subgrade Reaction ……..... 45

3.4.3 Forces ……..... 46

3.4.4 Flexural Rigidity ……..... 47

3.5 Numerical Solution of the Analysis Model of Lateral Load-Bearing Capacity ……..... 48

3.6 Effects of the Forces on the Wellhead ……..... 51

3.7 Effects of the Distance between Mudline and Wellhead, Cement Return Height and Type of Foundation …….. 54

Chapter 4

Development of Numerical Model for Fatigue Analysis ……..... 57

4.1 Overview ……..... 57

4.2 Global Riser Model …… 59

4.2.1 Drilling Riser Properties ……..... 62

4.2.2 Conductor, Surface Casing and Cement Properties ……... 65

4.3 Soil Model ……..... 65

4.3.1 Selection of Soil Parameters ……..... 70

4.4 Verification of Numerical Model ……... 74

4.5 Environmental Load ……... 75

4.5.1 Water information …….. 75

4.5.2 Waves ……..... 76

4.5.3 Current ……... 78

4.6 Modal Analysis …….. 78

4.7 Modelling Program (Parametric and Sensitivity Studies) ……. 79

4.7.1 Effects of Waves …… 79

4.7.2 Effects of Current ……..... 82

4.7.3 Water Depth Sensitivity Analysis …….. 85

Chapter 5

Effect of Soil Models on Riser Performance ……... 88

5.1 Modal Analysis Results of Riser……..... 88

5.2 Soil Models Investigation ……..... 88

5.2.1 Comparison of Result ……. ……... 90

Chapter 6

Wellhead Fatigue Performance on Proposed Soil Models ……. 94

6.1 Introduction …… 94

6.2 Fatigue Damage Assessment ……. 94

6.3 Fatigue Analysis Methodology …….. 95

6.3.1 Global Response Analysis …….. 96

6.4 Impact of Soil Models on Wellhead Fatigue Performance ……..... 97

Chapter 7

Conclusions and Recommendations for Future Research ……... 101

7.1 Conclusions …….. 101

7.2 Recommendations for Future Research ……... 102

References ……. 104

APPENDICES ……. 108

Appendix A: Modal Analysis ……..... 108

Appendix B: Irregular Motion Analysis ……..... 111

Appendix C: Fatigue Damage for Varying Water Depth …….. 114

Appendix D: Damage Summary Table …….. 117

List of Tables

Table 2-1: Design Fatigue Factors ……... 25

Table 4-1: Material Properties for Steel ……... 62

Table 4-2: Geometry and Weight Input for OrcaFlex ……. 63

Table 4-3: Stiffness and Hydrodynamic Properties …….. 64

Table 4-4: Conductor, Surface Casing and Cement Properties …… 65

Table 4-5: Natural Period for the First Two Modes ……... 74

Table 4-6: Sea Data …… 75

Table 4-7: Significant Wave Height and Corresponding Peak and Zero-Crossing Periods …... 78

Table 4-8: Natural Periods …….. 79

Table 4-9: Regular Sea Parameter …… 80

Table 4-10: Load Case for Current …….. 82

Table 4-11: Fatigue Life for Varying Water Depths …… 85

List of Figures

Figure 2-1: Example of Well Construction Sequence Using Drilling Riser Operated from MODU ……... 6

Figure 2-2: Examples of Mobile Offshore Drilling Units …… 7

Figure 2-3: Schematic Overview of the System ……... 8

Figure 2-4: Schematic of Subsea Wellhead System ……... 10

Figure 2-5: Internal Forces Acting on a Submerged Body Segment …….. 13

Figure 2-6: Pipe In-Wall Stresses for Two Equivalent Stress Systems ……..... 15

Figure 2-7: 2D Beam Element ……..... 17

Figure 2-8: Change in Geometry due to Resisting Forces ……. 18

Figure 2-9: 3D Beam Element ……..... 20

Figure 2-10: Stress Cycling Involving a Detailed Fatigue Assessment ……. 23

Figure 2-11: Calculation of Soil-Structure Spring Stiffness in Riser Analysis Program ……... 28

Figure 3-1: Marine riser model …….. 32

Figure 3-2: Modal Responses Considering the Combined Wave-Current Interaction……... 40

Figure 3-3: Dynamic Moment Responses Considering Combined Wave-Current Loads ……. 42

Figure 3-4: Shear Force Responses Considering Combined Wave-Current Loads ……... 42

Figure 3-5a: Dynamic Moment Response at the Middle point …….. 43

Figure 3-5b: Shear Force at the Bottom of the Riser ……. 43

Figure 3-6: Numerical Grid of Casing String…….. 48

Figure 3-7: Transverse Displacement ……..... 52

Figure 3-8: Rotation Angle ……. 53

Figure 3-9: Moment ……..... 53

Figure 3-10: Shear Force ……..….. 53

Figure 3-11: Subgrade Reaction ……. 54

Figure 3-12: Transverse Displacement …….. 55

Figure 3-13: Moment ……. 56

Figure 4-1: Drilling Riser System Configuration and Coupled Analysis Models …….. 58

Figure 4-2: Drilling Riser System Configuration and Decoupled Analysis Models ……. 59

Figure 4-3: Schematic of Riser Stack-Up and Wellhead Model Created in OrcaFlex ……... 61

Figure 4-4: Comparison between P-y Springs Measured in Centrifuge Tests on Kaolinite and Computed Using the FEA Method with API Recommendation …….. 67

Figure 4-5: P-y Curves as Per Equation 1, Compared with API and Matlock Curves for Large Embedment Depths ……. 68

Figure 4-6: Example of Non-Linear Springs that Represent the Lateral Soil Support of the Well 71

Figure 4-7: P-y Curve Stiffness 72

Figure 4-8: P-y Curve for Large Displacement 73

Figure 4-9: P-y Curve for Small Displacements 73

Figure 4-10: First Mode Shape 74

Figure 4-11: Second Mode Shape 75

Figure 4-12: JONSWAP Spectrum 77

Figure 4-13: Wellhead Bending Moment at Sea State 1 80

Figure 4-14: Wellhead Bending Moment at Sea State 2 81

Figure 4-15: Wellhead Bending Moment at Sea State 3 81

Figure 4-16: Wellhead Shear Force at Current Speed of 0.72m/s 83

Figure 4-17: Wellhead Shear Force at Current Speed of 1.25m/s 84

Figure 4-18: Wellhead Shear Force at Current Speed of 1.55m/s 84

Figure 4-19: Fatigue Life for Water Depth of 100m 86

Figure 4-20: Fatigue Life for Water Depth of 200m 86

Figure 4-21: Fatigue Life for Water Depth of 300m 87

Figure 5-1: Wellhead Bending Moment for Sea State 1 89

Figure 5-2: Wellhead Bending Moment for Sea State 2 ……... 90

Figure 5-3: Bending Moment for Matlock API Model for Sea State 1 ……. 91

Figure 5-4: Bending Moment for Jeanjean Model for Sea State 1 ……..... 91

Figure 5-5: Bending Moment for Zakeri et al. Model for Sea State 1 ……... 92

Figure 5-6: Bending Moment for Matlock API Model for Sea State 2 ……. 92

Figure 5-7: Bending Moment for Jeanjean Model for Sea State 2 …….93

Figure 5-8: Bending Moment for Zakeri et al Model for Sea State 2 …… 93

Figure 6-1: Wellhead Fatigue Methodology Flowchart …… 96

Figure 6-2: Fatigue Damage for Load Case 1 ……..... 98

Figure 6-3: WH fatigue Life for Load Case 1 ……..... 98

Figure 6-4: WH fatigue Damage for Load Case 2 ……. 99

Figure 6-5: WH fatigue Life for Load Case 2 ……..... 100

List of Abbreviations

API	American Petroleum Institute
BM	Bending Moment
BOP	Blowout Preventer
CPT	Cone Penetration Test
ECA	Engineering Criticality Assessment
FE	Finite Element
FPU	Floating Production Unit
GoM	Gulf of Mexico
5Gmax	Five Times the Maximum Shear Modulus in Clay
HPH	High Pressure Housing
Hs	Significant Wave Height
JONSWAP	Joint North Sea Wave Project
LFJ	Lower Flex Joint
LMRP	Lower Marine Riser Package
LPH	Low Pressure Housing
LRS	Lower Riser Section
MODU	Mobile Offshore Drilling Unit
MWL	Mean Water Level
Tp	Peak Period
Tz	Mean Up-Crossing Period
UFJ	Upper Flex Joint
WH	Wellhead

Chapter 1

Introduction

1.1 Background

Typical offshore drilling operations are carried out using drilling risers and subsea Blowout Preventer (BOP) stacks deployed from drilling rigs. The BOP is placed on top of the subsea wellhead sometimes called the mudline wellhead which is located at sea bottom.

While drilling the oil well, surface pressure control is provided by a blowout preventer (BOP). If the pressure is not contained during drilling operations by the column of drilling fluid, casings, wellhead, and BOP, a well blowout could occur.

The wellhead provides the suspension point and pressure seals for the casing strings that run from the bottom of the hole sections to the surface pressure control equipment. It is worthy of note that hydrodynamic forces acting on the drilling riser and drilling unit will cause dynamic movement which will be transmitted to the wellhead system and can lead to fatigue accumulation in the subsea wellhead. Fatigue damage also arises from stress changes in the conductor which are generated by environmental loads such as waves acting on the vessel and the riser. Structurally, the function of the subsea wellhead is for supporting the weight of the subsea BOP stack during the drilling operations. Hence, a structural failure in the wellhead might lead to blowouts which can cause catastrophic effects on the environment such as the deepwater horizon oil spill, also referred to as the BP oil spill which occurred in the Gulf of Mexico (GoM) on the BP-operated Macondo Prospect. Since safety is a top priority during oil and gas production, it is extremely important to

ensure that special care is taken during the detailed engineering design of the wellhead system to prevent any possibility of failure.

The most popular method of estimating fatigue damage of the subsea wellhead is to perform a global and a local finite element analyses with the main intent to predict the fatigue damage in system components for the life of the well. For this purpose, operational inputs are appropriately applied to engineering models of systems and sub-systems to predict local responses, which are then combined with material properties and damage models, (DNV-RP 2015). Both the fatigue and strength analyses can be examined from geotechnical point of view with inputs for seabed-structure interaction modelling which is the main focus of this thesis. Furthermore, complex modelling requirements exist and numerous analysis methods exist for the wellhead system.

The soil response acting on the conductor is generally modelled using Winkler springs type which is defined as a function of the lateral soil-resistance displacement (P-y) relationship. The soil stiffness are highly dependent on the soil type and strength properties and will directly affects the amplitude of stress cycles predicted in the subsea wellhead system.

For the purpose of this study, the impact of seabed soil interaction on the subsea wellhead fatigue for drilling riser is carefully examined.

1.2 Objectives

The main objectives of this thesis are:

- Review literature to acquire an in-depth knowledge of the field as well as find the most suitable soil P-y model for performing fatigue damage assessment in the subsea wellhead system
- To perform a fatigue assessment in a subsea wellhead system based on the numerical models
- To investigate the effect of seabed soil interaction on wellhead fatigue on drilling risers by performing a global drilling riser model in OrcaFlex
- To perform parametric studies in order to investigate their effects on estimated wellhead fatigue damage.

1.3 Outline of the Thesis

This thesis is composed of seven chapters. The first chapter is the introduction and the main objectives of the thesis as well as its contribution to subsea wellhead fatigue analysis.

Chapter two presents the system description, overview of offshore drilling and marine riser system to gain more knowledge on the system functionality and operations. Basic knowledge of marine riser mechanics are discussed in this chapter. Also basic concepts of fatigue is discussed with a focus on fatigue as a challenge in soil-structure interaction. An overview of soil modelling approach is also discuss.

Chapter three gives insight on the lateral load-bearing capacity of conductor and surface casing by performing an analysis model of the lateral load-bearing capacity to be considered during the design of the wellhead.

Chapter four presents the methodology and provides information about the development of the numerical model with focus on the global riser model and selection of soil parameters. Finite Element analysis tool, OrcaFlex is used in this thesis to perform the global riser analysis. OrcaFlex is a recognized software used in the offshore oil and gas industry for the analysis of offshore marine system including global analysis of riser systems.

The effect of soil models on riser performance is investigated in chapter five and the results of the bending moment diagrams are presented.

Chapter six presents the impact of the soil models on wellhead fatigue performance and explains the analysis methodology of the subsea wellhead fatigue analysis

Finally, chapter seven concludes the research work and recommendations for future study.

1.4 Contribution in Subsea Wellhead Analysis

Offshore drilling continues to move into deeper to ultra-deepwater depths and more harsh environments. The soil-conductor interaction which is strongly influenced by the seabed properties may affect the global integrity and design condition of the wellhead. As a result of this, the lateral response of soil to force applied to the lower boundary condition and associated fatigue loading transmitted to the wellhead and conductor systems are of paramount importance in assessing the structural integrity of the wellhead against fatigue. In addition, identifying the effects of bending moment on subsea wellhead fatigue will help to understand the parameters affecting wellhead fatigue.

Chapter 2

Literature Review

2.1 Overview of Offshore Drilling

Drilling is performed using a Mobile Offshore Drilling Unit (MODU) or a Floating Production Unit (FPU). The rig is a complex equipment containing the drills, pumps and other machinery needed to drill the oil well. Hence, the deeper the well, the stronger and more reliable the rig will need to be.

Construction of well starts by first making the initial drilling for the oil well in open water using a drill bit with the conductor casing, which may involve the use of a template and/or other reinforcing structures. The conductor casing is set to a sufficient depth usually below the mudline in order to support the weight of the wellhead, subsea stack and internal casing strings. While drilling, drilling fluid mostly bentonite or a combination of water and other chemicals are injected into the well to cool the drill bit, flush out bits of broken rock and balance hydrostatic pressure. Thereafter, the conductor casing with Low Pressure Housing (LPH) is installed and drilling continues, later on the wellhead housing, High Pressure Housing (HPH) is installed and cemented. After cementing of the surface casing with HPH, the marine riser and drilling equipment are then connected to the HPH. From this stage onwards, fatigue loading is transmitted to the wellhead/casing system for the remainder of the drilling operations. For this purpose an assessment of the fatigue is necessary to ensure that the wellhead does not fail during operation. Its structural integrity must be such that it will withstand the load imposed by the complete system. Figure 2-1 contains a schematic showing a simplified example of a well construction sequence for a drilling riser operated from a MODU (DNV, 2015)

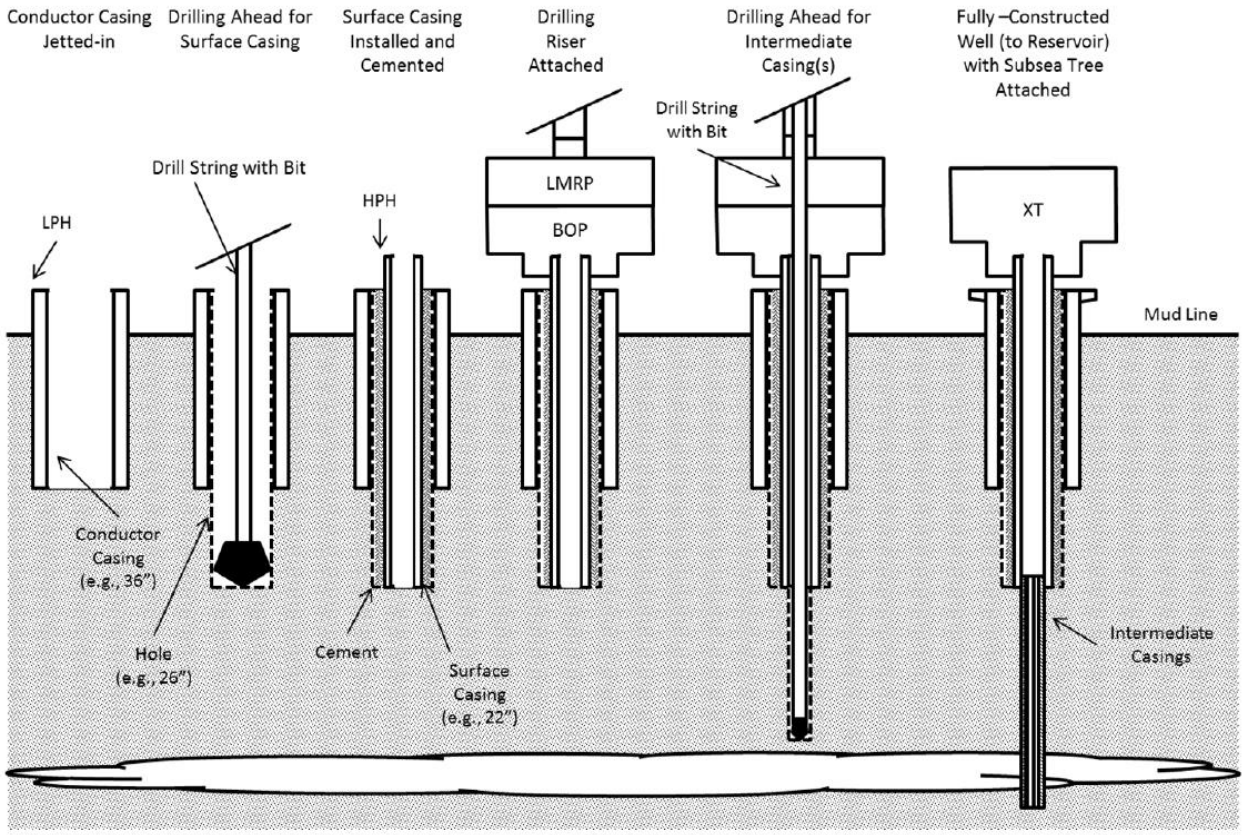

Figure 2-1: Example of well construction sequence using drilling riser operated from MODU (DNV, 2015)

2.1.1 Drilling Riser

Riser drilling is a very essential and indispensable part of the offshore oil industry and is used basically in conveying fluids from the seafloor to an offshore floating production structure or a drilling rig. A drilling riser installed in 100 m water depth operated by semi-submersible vessel also known as MODU is selected for this study. The rig is a complex equipment containing the lower marine riser package (LMRP), subsea Blowout Preventer (BOP) connected to the wellhead at the seabed, conductor, casing and other components needed to drill the oil well. A typical drilling

system comprises of a Lower Flex Joint (LFJ) and Upper Flex Joint (UFJ). The UFJ makes up the topmost part of the LMRP. The function of the Flex joint is to allow rotation of the riser with minimal motion thereby reducing bending moments generated at critical structural interfaces. It also exhibits a non-linear behaviour and this has to be taken into account during the analysis to avoid non-conservative results. Figure 2-2 shows typical examples of mobile offshore drilling rigs.

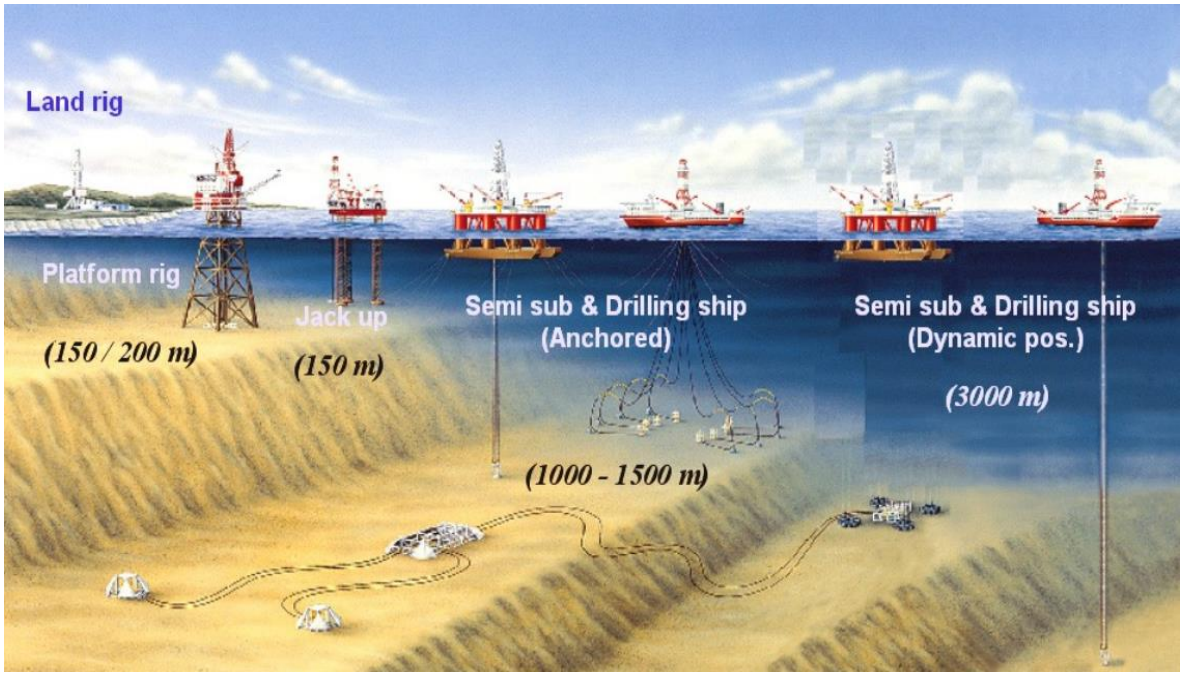

Figure 2-2: Examples of Mobile Offshore Drilling Units (Mishra, 2017)

2.1.2 System Description

Deepwater drilling is mostly performed using the marine drilling risers equipped with BOP stacks connected to the subsea wellhead and accessed from a mobile drilling unit (MODU). The MODU and riser are exposed to environmental loads from waves, currents and wind. During operations, the riser exhibits vibration due to wave-induced motion of the drilling unit and direct wave loading of the riser as well as VIV. The motion due to these vibrations will transfer dynamic loads to the wellhead system which can result in fatigue in the wellhead system. A schematic of the system is shown in Figure 2-3.

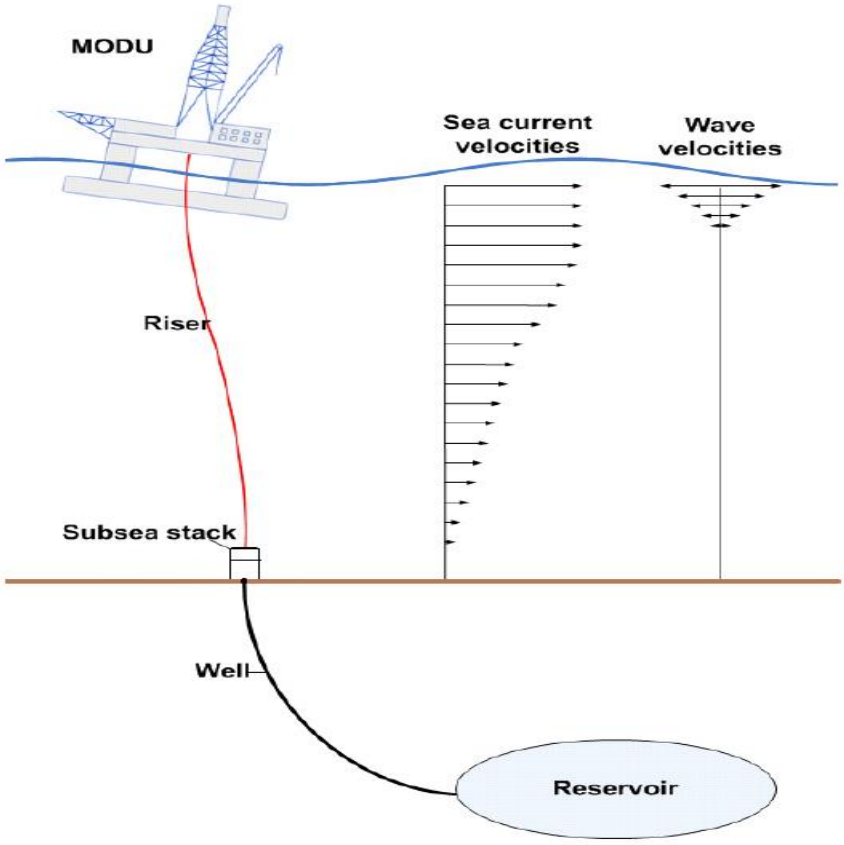

Figure 2-3: Schematic overview of the system (DNV, 2015)

2.1.3 Subsea Wellhead System

The wellhead is a pressure-containing vessel that provides a means to hang off and seal off casing used in drilling the well. Its main purpose is to support the BOP. Once drilling is complete, the wellhead will provide an interface for the production tubing string and the subsea production tree. The subsea wellhead is located on the seabed and must be installed remotely with running tools and drillpipe. Wellheads must be designed for high structural loads imposed (i.e. Maximum strength and capacities) during drilling, workover or well completion operations. These processes will be discussed later on in this chapter. Additionally, the wellheads must support the casing weight and it must also be able to withstand sufficient amount of forces imposed by both external and internal pressure. Loads that are generated by reservoir fluids would be internal, i.e., reservoir pressures and thermal growth during production. External loads will be imposed from the surroundings (Reinås, 2012). The external loads are transmitted from a connected riser which can be static and cyclic combinations of bending and tension. Excessive cyclic loads will cause fatigue damage to the well since the well can only accommodate a limited amount of fatigue damage without failure. The well should be designed to withstand environmental loads imposed by the BOP/marine riser. If the wellhead fails, this may pose a serious consequence as there will be no pressure vessel contact, hence a potential threat to the integrity of the well. The design life for the wellhead is normally 25 years as per DNV.

In the industry, the design of the wellhead system is normally reviewed together with the Workover, Tree and Tubing Hanger Systems to establish a cross-system project standard for hydraulic fittings. The wellhead and the foundation shall be capable of withstanding the installation and environmental loads by the BOP/marine riser. Figure 2-4 shows a typical subsea wellhead system with naming conventions used in this thesis.

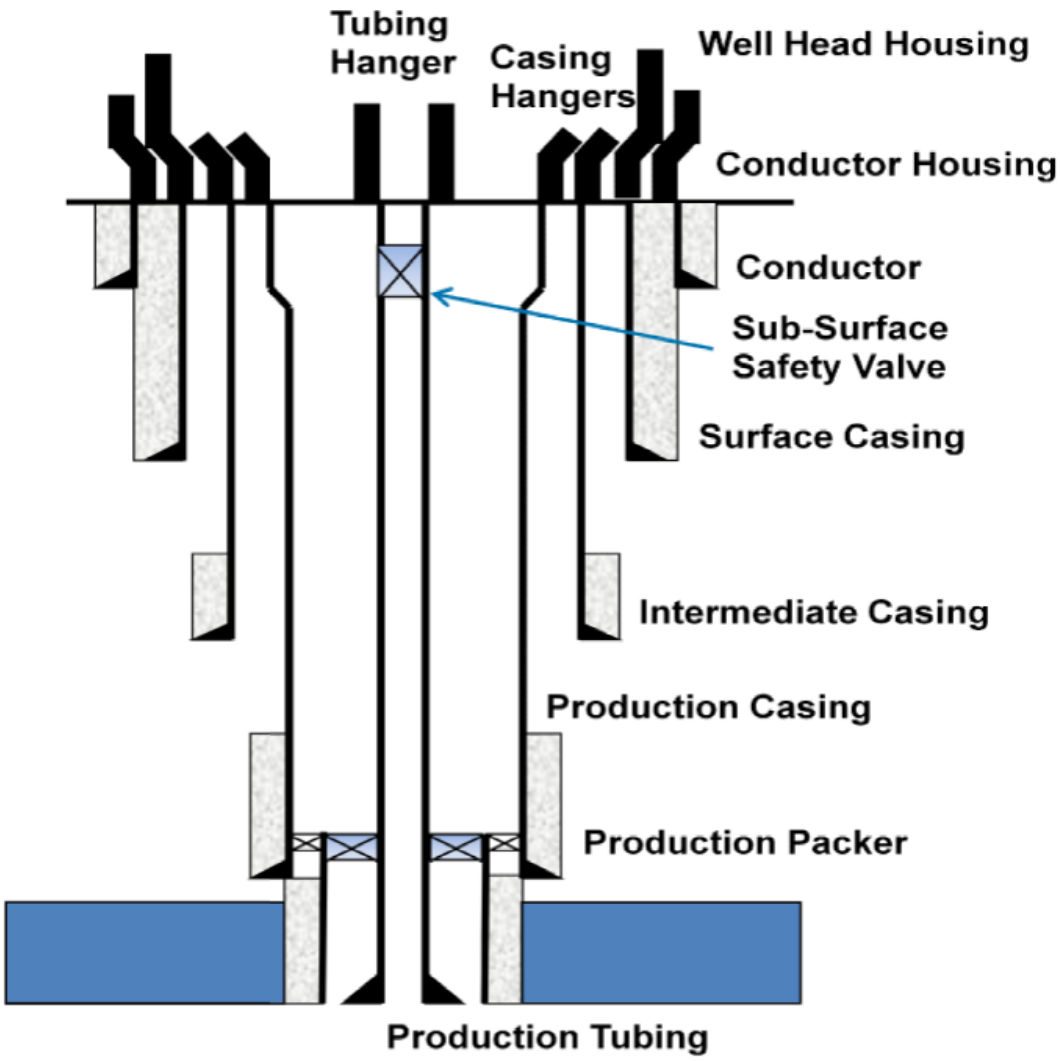

Figure 2-4: Schematic of Subsea Wellhead System (Reinås, 2012).

The subsea wellhead system comprises the high pressure housing (HPH) also known as the wellhead housing and the conductor housing also called the Low Pressure Housing (LPH). The conductor housing is essentially the top of the casing conductor. In addition, the HPH provides pressure integrity for the well.

In this study, a simple two-pipe wellhead system comprising a conductor pipe (diameter 762 mm, thickness 25.4 mm) and a surface casing pipe (diameter 536.4 mm, thickness 33.3 mm) was considered. The conductor casing is welded to the base of the LPH while the surface casing is welded to the base of the HPH. The annular space between the conductor and the surface casing is cemented from the casing bottom at 186.5 m below the MWL to 10 m below the seabed.

2.2 Marine Riser Mechanics

2.2.1 Effective Tension and Apparent Weight

The weight of the riser is supported by the top tension. The application of effective tension to riser dynamic cases is of paramount importance. The influence of tension, pressure and weight on pipe and risers will be discussed here.

The effective tension distribution along the riser is mainly governed by functional loading due to applied top tension and the effective weight of the riser. The drilling riser is liable to buckle if the effective tension is negative. However, the effective tension equation can be derived in different ways. For the purpose of this research work, Sparks C.P method will be presented. This equation is the same as the equation used for calculating effective tension in OrcaFlex (Hovland, 2014)
In the discussion of riser behavior, the concept of buoyancy cannot be overemphasized as far as offshore industry is concern.

Confusion arises when discussing the buoyancy of part of a submerged object such as a segment of riser, since it is subject to a pressure field that is not closed. According to Sparks (2007), the confusion is often considered wrong if the riser pipe concerned is vertical and of uniform section. The wall of such a riser is continuous. Hence, the pressure of the fluid will act only horizontally

on the segment and tends to have no vertical component. In this case, it is quite tempting to conclude that such a riser segment has no buoyancy. Since the segment can be positioned anywhere along the riser length, that would mean that the entire riser has no buoyancy, except at the surface of the lower end and hence Archimedes' principle is not hold.

From basic Physics, Archimedes' principle also known has law of buoyancy states that: "If an object is completely or partially submerged in a fluid, it experiences a force, buoyancy which is equal to the weight of the fluid displaced by the object. This force occurs as a resultant of the closed pressure field in the displaced fluid and will act vertically in the center of the object.

For Archimedes' principle to be valid, the following conditions must be satisfied (Sparks, 2007)

- Internal forces or stresses is not mentioned
- The law is only valid for completely closed fields. For objects in the water surface where the pressure is zero, the field can be considered closed.

In the calculation of the internal forces on a part of a submerged object, it is important to take into account the case where the pressure field is not closed. Figure 2-5 shows the forces acting on the submerged body segment, displaced fluid including the closed pressure field and equivalent system. Superposition is used to determine the internal forces. The external pressure field can be calculated by applying Archimedes' law.

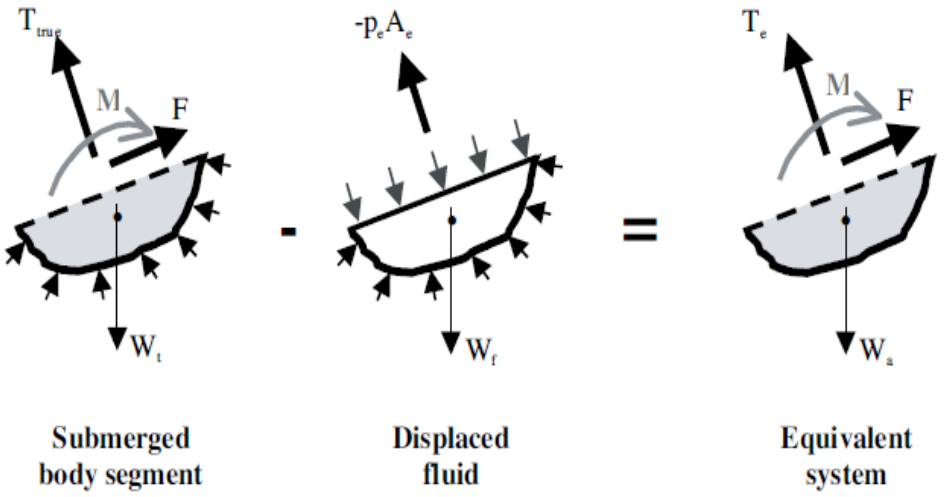

Figure 2-5: Internal forces acting on a submerged body segment (Sparks, 2007)

By adding pressure as shown in the middle sketch of Figure 2-5, if the forces acting on the displaced fluid segment is subtracted from the forces on the body segment, the pressure field that acts below the body is conveniently eliminated. Hence, the force $p_e A_e$ remains. Where p_e and A_e are the pressure in the fluid and cross-sectional area of the section respectively. Since tension must be positive, the negative force is termed tensile force.

The shear force (F), and the moment (M) are the same for the segment as for the resulting equilibrium. However, the relationship between the resulting tension (i.e., effective tension, (T_e)), and true tension, T_{true} is expressed below (Sparks, 2007):

$$T_e = T_{true} — peA_e = T_{true} + p_e A_e \quad (2.1)$$

The effective tension can be expressed as

$$T_e = T_{tw} - p_i A_i + p_e A_e \quad (2.2)$$

where,

T_{tw} = wall tension

p_i = Internal pressure

p_e = External pressure

A_i = Internal cross-sectional stress area

A_e = External cross-sectional stress area

Similarly, the apparent weight w_a which is the difference between the weight of the segment, w_t and the displaced fluid,w_e, is given by the expression (Sparks, 2007):

$$w_a = w_t - w_e \tag{2.3}$$

At any point in the riser, the effective tension and apparent weight can be used to find the equilibrium of a riser segment. Even though, both methods are valid and applicable, it is often more preferred to use the effective tension since it is more convenient and more accurate.

The effective tension is used in computer programs for both static and dynamic analysis of marine risers, as well as for calculation of buckling load and geometric stiffness mostly due to tension in a slender beam (Stokvik, 2010).

2.2.2 Stresses

When a riser or a cylindrical pipes made from elastic materials is exposed to tension and external and internal pressures, it experiences stresses. According to Sparks (2007), the distribution of stresses across the pipe sections depends on the material. The axial and circumferential forces generated by tension and pressure in the pipe or riser wall do not depend on the properties of the pipe material. For instance, in the case of flexible pipes where the stress distribution depends on

the details of the pipe wall construction and the distribution can be conveniently controlled by the design engineer. For risers made from isotropic materials the distribution is dependent on mechanical principles over which the designer has no control.

The Von Mises stress failure criterion is considered to be the most accurate criterion for ductile materials and most codes require the Von Mises equivalent stress to be checked.

Combination of stresses in the riser cause yielding and it is of paramount importance to decide on the limit stress criteria for a given riser during the analysis.

Sparks (2007) gave the equation for Von Mises' equivalent stress for the general cases of triaxial stress as follows:

$$2\sigma_{vm}^2 = (\sigma_1 - \sigma_2)^2 + (\sigma_2 - \sigma_3)^2 + (\sigma_3 - \sigma_1)^2 + 6(\tau_{12}^2 + \tau_{23}^2 + \tau_{31}^2) \quad (2.4)$$

where,

$\sigma_1, \sigma_2, \sigma_3$ represent axial stresses in the three directions (x, y, z)

$\tau_{12,}\tau_{23}, \tau_{31}$ represent the shear stresses

Yielding will occur when the equivalent Von Mises stress equals the yield stress of the material.

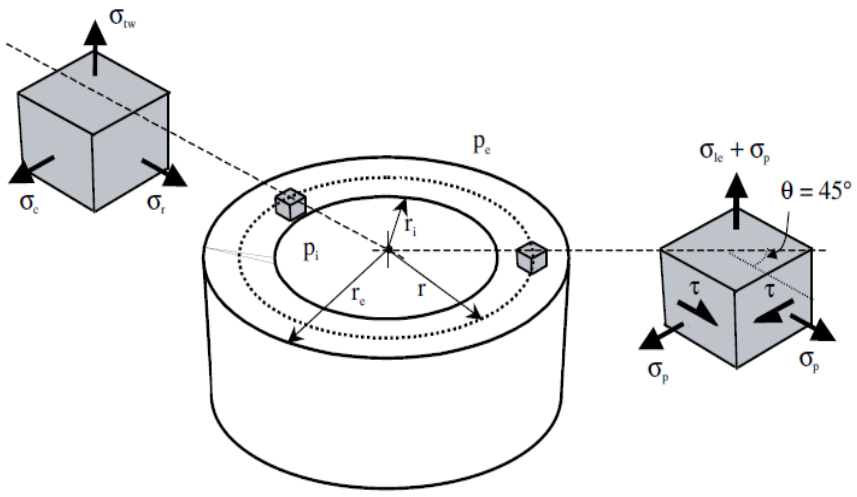

Figure 2-6: Pipe in-wall stresses for two equivalent stress systems (Sparks, 2007)

Sparks (2007) also opined that equation 2-5 can be applied to the left-hand stress cubes of figure 2-6 showing the principal stresses for which shear stresses are zero to give:

$$2\sigma_{vm}^2 = (\sigma_{tw} - \sigma_c)^2 + (\sigma_c - \sigma_r)^2 + (\sigma_r - \sigma_{tw})^2 \quad (2.5)$$

2.2.3 Strains

Strains will affect risers in different ways therefore the correct calculation of axial strains is of great importance during the design of riser. Axial strains can influence the required stroke of riser tensioners in the case of near-vertical risers and has to be taken into consideration when analyzing the stability of drilling riser choke and kill lines. Similarly, for risers without tensioners, differential strains between adjacent risers influence the profile of the riser as well as the riser interaction (Sparks, 2007).

The principal strains are related to the principal stresses by Young's modulus *E* and Poisson's ratio ν for the case of elastic isotropic pipes. The axial strain ε_a, is given by (sparks, 2007) as:

$$\varepsilon_a = \frac{1}{E}(\sigma_{tw} - \nu\sigma_c - \upsilon\sigma_r) \quad (2.6)$$

where,

σ_{tw} is the axial stress

σ_c is the circumferential stress

σ_r is the radial stress

2.2.4 Finite Element Formulation

The finite element method (FEM) is a general and efficient tool and can be used for numerous structural applications and is often applied in the analysis of marine risers. From a FEM, these problems seem less complex, often adopting beam or bar elements in one single chain (Larsen, 1990). A top tensioned riser, like the drilling riser has a statically determined initial configuration. Risers are normally modeled using beam elements, and the matrices can be found using the corresponding finite element formulation. The elastic stiffness matrix for a linear 2-dimensional beam element and its degree of freedom is shown in Figure 2-7

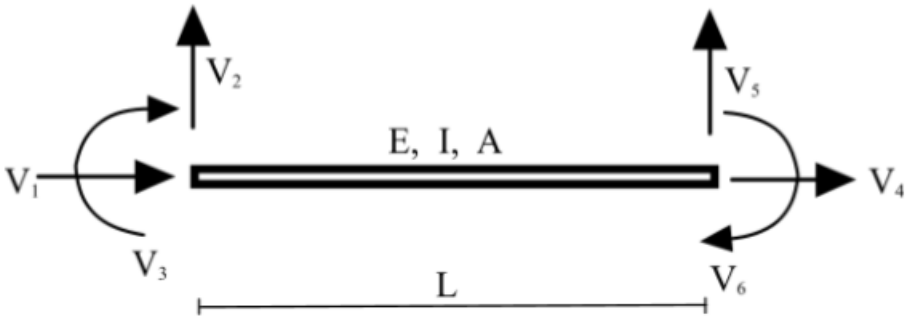

Figure 2-7: 2D Beam Element

In the finite element analysis, the beam elements of either two or three dimensions having length of *L* are used in the building up of the whole riser. Hence, the axial stresses and strains, node positions and effective tension can be calculated by direct inspection of vertical equilibrium (Stokvik, 2010). To characterize structural behavior, key-words such as large deformations, small (elastic) strains, and geometric stiffness (lateral displacements) are normally used.

The geometric stiffness is more important than elastic stiffness in the sense that Geometric stiffness is the equilibrium obtained by change of geometry whereas the elastic stiffness is the equilibrium obtained by change of elastic stresses. Since the drilling riser is supported by top tension in order to increase the lateral stiffness of the riser, it is worthy of note that without the top tension, the riser will experience large displacement when it is subjected to lateral forces such as waves and currents due to its long and slender structure with minimal elastic bending stiffness (EI). The incessant increase in stiffness is as a result of the counteraction between lateral components of the tension and the lateral forces that the riser is subjected to, hence the additional lateral stiffness that occurs is called geometric stiffness which will be discussed in this chapter.

In Figure 2-7, the stiffness of the beam element has contributions from the element stiffness itself and the stiffness that occurs as a result of change in geometry due to external forces.

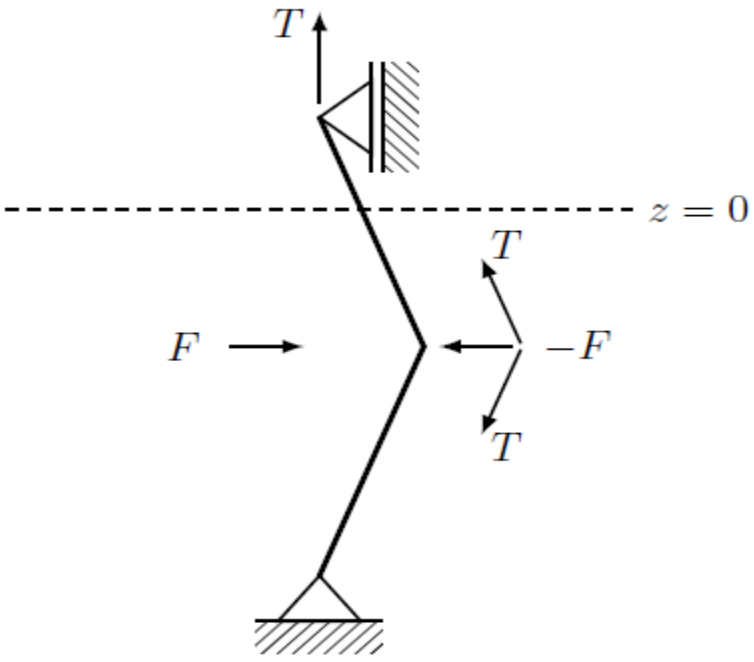

Figure 2-8: Change in geometry due to resisting forces (Hegseth; 2014).

The geometric stiffness matrix includes both the effects due to beam curvature and rope (Larsen, 1990) as shown in Figure 2-8. It also takes into account that the structure will change its geometry when it is subjected to external loads which will in turn affect its equilibrium. One has to consider the second order strains in the beam in order to derive the stiffness matrix (Larsen, 1990).

Larsen (1990) gave the equation for the total stiffness matrix, k for the element as the sum of the beam stiffness matrix k_E, and the geometric stiffness matrix, k_G as follows:

$$k = k_E + k_G \tag{2.7}$$

The stiffness of the element can be transformed to the global system by use of a transformation matrix. In the case of a large displacements and rotations found in marine risers and pipelines, a beam element with no limitations on displacement is required, hence the use of 3-D elements is with 12 degrees of freedom is adopted in this case (Larsen, 1999).

Figure 2-9 illustrates how the 12 nodal degrees of freedom for the 3-dimensional beam element are defined in relation to the local *x, y, z* system. The beam theory is based on the following assumptions as proposed by Larsen (1999).

- Lateral contraction caused as a result of axial elongation is disregarded
- A cross-section of the beam remains plane and perpendicular during deformation
- Shear deformations as a result of lateral loading are neglected
- The strains are infinitesimal

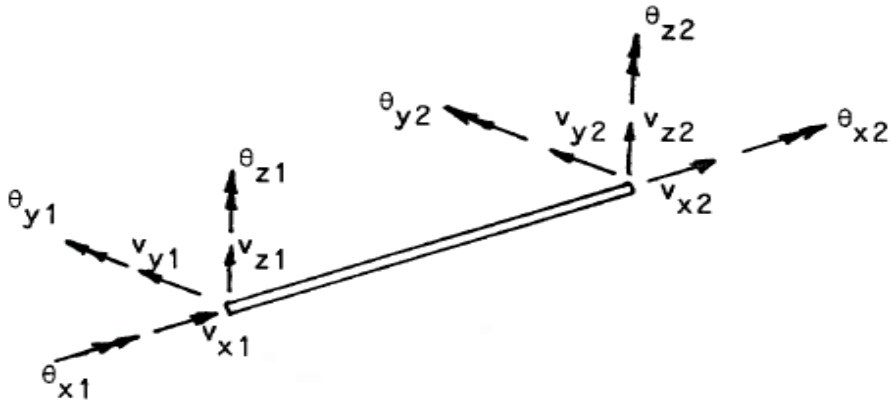

Figure 2-9: 3D Beam Element (Larsen, 1999)

2.3 Basic Concepts of Fatigue

This section explains the theory related to the fatigue calculation such as fatigue loading, development of S-N curves, cumulative damage assessment, stress concentration factor etc. According to (DNV, 2015), the fatigue assessment of subsea wellhead is mainly based on the S-N curve and Miner-Palmgren hypothesis which will be discussed in more details.

Since this thesis is focused on wellhead fatigue, it is necessary to understand how fatigue affects the wellhead during offshore drilling. The fatigue capacity of a system simply means the tendency of the system to accommodate cyclical loading before failure takes place.

The subsea wellhead is usually connected to the MODU through the drilling riser as shown in Figure 2-3. The wellhead is subjected to dynamic loads and these loads are a result of the vessel motion and riser caused by waves and current which are likely to generate crack growth thereby altering the structural integrity of the wellhead. Excessive bending loads can be imposed on the wellhead during drilling and completion operations especially if the vessel offsets and riser tensions are not controlled and this becomes a substantial issue. The aim of fatigue design is to

ensure that the structure has an adequate fatigue life. Normally, fatigue life on offshore structures is estimated to be 20 years (DNV, 2010). In order to ensure that the wellhead is fit for its intended purpose, a fatigue assessment, which is usually supported by a detailed fatigue analysis, is carried out since it is subjected by fatigue loading.

Since the BOP is placed on top of the subsea wellhead, it can impose large loads in the wellhead which will affect the structural integrity of the wellhead.

2.3.1 Fatigue Damage of Wellhead

Marine structures are subjected to dynamic loads and cracks may be initiated due to the cumulative effect of varying loads. Fatigue is caused by cyclic loads where the loads (stresses) are usually smaller to cause immediate failure. Hence, failure will not occur suddenly, instead the structure will fail after a certain number of load cycles.

According to Berge, (2006), the fatigue history of a structure can be divided into three stages:

- Initiation
- Crack growth
- Final failure

For fatigue life estimation of marine riser, only the initiation and crack growth stages are of interest. The initiation stage which is based on an elastic-plastic strain model is the first phase of fatigue and is caused by local yielding at the surface of the material. The initiation method relies on accurate material properties and specific test as the case may be (DNV, 2011). For an un-welded component, most of the fatigue life is spent in initiation stage, whereas for a welded component, the majority of the fatigue life is spent in crack growth stage. The fatigue damage is different for the two stages and is influenced by the stress component. Crack initiation stress component is

governed by yield, i.e. the von Mises stress, the crack growth is governed by the maximum principal stress (DNV, 2011)

Damage can be due to cyclical fatigue loading, hence, the load cycle will usually not have a constant amplitude due to variation of loads emanating from waves, currents and wind. When carrying out fatigue analysis of a structure, the point of interest is the stress acting over a given time. Since the acting stress is estimated based on loading, it is necessary to carefully examine the nature of the loading which comprises combinations of shear force and bending moment.

The loading may be considered as a stochastic process in case of environmental loading whereby different load amplitudes have a corresponding probability of occurrence and are randomly determined and may not be predicted precisely (Harildstad et al, 2013).

2.3.2 S-N Curves

The Stress to Number of cycle curves usually abbreviated as S-N curves is the graphical representation of the dependence of fatigue life (N) on fatigue strength (S). It is used to calculate the damage at the weld location. The fatigue life of a structural component is usually expressed by an S-N curve where the number of cycles to failure is plotted against stress range as shown in Figure 2-10.

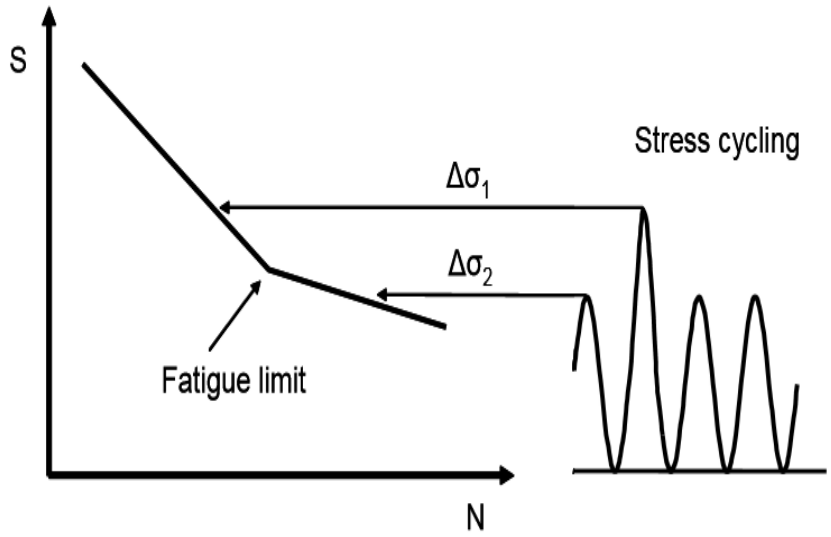

Figure 2-10: Stress cycling involving a detailed fatigue assessment (DNV, 2010)

Basically, the fatigue design which is based on the use of S-N curves are obtained from fatigue tests. According to DNV (2010), the S-N curves are associated with 97.7 percent probability of survival. There are several locations of potential fatigue failure in a wellhead system with some of the components comprising of forged parts and others are made of welds and sheet metal.

Most of the fatigue life is associated with growth of small crack that tends to grow faster as the crack size increases until fracture. A welded joint experiences a less crack growth than the base material notwithstanding the fact that the base material has a higher fatigue resistance. The initiation period of a fatigue crack takes longer time for a scratch in a base material than at a weld root (DNV, 2010).

2.3.3 Cumulative Damage Assessment

In order to determine how many stress cycles structures are able to resist before failure, a cumulative damage assessments are performed. Its main input is stress-to-time series for a given hot spot on the structure. The data is first processed and presented as stress range.

The most common method to carry out cumulative fatigue damage calculation is by using Miner-Palmgren summation technique owing to its simplicity and accuracy. It uses S-N curve data to calculate the damage. In this method, the damage is assumed to be constant per load cycle (Almar-Næss et al, 1985). The expression for the fatigue damage is given by:

$$D = \frac{1}{N} \tag{2.8}$$

Where N is the number of cycles to failure for a given stress range.

For loading with variable amplitude having k blocks of different stress ranges, the damage becomes:

$$D = \sum_{i=1}^{k} \frac{n_i}{N_i} \tag{2.9}$$

Where n_i represents the number of load cycles accumulated at the given stress level in block *i*.

The fatigue failure criterion for the structure also known as the fatigue design criterion states that failure will occur if the total fatigue damage is greater or equal to one.

$$D_{fat} \geq 1 \tag{2.10}$$

A design fatigue factor (DFF) is often applied as per DNV (2010) to reduce the probability of fatigue failure. The DFF depends on the consequences of failures and availability for inspection. Equation 2.11 gives the expression for the failure criterion with the design factor:

$$DFF.D_f \geq 1 \tag{2.11}$$

The choice of DFF is based on the safety classes as shown in Table 4-1. For drilling operations such as wellhead fatigue analysis, a high safety class (DFF = 10) must be considered in the analysis.

Table 2-1: Design fatigue factors, DFF (DNV-OS-F201)

Safety Class		
Low	Normal	High
3.0	6.0	10.0

The closed form approach may also be used as an alternative method to calculate fatigue damage if the stress range distribution can be represented by a two-parameter Weibull distribution. This approach is derived from the Palmgren-Miner Summation and is presented in the DNV-RP-C203

The Weibull distribution for stress ranges is given by the expression below:

$$Q(\Delta\sigma) = \exp\left[-\left(\frac{\Delta\sigma}{q}\right)^{h}\right] \quad (2.12)$$

$$q = \frac{\Delta\sigma_0}{(\ln n_0)^{1/h}} \quad (2.13)$$

where,

$Q(\Delta\sigma)$ is the probability of the stress range $\Delta\sigma$

q is the Weibull scale parameter

h is the Weibull stress range shape distribution parameter

$\Delta\sigma_0$ is the largest stress range out of n_0 cycles

The equation for fatigue damage using the closed form approach can further be expressed as:

$$D = \frac{v_0 T_d}{\bar{a}} q^m \Gamma\left(1 + \frac{m}{h}\right) \quad (2.14)$$

where,

T_d is the design life expressed in seconds

q is the Weibull stress range scale distribution parameter

v_0 is the average zero-crossing frequency

$\Gamma\left(1+\frac{m}{h}\right)$ is the gamma function

Equation 2.14 is applicable only for single slope S-N curves

2.3.4 Stress Concentration Factor

A stress concentration factor normally abbreviated as SCF is defined as the ratio of hot spot stress range to the nominal stress range.

Mathematically,

$$SCF = \frac{\Delta\sigma_{hotspot}}{\Delta\sigma_{nominal}} \tag{2.15}$$

SCF is used in the evaluation of fatigue damage of offshore structures. These stresses are due to geometrical irregularities like welds and cut-outs. The nominal stress can be obtained from the net cross section of the component while the hotspot stresses are obtained by conducting a local FE analysis or by using appropriate S-N curve as per DNV (2010).

2.4 Fatigue as a Challenge in Soil-Structure Interaction

An important factor to be considered during the analysis of wellhead is the interaction of the soil with the conductor. Since the wellhead is to transfer loads from the BOP and the conductor to the soil, accurate determination of soil properties is importance for fatigue damage in the subsea wellhead. Fatigue stresses in a subsea wellhead are primarily due to environmental loads acting on the vessel and the riser system. The soil stiffness related to the wellhead location can be obtained by adopting P-y curves i.e. pressure-displacement curves.

2.5 Overview of Soil Modelling Approach

Soil response modelling plays an important role in well fatigue analysis and there is need for developing appropriate soil models for well fatigue analysis. The bending and axial stresses in the subsea wellhead has to be accurately determined in this aspect. This thesis takes into account the response of soil on wellhead fatigue.

Jeanjean (2009) was the first to note that the application of backbone curves for fatigue analysis is not appropriate by performing an assessment of P-y curves for soft clays from a series of physical experiments complemented by Finite Element Analysis. Comparisons were made between the P-y curves generated from centrifuge testing and FE analyses and concluded that the lateral P-y curves provided by API RP 2A (2000) which is based on the work of Matlock (1962) are too soft and underestimate the ultimate unit pressure acting on the conductor. A monotonic backbone curve was proposed to generate P-y curves for soft clays with a more appropriate stiffness. It was investigated that the lateral soil resistance under the monotonic backbone P-y curve in soft clays are both stiffer and stronger than those of the API recommendations. The work of Jeanjean

confirms that the methodology used by the FEA software to derive the unload-reload cyclic stiffness from the monotonic FEA P-y curves is conservative to determine the fatigue life below mudline (BML) since it gave a reduction in cyclic stresses and increased in fatigue life and will be unconservative to estimate fatigue above the mudline (Jeanjean, 2009). Figure 2-11 shows the soil-structure interaction modeled as a linear spring with a stiffness equal to the tangent modulus of the P-y curve taken at the mean load of the load cycle.

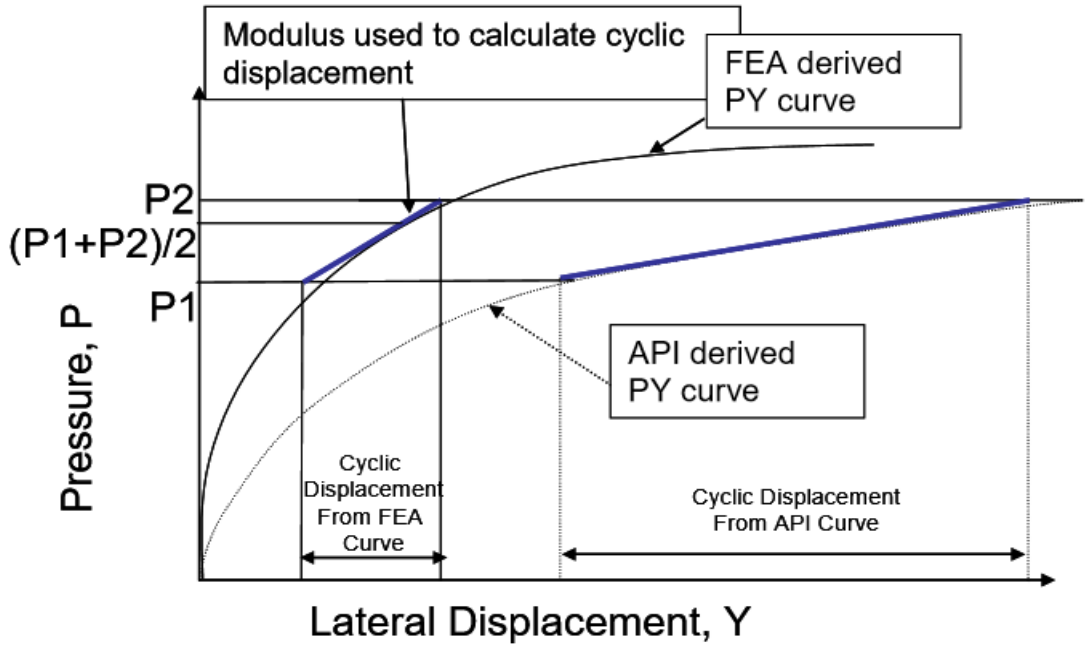

Figure 2-11: Calculation of Soil-structure spring stiffness in riser analysis program (Jeanjean, 2009)

Zakeri et al. (2015) also performed an extensive study that involved physical experiments in a geotechnical centrifuge with complementary numerical analyses to develop soil response model specifically for conductor fatigue analysis that is applicable to wide range of soil and load conditions. Two approaches were developed for conductor fatigue analysis. The first approach utilizes Winkler springs to model the soil response based on relationships obtained from the centrifuge model tests for the fully degraded secant stiffness at the steady-state condition, K_{sec_ss}

taken as a function of cyclic displacement. The first approach is also called the simplified approach or secant stiffness approach and it does not also consider the transient phase for soil degradation. The second approach was developed by performing a numerical modelling and applying a kinematic hardening model in the FE program to simulate the unload-reload behavior of the soil. This approach is also referred to as the "Kinematic Hardening (KH) approach", since it offers the advantage of simulating the soil reactions through a constitutive mechanics-based framework (Zakeri et al, 2015).

The centrifuge testing program conducted by Zakeri et al (2015) and completed in 2013 consisted of series of centrifugal tests followed by the development of laboratory testing apparatus calibrated to the centrifuge data for direct P-y relationships measurement. According to Zakeri et al (2015), the centrifuge testing program comprises four series of test given as follows:

Series 1: this involved displacement-controlled test in normally consolidated kaolin clay

Series 2: this involved displacement-controlled tests in medium-dense sand

Series 3: this involved displacement-controlled test in normally consolidated Gulf of Mexico (GoM clay).

Series 4: this involved displacement-controlled test in over-consolidated (stiff) natural clay.

Zakeri et al presented the results in two papers. The papers deal with geotechnical aspects of well conductor fatigue analysis. The first paper, which is the part I gives an insight of the technique of conductor fatigue analysis and the function of foundation soils and further presents an overview of the centrifuge testing program accompanied by detailed analysis of series 1 test results. The series 1 test has four model conductors which are installed in kaolin clay and subjected to displacement-control loading conditions with the intent to develop a better understanding of the mechanisms associated in the soil-conductor interaction for the development of soil constitutive

P-y models to be implemented into numerical analysis. Series 1 test also produce soil resistance-displacement data to be applied for variable loading conditions with random and harmonic excitations.

The second paper, part II, presents the results of series 2-4 along with the fatigue soil model developed for estimating conductor fatigue analysis.

Chapter 3

Analysis of Drilling Riser and Conductor for Deepwater Drilling

This section explains the analysis of the strength and stability of drilling riser, lateral load bearing capacity of conductor and surface casing for deepwater drilling.

Jin et al. (2007), carried out some studies on the strength and stability analysis of deep sea drilling risers by analyzing the influence of vortex-induced vibration (VIV) on the strength and stability of marine drilling risers. Jin et al. (2007) established a simplified analytical model and developed a method for calculating vortex induced dynamic response.

Guan et al. (2009) performed an analytical model for the lateral load-bearing capacity of conductor and surface casing in deepwater drilling and its analysis was based on the pile foundation theories and material mechanics by considering the axial and lateral loads, variable stiffness of casing string and the nonlinear response between casing string and soil in deepwater drilling operations.

A series of numerical methods was adopted to solve these models and are presented in this chapter.

3.1 Vibration Equation of Marine Risers

A simplified analytical model has been established by Jin et al. (2007) to analyze the influence of vortex-induced vibration (VIV) on the strength and stability of marine risers. A method for estimating vortex-induced dynamic response was developed. The marine riser model can be idealized as a vertical beam in water as shown in Figure 3-1. The *x*-axis is parallel to the flow velocity of current and the propagation direction of wave, *z*-axis is the vertical axis of the riser in its undeflected configuration and *y*-axis is perpendicular to both as shown in Figure 3-1.

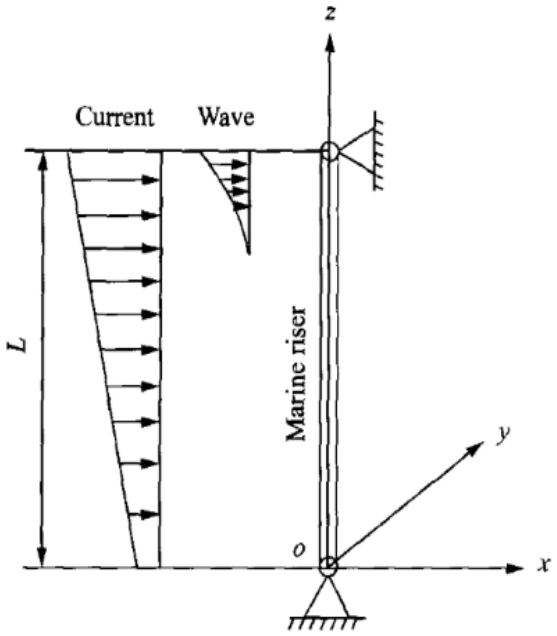

Figure 3-1: Marine riser model (Jin et al, 2007)

Dong (1994) proposed an equation for the transverse motion of the marine riser with the assumption that the wave is a linear wave with low amplitude and uniform mass distribution of the riser and cross section variation in the *z* direction. This equation is presented below.

$$EI \cdot \frac{\partial^4 y}{\partial z^4} - T_0 \cdot \frac{\partial^2 y}{\partial z^2} + c \cdot \frac{\partial y}{\partial t} + m \cdot \frac{\partial^2 y}{\partial t^2} = F_y(z,t) \qquad (3.1)$$

where,

EI is the flexural stiffness of the riser, N.m^2

T_o is the top tension, N

C is the viscous damping coefficient

m is the mass of the beam per unit length, kg/m

F_y (z, t) is the total external fluid force per unit length in the y-direction, N/m

$$F_y(z,t) = F_L(z,t) - F_r(z,t) \tag{3.2}$$

where,

F_L is the vortex lift force per unit length measured in N/m. It is defined as the fluid damping force caused by the motion of the riser in y direction

$F_r(z, t)$ is the nonlinear fluid damping force caused by the motion of the riser in the y-direction.

$F_L(z, t)$ can also be expressed as follows:

$$F_L(z,t) = \frac{1}{2}\rho D(V_c + u)^2 C_L \cos(\omega_s t) = K_L(z) \cdot C_L \cos(\omega_s t) \tag{3.3}$$

where,

ρ is the density of seawater, kg/m^3

D is the external diameter of the riser, m

C_L is the lift coefficient

ω_s is the vortex shedding frequency, rad/s

K_L is the lift force distribution coefficient, kg/s^2 and can be expressed as follows:

$$K_L(z) = \frac{1}{2}\rho D(V_c(z) + u)^2 \tag{3.4}$$

V_c is the flow velocity of current and is a linear function of water depth expressed as:

$$V_c(z) = a + bz \tag{3.5}$$

Applying the linear wave theory, the horizontal velocity of wave *u* can be described as follows:

$$u = u(z,t) = \frac{\pi \cdot H}{T_w} e^{k(z-1)} \cos(\omega_w t) \tag{3.6}$$

where,

H is the wave height, m

T_w is the wave period, s

ω_w is the wave circular frequency, rad/s

l is the length of riser, m

k is the wave number, $k = 2\pi/L_w$, and L_w is the wavelength, m.

$F_r(z, t)$ can be described by Morison Equation:

$$F_r(z,t) = \frac{1}{2}\rho D C_d y'|y'| + C_a \rho \frac{\pi D^2}{4} y'' \tag{3.7}$$
$$= K_d C_d y'^2 \operatorname{sgn}(y') + m' y''$$
$$K_d = \frac{\rho D}{2}$$

$$m' = \frac{\rho C_a \pi D^2}{4}$$

where,

m' is the mass of adhered water per unit length, kg/m

C_d is the fluid damping coefficient and C_a is the coefficient of additional mass

The vortex-induced vibration (VIV) response of the risers can be calculated as follows, assuming that the riser is a beam simply supported at both ends, and its boundary conditions are as follows (Jin et al, 2007):

$$\left.\begin{aligned} y(0,t) &= 0 \quad \frac{\partial^2 y(0,t)}{\partial z^2} = 0 \\ y(l,t) &= 0 \quad \frac{\partial^2 y(l,t)}{\partial z^2} = 0 \end{aligned}\right\} \tag{3.8}$$

Using the Galerkin method, Eq. 3.1, a partial differential equation, is transformed into a group of nonlinear ordinary differential equations (Jin et al, 2007). Note that Galerkin's method provides powerful numerical solution to differential equations and modal analysis.

The lateral displacement y (*z*, *t*) can be expressed as a series of vibration mode shapes given as:

$$y(z,t) = \sum_{n=1}^{\infty} y_n(t)\sin(\lambda_n z) \tag{3.9}$$

$$\lambda_n = \frac{n\pi}{l}$$

Substituting Eq. (3.3), Eq. (3.7) and Eq. into Eq. (3.2), total external fluid force per unit length in the y-direction will be obtained. Also, by rearranging Eq. (3.1) via substituting Eqs. (3.9) and (3.2) and applying the Galerkin method, we obtain:

$$y'' + \left[\lambda_{b_n}^2 + \lambda_{C_n}^2\right]y_n + \frac{c_n}{\overline{m}}y_n' + \frac{2D_n}{l\overline{m}} = \frac{2C_L}{l\overline{m}}\cos(\omega_s t)\int_0^l K_L(z)\sin(\lambda_n z)dz \tag{3.10}$$

$$\overline{m} = m + m'$$

$$\lambda_{B_n}^2 = \lambda_n^4 (EI / \overline{m})$$

$$\lambda_{C_n}^2 = \lambda_n (T_0 / \overline{m})$$

$$C_n = 2\overline{m}(\lambda_{B_n}^2 + \lambda_{C_n}^2)^{1/2} \zeta_s$$

where,

$\overline{m}$ is the virtual mass per unit length of riser, kg/m

$\lambda_{B_n}^2$ is the natural frequency of bending vibration of the riser

$\lambda_{C_n}^2$ is the natural frequency of axial vibration of the riser

C_n is the viscous damping coefficient

ζ_s is the dimensionless damping ratio of the structure

D_n is defined by Eq. (3.11), and the nonlinear damping term can be obtained by numerical algorithm (Jin et al., 2007):

$$D_j = K_d C_d \int_0^1 sgn(y') y'^2 \sin(\lambda_j z) dz \qquad j = 1,2,3,\ldots n \tag{3.11}$$

$$y' = y'(z,t) = \sum_{i=1}^{n} y_i'(t) \sin(\lambda_n z) \tag{3.12}$$

D_n defined by Eq. (3.11) is a quadratic function of y_i'

Dynamic displacement *y (z, t)* can be expressed by Eq. (3.9).

Dynamic moment is then given according to Ma et al. (2000) as follows:

$$M(z,t) = EI\frac{\partial^2 y}{\partial z^2} = EI\sum_{n=1}^{\infty}\lambda_n^2 y_n(t)\sin(\lambda_n z) \tag{3.13}$$

Dynamic shearing force is expressed as follows:

$$Q(z,t) = EI\frac{\partial^3 y}{\partial z^3} = EI\sum_{n=1}^{\infty} y_n^3\, y_n(t)\cos(\lambda_n z) \tag{3.14}$$

The fatigue life of the marine riser can be estimated using Palmgren-Miner theory. Hence, the damage criterion is given by:

$$D_i = \sum_i \frac{n(\Delta\varepsilon_i)}{N(\Delta\varepsilon_i)} \tag{3.15}$$

where,

$n(\Delta\varepsilon_i)$ is the number of cycles of alternate strain occurred in the range of $\Delta\varepsilon_i$ and can as well be expressed as:

$$n(\Delta\varepsilon_i) = f_i t_i \tag{3.16}$$

f_i is the frequency corresponding to the *i*th amplitude measured in rad/s and t_i is the vibration time, in seconds.

Similarly, the denominator in Eq. (3.15) can be obtained from the relevant S-N curve and it is related to the equation below:

$$N(\Delta\varepsilon_i) = c.(\Delta\varepsilon)^{-b} \tag{3.17}$$

where *c* and *b* are constants.

The symbol $\Delta\varepsilon$ is the maximum difference of strain in one cycle and is indicated in the middle point of the riser having two joint and is expressed as follows:

$$\Delta\varepsilon = \pi^2 A_o (\frac{D}{L})^2 \tag{3.18}$$

where A_o is the amplitude of the middle point of riser, m. By substituting Eqs. (3.16), (3.17) and (3.18) we can obtain the value of D_i for t = 1 year as follows:

$$D_i = \sum_i \frac{f_i t_i A_{0,i}^4 \left(\frac{D}{L}\right)^8}{6.745 \times 10^{-12}} \tag{3.19}$$

Assuming $T_i = \frac{t_i}{3600\times365}$ and substituting it into Eq. (3.19), we can obtain the fatigue lifetime of the riser in years as follows:

$$D_i = \frac{5.133\times10^{-18}(\frac{L}{D})^8}{f_n \sum_i (\frac{f_i}{f_n}) T_i A_{o,i}^4} \tag{3.20}$$

3.2 Analysis of Dynamic Response of Riser

The natural frequencies of marine risers tend to decrease with increasing length. However, resonance is likely to occur when the natural frequency of the riser is close to the vortex shedding frequency. Applying Runge-Kutta Method, the equations can be reduced as follows:

$$Y_1 = y_1 \tag{3.21}$$

$$Y_2 = \frac{dY_1}{dt} = \frac{dy_1}{dt} = y_1' \tag{3.22}$$

$$Y_3 = y_2 \tag{3.23}$$

$$Y_4 = \frac{dY_3}{dt} = \frac{dy_2}{dt} = y_2' \tag{3.24}$$

$$Y_5 = y_3 \tag{3.25}$$

$$Y_6 = \frac{dY_5}{dt} = \frac{dy_3}{dt} = y_3' \tag{3.26}$$

$$Y_7 = y_4 \tag{3.27}$$

$$Y_8 = \frac{dY_7}{dt} = \frac{dy_4}{dt} = y_4' \tag{3.28}$$

Where Y_1, Y_2, Y_3, Y_4, Y_5, Y_6, Y_7 and Y_8 are values of iterations in meters.

The first four modal response $y_1(t)$, $y_2(t)$, $y_3(t)$ and $y_4(t)$ caused by combined wave-current interaction were calculated and shown in the figures below:

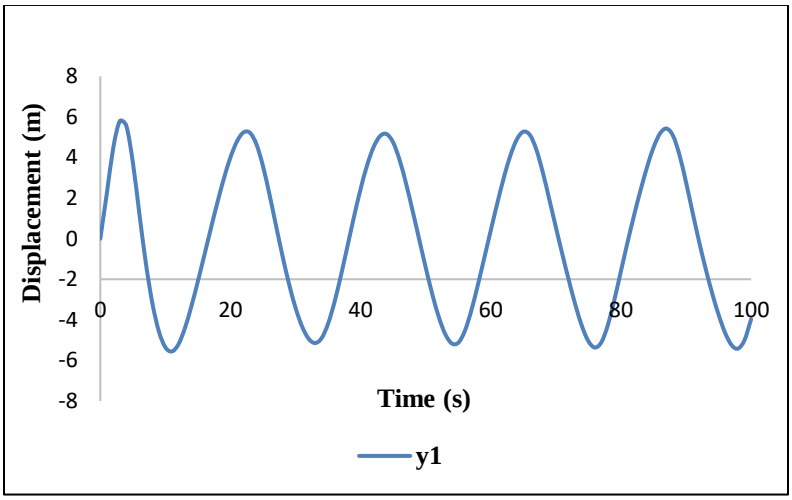

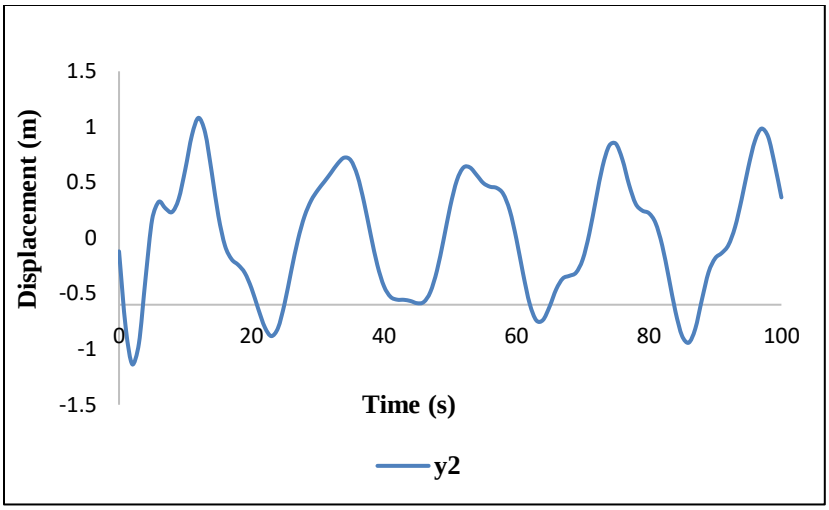

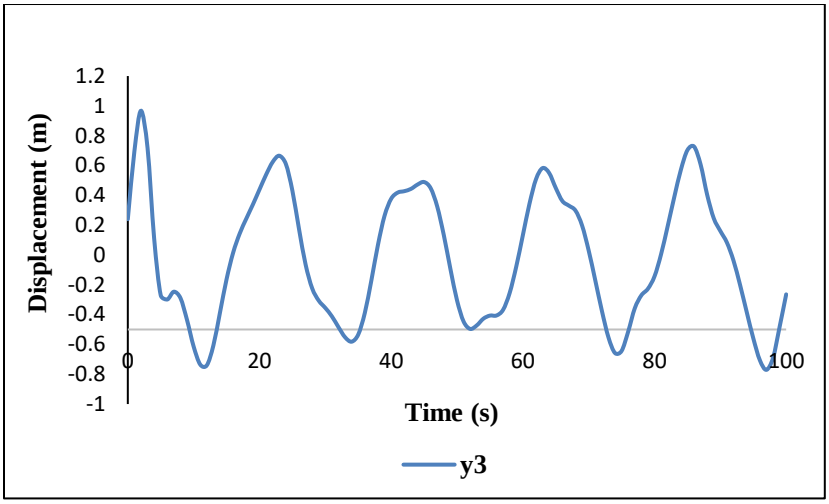

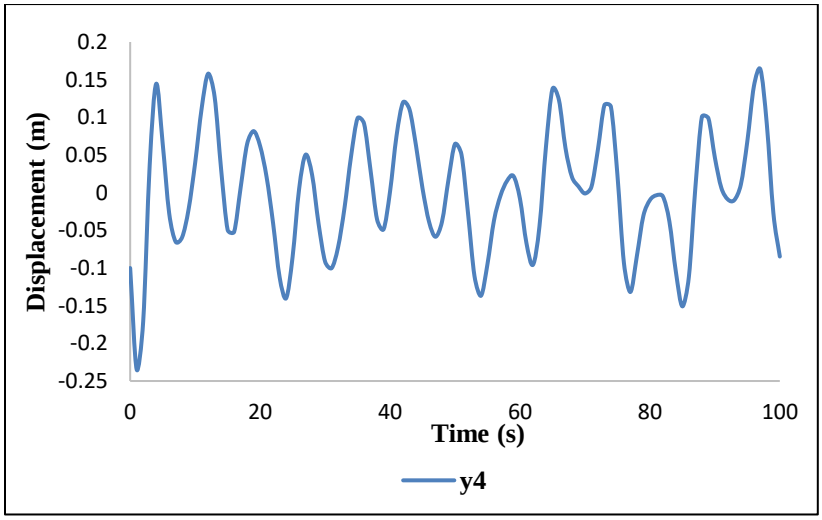

Figure 3-2: Modal response considering the combined wave-current interaction

Eq. (3.13) can be modified as follows:

$$M(z,t) = EI\frac{\partial^2 y}{\partial z^2} = EI\left\{y_1(t)\sin(\frac{\pi z}{l}) + 4y_2(t)\sin(\frac{2\pi}{l}) + 9y_3(t)\sin(\frac{3\pi z}{l}) + 16y_3(t)\sin(\frac{4\pi z}{l})\right\} \quad (3.29)$$

Hence, $z = l/2$, for the middle point of the riser. Therefore the dynamic displacement becomes:

$$M\left(\frac{l}{2},t\right) = EI\frac{\partial^2 y}{\partial z^2} = EI\left\{y_1(t)\sin(\frac{\pi z}{l}\right) + 9y_3(t)\sin(\frac{3\pi z}{l})\right\} \quad (3.30)$$

Eq. (3.30) shows that $y_3(t)$ has a significant influence on the bending moment when, $z = l/2$,

Figures 3-3 and 3-4 show the responses of dynamic moment and dynamic shear force when the primary resonance generates. Figure 3-5 shows the responses of dynamic moment at the middle point and the dynamic shear force at the bottom of the riser.

Since the natural frequency of marine risers increases with top tension, vortex-induced vibration can be avoided by increasing the top tension.

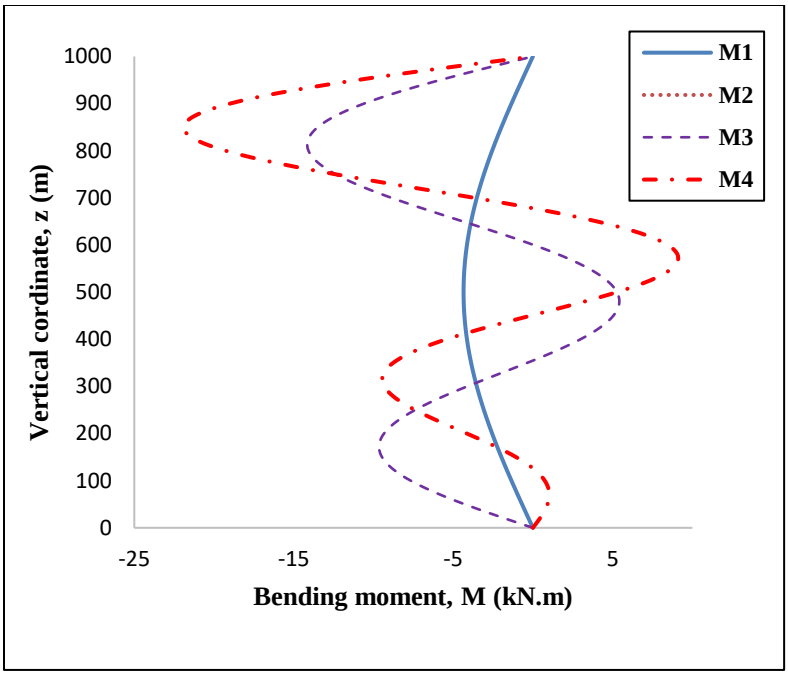

Figure 3-3: Dynamic moment responses considering combined wave-current loads

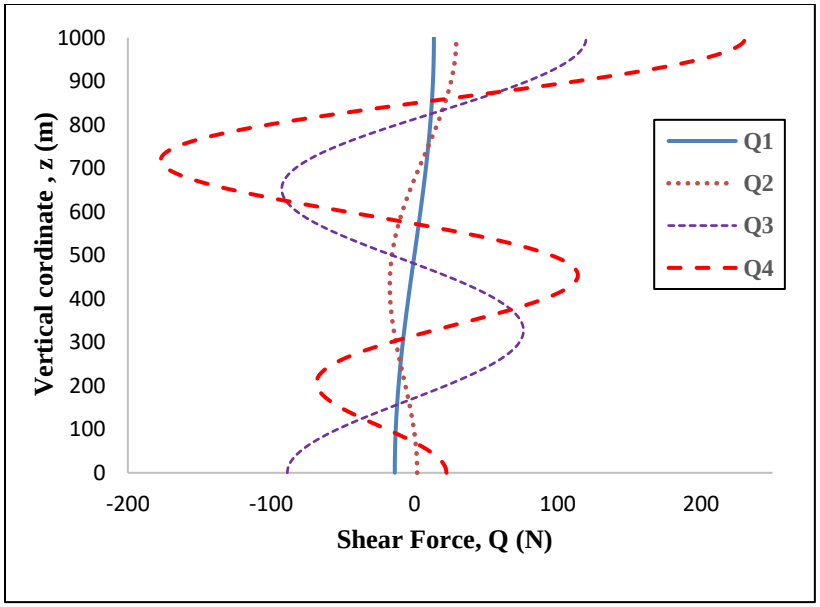

Figure 3-4: Shear force responses considering combined wave-current loads

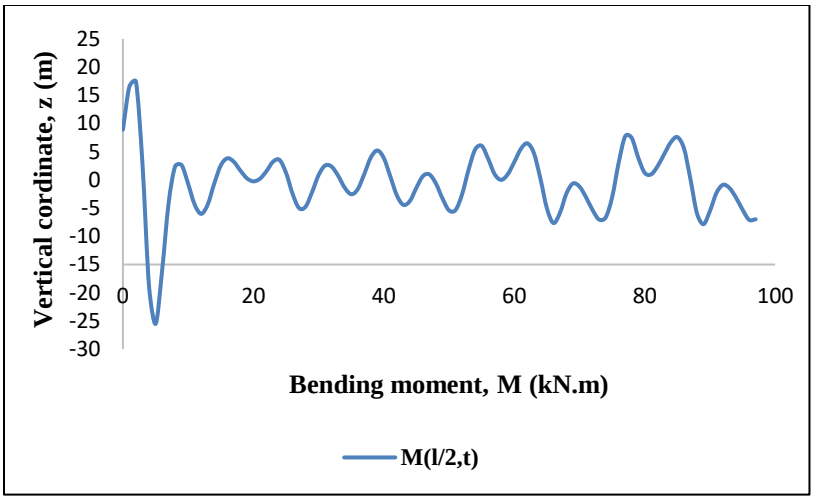

Figure 3-5a: Dynamic moment response at the middle point

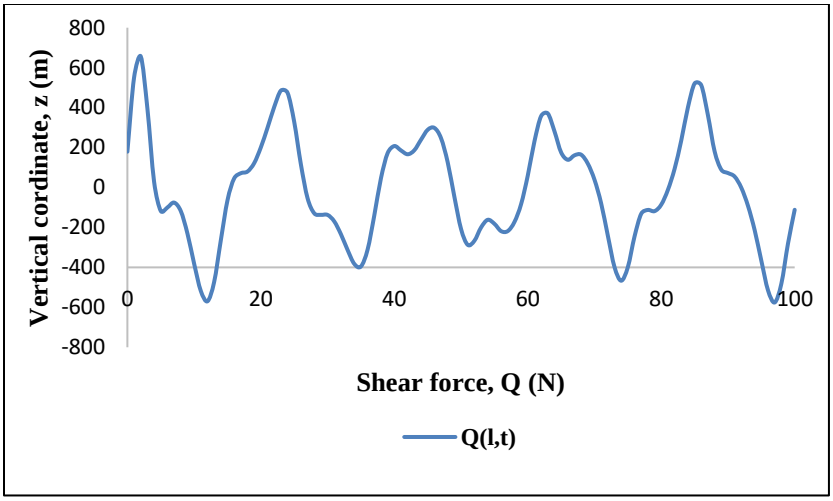

Figure 3-5b: Shear force at the bottom of the riser

From the analytical results, it can be concluded that the first-order mode dynamic response is greater than higher-order mode responses primary resonance. In addition, the natural frequency of a riser decreases with increasing length, but increases with increasing top tension

3.3 Lateral Load-Bearing Capacity of Conductor and Surface Casing

Since the force transferred to wellhead through the bottom joint of the riser and the weights of BOP stack and all casing strings themselves have been undertaken by conductor and surface casing, vertical load-bearing capacity is important for determination of running depth of conductor and providing basis for prohibition of wellhead sinking (Guan et al, 2009). This section provides a theoretical basis for the stability analysis of wellhead of deepwater drilling and for the process design of conductor and surface casing.

3.4 Analysis Model of Lateral Load-Bearing Capacity for Conductor

An analysis model of lateral load-bearing capacity suitable for conductor and surface casing for deepwater is presented.

3.4.1 Force Analysis

Casing string and the above BOP stack and riser are joined by the subsea wellhead. Forces from the ocean environment transferred to the subsea wellhead from the risers, making it bear some transverse moment and vertical force. Assuming the transverse moment acting on the top of the riser (wellhead) is M and the vertical force is N. Continuous distributed reaction has been generated by the foundation under the mudline which supports the casing strings.

An infinitesimal section is taken from the string, with Q representing the shear of the string and M representing the moment. Deflection differential equation of pipe string under the interaction of transverse moment and vertical force is then obtained according to the mechanical equilibrium relationship.

$$\frac{d}{dx^2}\left[EI(x)\frac{d^2y}{dx^2}\right]+\frac{d}{dx}\left[N(x)\frac{dy}{dx}\right]+D(x)\cdot p(x,y)=0 \tag{3.31}$$

Where: $EI(x)$ $(\mathrm{kN}\cdot\mathrm{m}^2)$ is the flexural rigidity changes along x axis, $N(x)$ (kN) is the axial force changes along x axis, $D(x)$ (m) is the variable outer diameter of the pipe string, $p(x,y)$ is the subgrade reaction per unit area: $p(x,y)=\bar{p}(x,y)/D(x)$ (kPa). Pipe strings above the mudline do not suffer from the subgrade reaction: $p(x,y)=0$.

3.4.2 Subgrade Reaction

According to different assumed conditions, the calculation methods of the subgrade reaction p can be divided into 3 kinds：

1. Limit of subgrade reaction method. Without considering the deformation of the foundation itself, p is the function of depth: $p=p(x)$;
2. Elastic subgrade reaction method. Assuming that p is proportional to the nth power of the deflection of the pipe string: $p=kx^m y^n$, where k is a coefficient determined by the properties of the foundation which is also related to the choice of the exponential m $(m\geq 0)$, n $(0<n\leq 1)$.
3. Elastoplastic subgrade reaction method. That is, the plastic region is analyzed with limit of subgrade reaction method while the plastic region is analyzed with elastic subgrade reaction method. Then the transverse reaction can be solved with the continuous condition of the boundary of the elastic region and the plastic region. Since it can describe the nonlinear characteristics between pipe strings and the foundation, it is able to make more

exact analysis on the lateral loading-bearing capacity with large displacement of pipe string comparing to other methods. It has been adopted in the API RP 2A named as $p-y$ curve method. When no experimental material is available, theoretical equations provided by the practice can be referred to for the calculation of the $p-y$ curve of clay and sandy soil.

Secant modulus of the subgrade reaction at depth x can be determined according to the $p-y$ curve $\left(E_s = p/y\right)$, and therefore p corresponding to different y can be determined $\left(p = E_s y\right)$.

Substitute p with $p = E_s y$ in equation (1), we have:

$$\frac{d}{dx^2}\left[EI(x)\frac{d^2y}{dx^2}\right]+\frac{d}{dx}\left[N(x)\frac{dy}{dx}\right]+D(x)\cdot E_s y = 0 \tag{3.32}$$

3.4.3 Forces

Risers in the deep-water conditions suffer from complex stress: the transverse component of the bottom tension, weight of the BOP and current force acting on it will render transverse moment M_t on the wellhead while the resultant force of the vertical component of the bottom tension and weight of the BOP is the vertical force N_t on the wellhead.

Axial force on the pipe string can be described as:

$$N(x)=\begin{cases} N_{\mathrm{t}}+W(x)\cdot x & \left(x \le x_{\mathrm{ml}}\right) \\ N_{\mathrm{t}}+W(x)\cdot x - F_{\mathrm{f}}(x)\left(x-x_{\mathrm{ml}}\right) & \left(x > x_{\mathrm{ml}}\right) \end{cases} \tag{3.33}$$

Where, x_{ml} is the length of the pipe string above the mudline (m), $W(x)$ is the weight of the pipe string per unit length (kN), $F_{\mathrm{f}}(x)$ is the soil friction on the external wall of the pipe string per unit length (kN).

3.4.4 Flexural Rigidity

If there is a double layer casing pipe structure with cement sheath at the upper cementing segment of the combination pipe string, the equivalent flexural rigidity K_1 is:

$$K_1 = E_{\mathrm{st1}}(I_{\mathrm{so}} + I_{\mathrm{si}}) + 0.6 \cdot E_{\mathrm{c}} I_{\mathrm{c}} \tag{3.34}$$

Where, E_{st1} is the modulus of elasticity of the steel of the pipe string (kPa), I_{so} is the moment of inertia of the surface casing (m^4), E_{c} is the modulus of elasticity of the cement sheath (kPa), I_{c} is the moment of inertia of the cement sheath (m^4).

If there is a double layer casing pipe structure at the upper segment of the combination pipe string without cement sheath, the equivalent flexural rigidity K_2 is:

$$K_2 = E_{\mathrm{st1}}(I_{\mathrm{so}} + I_{\mathrm{si}}) \tag{3.35}$$

If it is a combination structure of cement sheath and surface casing rather than a conductor at the lower section of the combination pipe string, the equivalent flexural rigidity K_3 is:

$$K_3 = E_{\mathrm{st1}} I_{\mathrm{si}} + 0.8 \cdot E_{\mathrm{c}} I_{\mathrm{c}} \tag{3.36}$$

3.5 Numerical Solution of the Analysis Model of Lateral Load-Bearing Capacity

Since the reaction between pipe string and the foundation is quite complex, the length L of the pipe string can be equally divided into n segments with difference method. The length of each segment is h. Set the top node of the pipe string as node 0 while the bottom node of the pipe string is node n. Prolonging the two ends and set virtual node -1, virtual node -2, virtual node n+1, and virtual node n+2 as shown in figure 3-6.

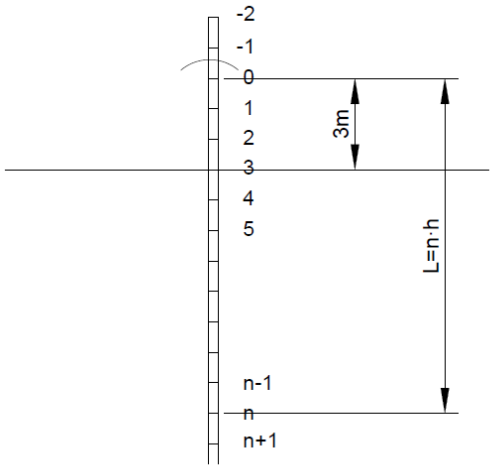

Figure 3-6: Numerical grid of casing string

The derivative scheme in Eq. (3.32) can be approximately substituted by the difference scheme. Then Eq. (3.32) becomes (n+1) difference equations.

$$\begin{cases} a_i y_{i+2} + b_i y_{i+1} + c_i y_i + d_i y_{i-1} + e_i y_{i-2} = 0 \\ a_i = (EI)_{i+1} \\ b_i = -2(EI)_{i+1} - 2(EI)_i + N_i h^2 \\ c_i = (EI)_{i+1} + 4(EI)_i + (EI)_{i-1} - 2N_i h^2 + D_i (E_s)_i h^4 \\ d_i = -2(EI)_i - 2(EI)_{i-1} + N_i h^2 \\ e_i = (EI)_{i-1} \end{cases} \tag{3.37}$$

Boundary condition: when there is a moment M_t at node 0 on the top of the pipe string, internal force of the pipe string will have the same value as it but in opposite direction, that is: $M_0 = -M_t$, $Q_0 = 0$. As for the pipe string which dives relatively deep in to the soil, the node at the bottom end can be regarded as a free end, that is: $M_n = 0$, $Q_n = 0$.

Difference of boundary conditions gives 4 equations. Together with equation (3.37), there are n+5 equations to solve the variables in n+5 nodes. Since the poor precision of matrix expunction computation, Gleser method is generally used to get the expression of y_i $(i = -2,-1,...,n+2)$ through transformation. Since $(E_s)_i$ varies nonlinearly, the calculation need to be performed by iteration. That is, first of all, a group of $(E_s)_i^o$ are assumed. There is no subgrade reaction on the pipe string above the mudline: $E_s = 0$. A group of y_i^o will be obtained after solving them for once, with which a group of p_i^0 will be obtained according to the $p-y$ curve. Then according to $E_s = p/y$, a new group of $(E_s)_i^1$ can be obtained. Using the new $(E_s)_i^1$ to repeat the iteration process until $\left|(E_s)_i^0 - (E_s)_i^1\right| < \varepsilon$, where ε is the allowable accuracy condition. The deflection (transverse displacement) of each node on the pipe string can be obtained, therefore rotation angle θ_i, moment M_i, shear Q_i, subgrade reaction p_i of each nodes can be calculated.

1. $$\begin{cases} \theta_i = -\dfrac{y_{i+1} - y_{i-1}}{2h} \\ M_i = -\dfrac{(EI)_i (y_{i+1} - 2y_i + y_{i-1})}{h^2} \\ Q_i = -\dfrac{(EI)_{i+1} y_{i+2} - \left[2(EI)_{i+1} - N_i h^2\right] y_{i+1}}{2h^3} + \dfrac{\left[(EI)_{i+1} - (EI)_{i-1}\right] y_i + \left[2(EI)_{i-1} - N_i h^2\right] y_{i-1}}{2h^3} - \dfrac{(EI)_{i-1} y_{i-2}}{2h^3} \\ p_i = (E_s)_i y_i \end{cases}$$

(3.38)

Example and analysis of influencing factors

Parameters of a deepwater well in a certain sea area are:

Conductor: length 85 m, outer diameter 914.4 mm, wall thickness 25.4 mm, weight per unit length 7.8 kN/m

Surface casing: length 650 m, outer diameter 508 mm, wall thickness 12.7 mm, weight per unit length 2.1 kN/ m, modulus of elasticity is 210 GPa

Cement sheath between two casing strings:

Modulus of elasticity is 18 GPa, weight per unit length is 45 kN/m

Length of pipe string above the mudline is 3m

Assuming in the adverse ocean environment maximum transverse moment conveyed to the wellhead is 3MN*m, vertical force is 1MN. To simplify the calculation, assuming it is clay layer from the mudline to 100 meters below it, of which the underwater bulk density is 7.0 kN/m^3 and the shear strength is 20 kPa.

3.6 Effects of the Forces on the Wellhead

As shown in Figure 3-7 to 3-11, an analysis was performed on the lateral load-bearing capacity of the combination pipe string under the interaction of different transverse moments and vertical forces.

The result illustrates transverse displacement, rotation angle, moment, shear, and subgrade reaction are almost zero when the depth goes over a certain value. That is, the forces on the wellhead only concentrate on a relatively short region at the upper pipe string and hardly bring any effects on the lower region.

Comparing the effects of different values of forces, the conclusion is that the transverse displacement on the top of pipe string has relatively obvious increase when the transvers moment is greater. Meanwhile, the moment and shear of the pipe string increase gradually with the increase of the transvers moment. Transverse displacement and moment become larger when there is a greater vertical force acting on the top of the pipe string. However, the effects of vertical force is not as obvious as the effects of the transverse moment. Forces undertaken by the subsea wellhead in deepwater drilling come from BOP stack above the wellhead, risers, drilling platform in the ocean environment. It’s very important to reasonably control the drifting of the platform and the drilling ship and tension force on the top of the risers to guarantee the stability of wellhead and pipe strings

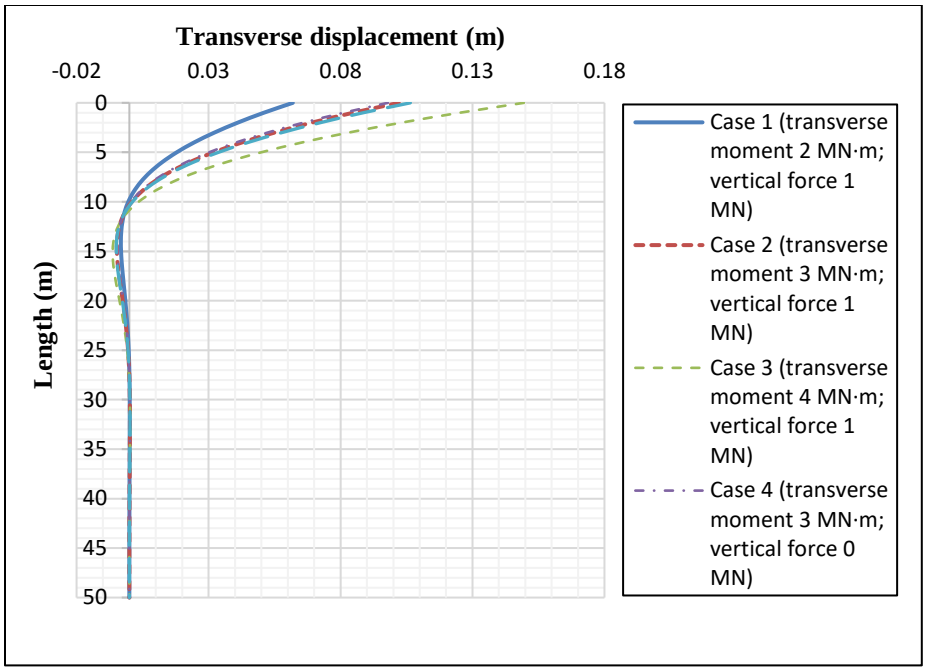

Figure 3-7: Transverse displacement

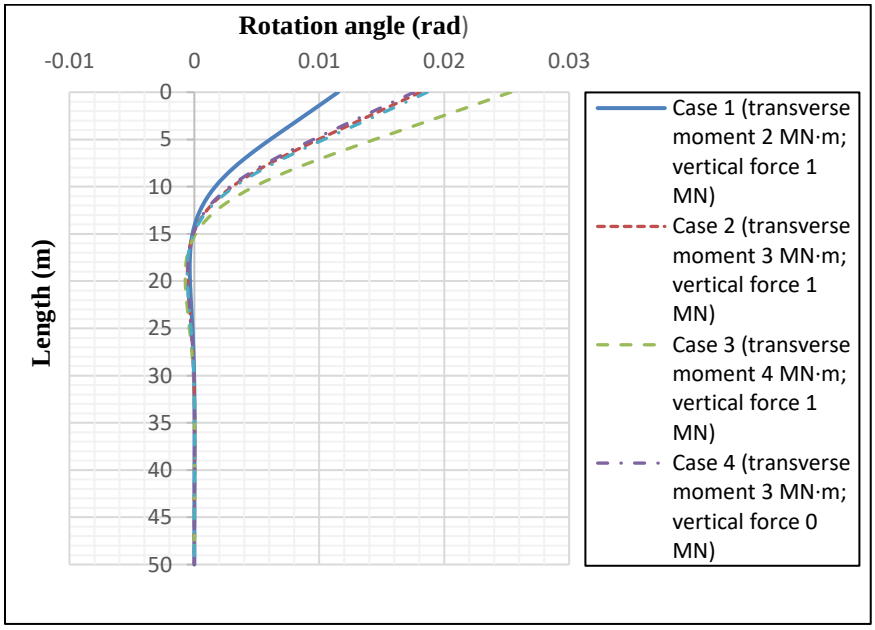

Figure 3-8: Rotation angle

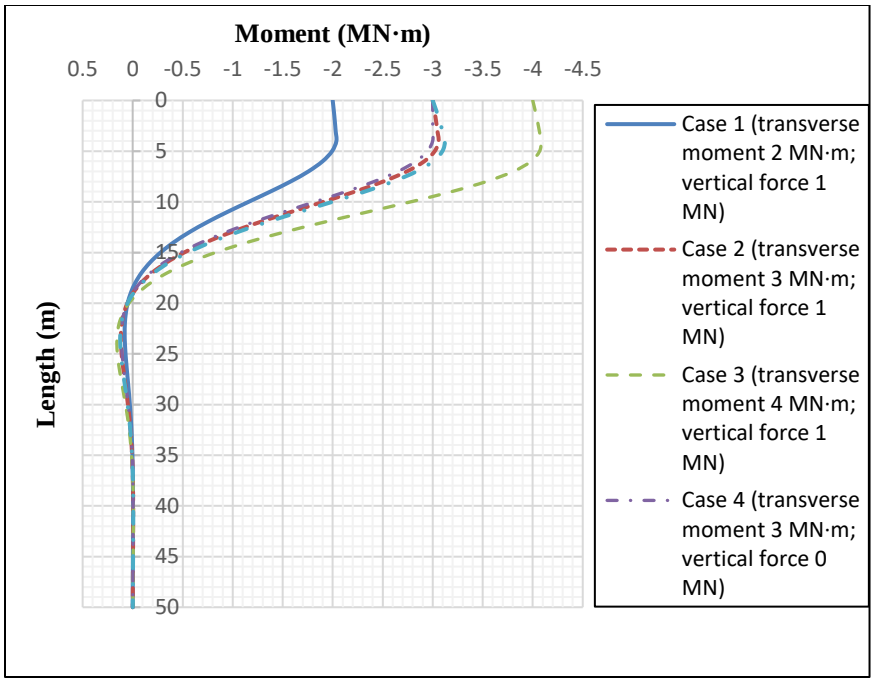

Figure 3-9: Moment

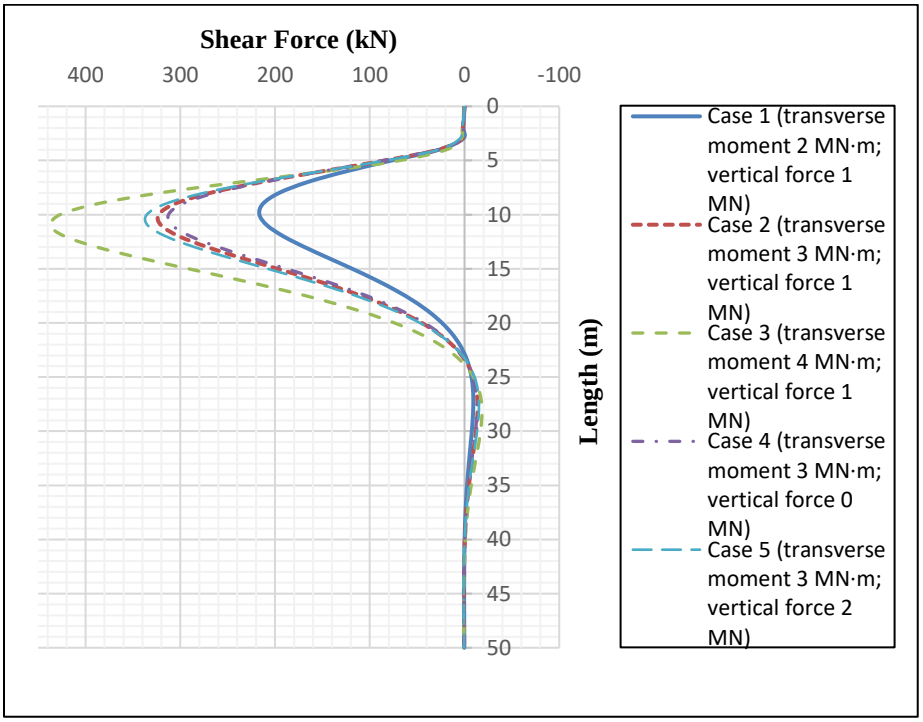

Figure 3-10: Shear force

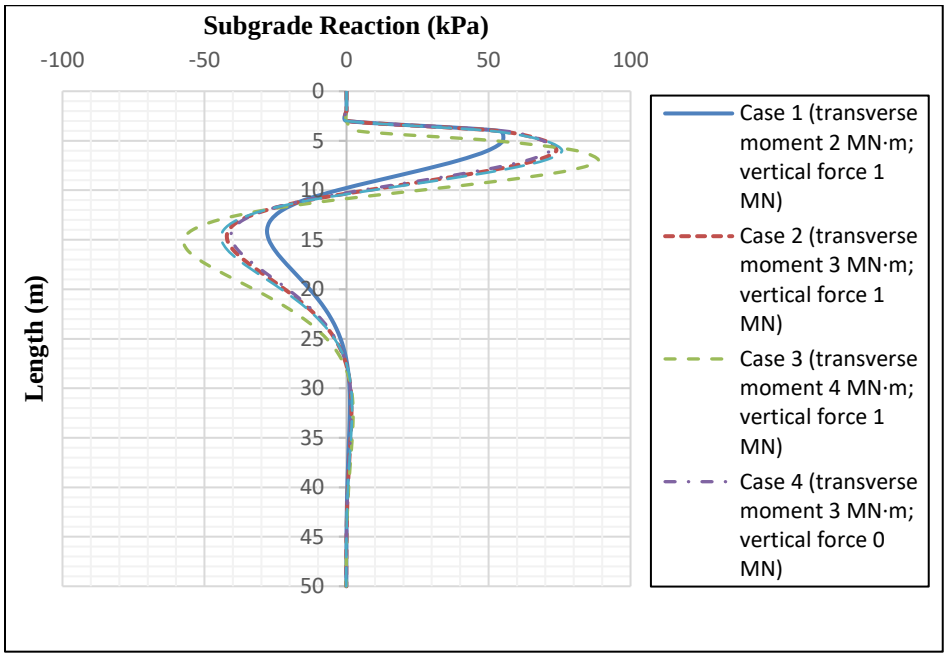

Figure 3-11: Subgrade reaction

3.7 Effects of the Distance between Mudline and Wellhead, Cement return Height and Type of Foundation

As shown in figure 3-12 and figure 3-13 analysis was performed on lateral load-bearing capacity of pipe string while changing the distance between mudline and wellhead, the return height of the cement sheath on the surface casing, and the type of the foundation (clayey soil or sandy soil). Where the assumptions of the sandy soil foundation are: from mudline to the depth of 100 meters below mud line, underwater bulk density as 10.0kN/m^3, internal friction angle as 30°, initial modulus as 14.7MN/m^3.

The results illustrate that the larger distance is between the wellhead and mudline, the greater transverse displacement and moment there will be. So scouring at the mudline has great effects on the lateral load-bearing capacity of the casing strings. Since relatively less contribution to the flexural rigidity of the combination pipe string has been made by the cement sheath, the return height of the surface casing does not have great effects on the transverse displacement and moment of the pipe string. When it is the sandy soil foundation, the transverse displacement and moment of the pipe string is smaller than those in the clayey soil foundation, meanwhile the length of the pipe being effected is also shorter (Guan et. al., 2009).

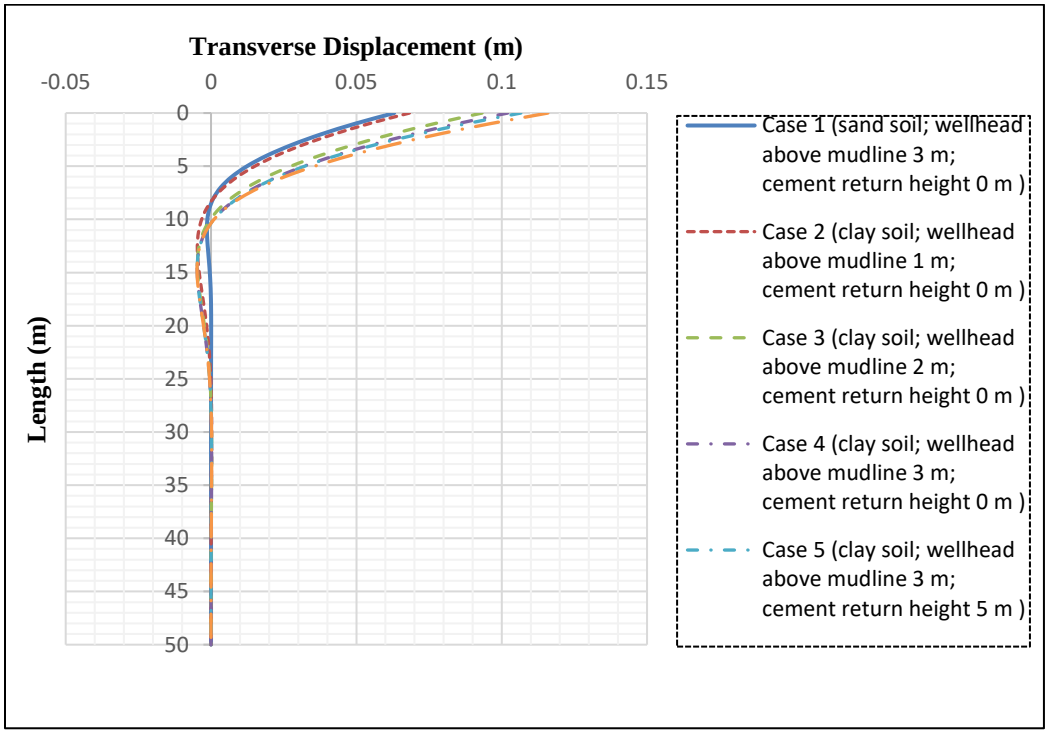

Figure 3-12: Transverse displacement

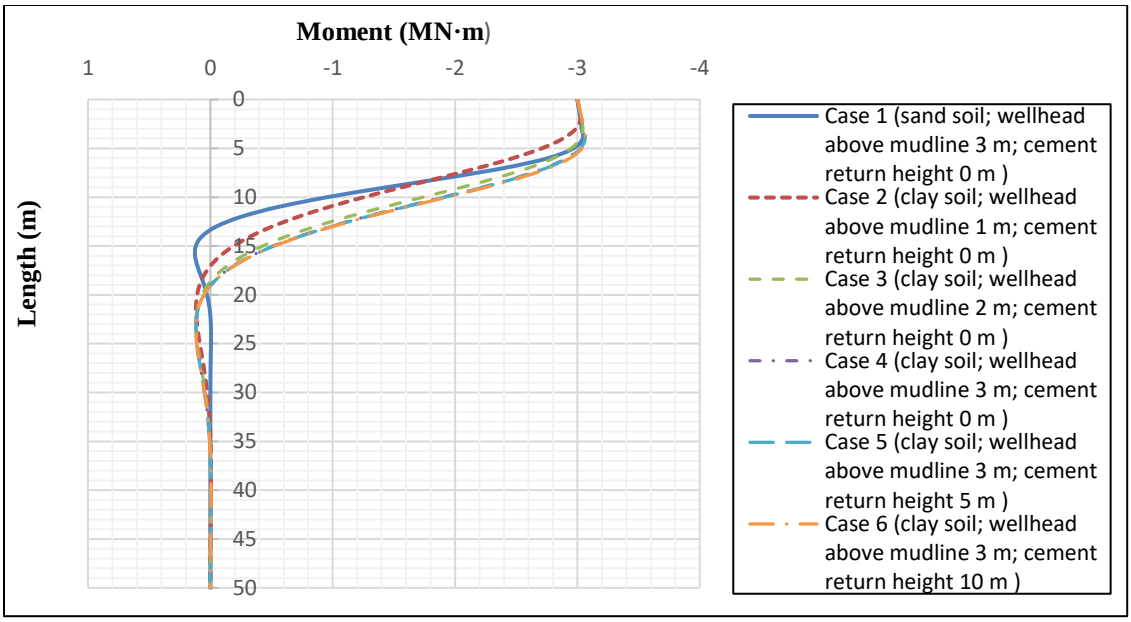

Figure 3-13: Moment

Distance between wellhead and mudline has relatively great effect on the lateral load-bearing capacity of the pipe string. Cementing sheath return height degree of the surface casing does not have great effect on the transverse displacement and moment of the pipe string while the type of the basement has some effects on the lateral load-bearing capacity of the pipe string.

Chapter 4

Development of Numerical Model for Fatigue Analysis

4.1 Overview

The fully coupled global analysis methodology is used in this thesis as shown in Figure 4-1. As the analysis is performed in shallow water, the response of the seabed soil-structure interaction is our main focus. In this study, the model stretches from the conductor to the upper flex joint. Environmental loads are applied to predict the riser behavior and the displacements of the conductor in the soil. By using this approach, it has been shown how the riser response and the wellhead are interdependent and also were impacted by seabed soil and cement levels. According to Jaiswal et al. (2016), the fully couple global model is the highest accurate numerical model of the drilling riser and wellhead system.

This thesis does not take into account the decoupled global model which entails the decoupling between the BOP and wellhead datum as shown in Figure 4-2. Jaiswal et al. (2016) in his paper gave an approach for the decoupled global model which entails replacing the local wellhead model by equivalent boundary conditions at the wellhead datum in the form of a combination of translational and rotational springs acting along *x* and *y* axes.

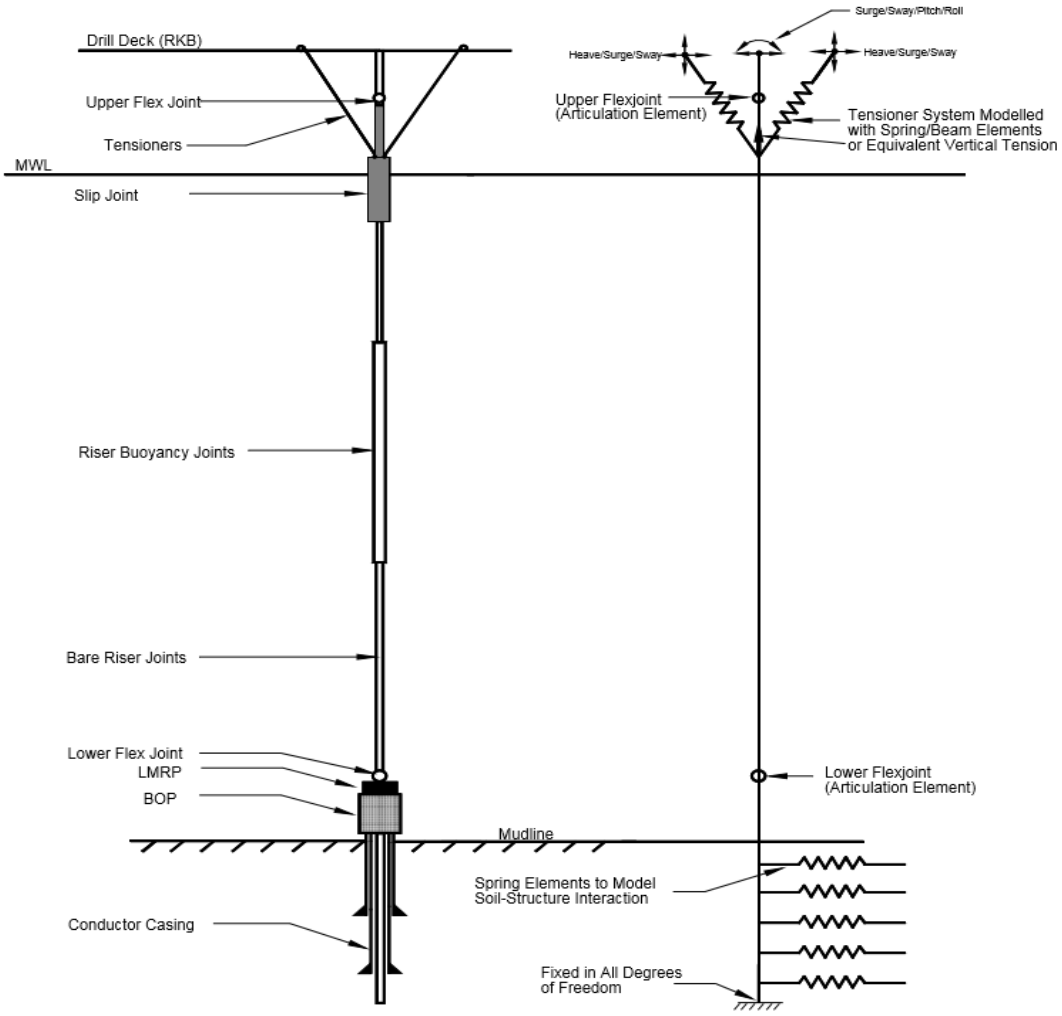

Figure 4-1: Drilling riser system configuration and coupled analysis models (ISO, 2010)

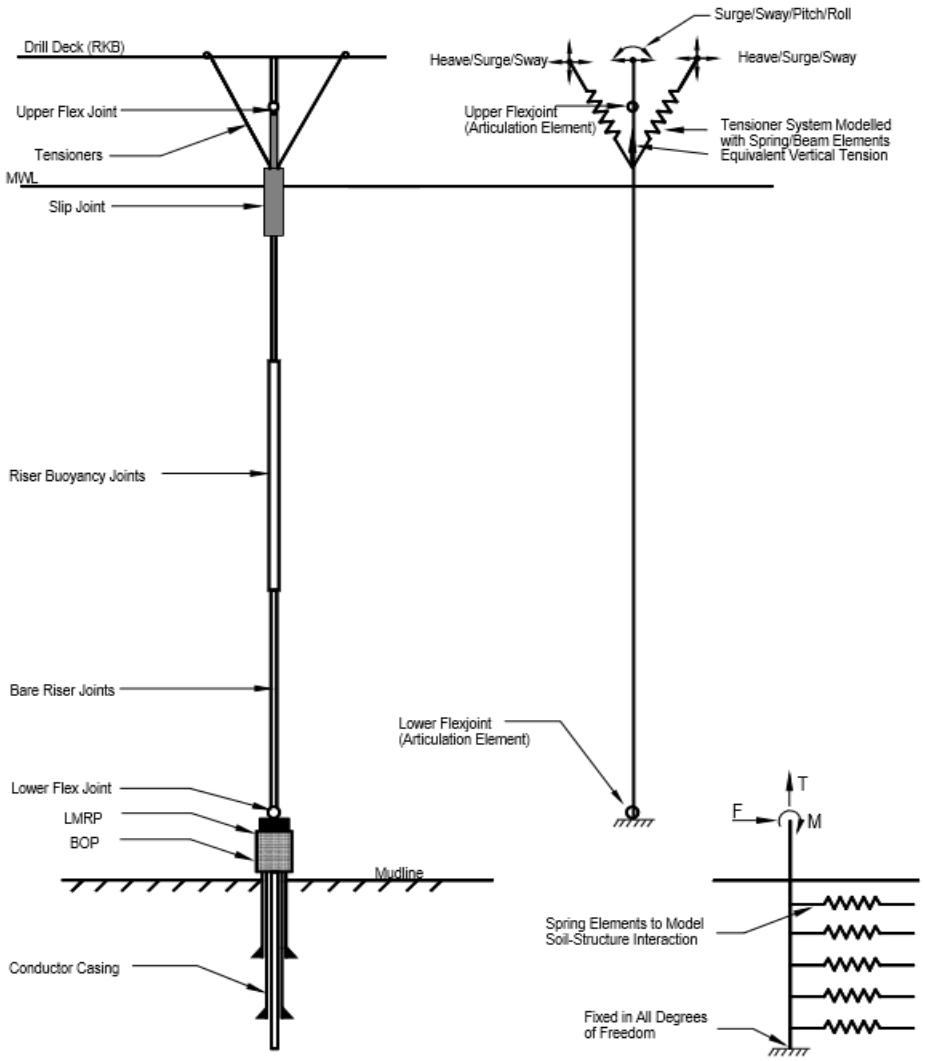

Figure 4-2: Drilling riser system configuration and decoupled analysis models (ISO, 2010)

4.2 Global Riser Model

A global load analysis, where the entire riser system is modelled, is performed using OrcaFlex software. The purpose of the global analysis is to obtain the bending moment at wellhead datum for all relevant sea states (i.e. waves) during the operation, hence, the results are strongly dependent on the environmental conditions. The global load analysis however, is performed in a coupled

manner with a lower boundary condition which involves the seabed soil. The main input parameters needed for the global riser analysis are given in this section.

The riser model comprises the lower and upper boundary conditions. The upper boundary consists of the vessel (MODU) which incorporates the diverter, tensioning systems and rotary table. The tensioner helps to minimize the MODU motion and excessive bending stresses under lateral wave, current and vortex shedding loads.

In OrcaFlex, the riser model is build up using lines, springs and buoys by using the graphical user interface in the program. This program has been used for the analysis of the wellhead on the seabed which is connected to the MODU by means of a top-tensioned riser.

In this model, the riser line starts at the Upper Flex Joint (UFJ) and ends at the wellhead. There is also a conductor casing which interacts with the seabed and it is our main focus in this study. The upper end of the riser is fixed at an elevation of 31.92 m above the mean water level (MWL) and supported by the tensioner system. There are four tensioners at elevation of 5.05m each with tension of 563.5 kN. The tensioners are modelled as springs with tension of 563.5 kN. The lower end of the riser is attached to the LMRP. The LMRP and BOP assembly are connected to the wellhead at the seabed through the spacer spool. The UFJ center of rotation is located at 27.5 m above MWL while the LFJ center of rotation is located 122.7 m below the MWL. The tensioners are connected to the tension ring (TR) located at 4.577 m above MWL. The UFJ is connected to the inner barrel also known as the slick joint which is positioned above the tensioner ring.

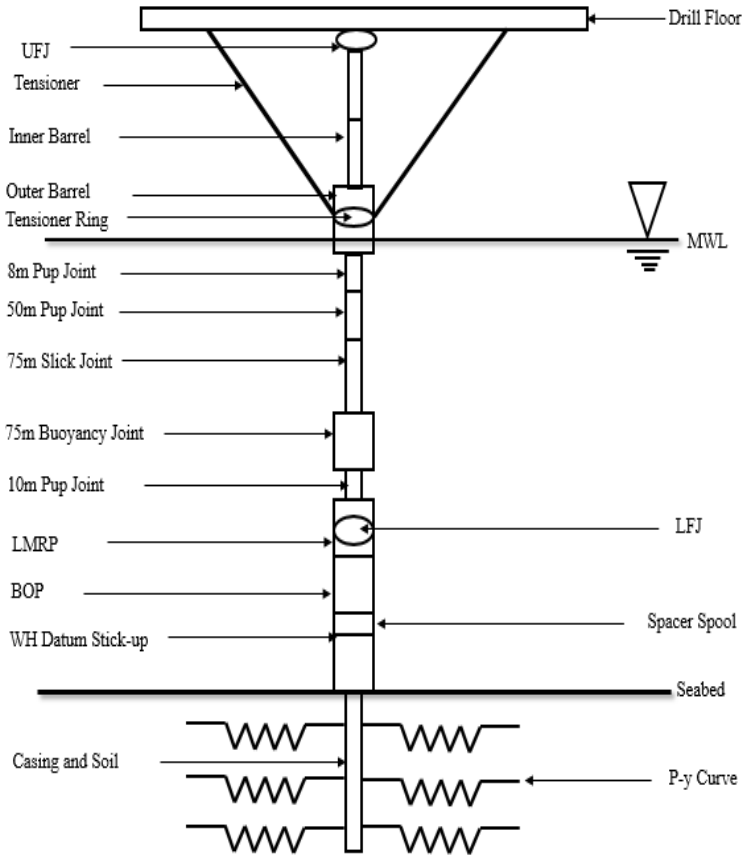

Figure 4-3: Schematic of riser stack-up and wellhead model created in OrcaFlex

The tensioner ring is modelled as a body with six degrees of freedom. In Orcaflex the body is represented as a 6D buoy and can transfer both moment and translation effects to and from the body to the connected lines. The main function of the 6D buoy is to act as a connection point for the tensioners since the springs cannot be connected to nodes on a line but can only be connected to end points. There is also a two pup joints that connects the outer barrel to the 23 m slick joint. Other components that make up the riser line are 23 m buoyancy joint and a 3 m pup joint connected between the buoyancy joint and the LMRP above lower flex joint (LFJ) center of rotation. The LMRP is fixed to the BOP. The lower packages (i.e., LMRP and BOP) are modelled

using cylindrical shapes in OrcaFlex with defined geometry (length, diameter etc.) A similar connection line (space spool) is also stretched from the BOP to the wellhead datum.

4.2.1 Drilling Riser Properties

The drilling riser stack-up and section properties are explained in this section. In addition to the riser, the model also has kill and choke lines which are fitted to the BOP stack. Note that the equivalent properties include the contribution of attached choke and kill auxiliary lines.

Table 4-1: Material properties for steel

Young's Modulus (E)	**Poisson's ratio (ν)**	**Density (Kg/m^3)**
210 GPa	0.3	7850

Table 4-2: Geometry and weight input for OrcaFlex

Section Description	Section Length (m)	Top End Elevation (m) from MWL	OD (m)	ID (m)	Dry Mass/Length (kg/m)
UFJ above rotation center	4.42	31.92	0.533	0.492	1778
UFJ below rotation center	1.922	27.5	0.533	0.492	1777
Slick Joint (SJ)-Inner barrel	7.833	25.578	0.533	0.492	893.7
SJ-above tension ring (TR)	12.695	17.745	0.66	0.61	1440
SJ-outer barrel &TR	0.946	5.05	0.66	0.61	15774
SJ-outer barrel btw TR & gooseneck	2.916	4.104	0.66	0.61	1440
SJ-outer barrel below gooseneck	6.556	1.188	0.66	0.61	1440
8m pup joint	7.62	-5.368	0.533	0.492	616.3
15m pup joint	15.24	-12.988	0.533	0.492	616.3
23m slick joint	45.72	-28.228	0.533	0.492	569.3
23m buoyancy joint	45.72	-73.948	1.235	0.492	963.8
3m pup joint	3.048	-119.668	0.533	0.492	1168
LMRP	6.472	-122.716	1.476	0.476	21951
BOP	6.664	-129.188	1.476	0.476	19817
Spacer spool	0.648	-135.852	1.476	0.476	6944

Table 4-3: Stiffness and hydrodynamic properties

Section Description	Bending Stiffness (Nm^2)	Axial Stiffness (N)	Torsional Stiffness (Nm^2)	Added mass Coeff-Normal	Drag Coeff-Normal	Drag Diameter (m)	Stress Diameter (m)
UFJ above rotation center	2.25E+08	6.84E+09	1.73E+08	1.1	1.0	0.53	0.533
UFJ below rotation center	2.25E+08	6.84E+09	1.73E+08	1.1	1.0	0.53	0.533
Slick Joint (SJ)-Inner barrel	2.24E+08	1	1.73E+08	1.1	1.0	0.53	0.533
SJ-above tension ring (TR)	5.24E+08	1.04E+10	4.03E+08	1.1	1.0	0.66	0.66
SJ-outer barrel &TR	5.24E+08	1.04E+10	4.03E+08	1.1	1.0	0.66	0.66
SJ-outer barrel btw TR & gooseneck	5.24E+08	1.04E+10	4.03E+08	1.1	1.0	0.66	0.66
SJ-outer barrel below gooseneck	5.24E+08	1.04E+10	4.03E+08	1.1	1.0	0.99	0.66
25ft pup joint	2.24E+08	6.82E+09	1.73E+08	1.1	1.0	0.86	0.533
50ft pup joint	2.24E+08	6.82E+09	1.73E+08	1.1	1.0	0.86	0.533
75ft slick joint	2.24E+08	6.82E+09	1.73E+08	1.1	1.0	0.86	0.533
75ft buoyancy joint	2.24E+08	6.82E+09	1.73E+08	1.1	1.0	1.235	0.533
10ft pup joint	2.24E+08	6.82E+09	1.73E+08	1.1	1.0	0.86	0.533
LMRP	4.72E+10	3.14E+11	3.63E+10	1	1.0	4.67	1.476
BOP	4.72E+10	3.14E+11	3.63E+10	1	1.0	4.67	1.476
Spacer spool	4.72E+10	3.14E+11	3.63E+10	1	1.0	4.67	1.476

4.2.2 Conductor, Surface Casing and Cement Properties

The properties of the conductor and surface casings and the cement are presented in Table 4-4. The annular space between the conductor and the surface casing is cemented from the casing bottom at 186.5m below the MWL to 10m below the seabed.

Table 4-4: Conductor, surface casing and cement properties

Description	**Conductor**	**Surface Casing**
Outer diameter (m)	0.7620	0.5364
Inner diameter (m)	0.7366	0.5031
Length (m)	48.3687	48.4042
Bending Stiffness (Nm^2)	1.76E+06	1.93E+05
Axial Stiffness (N)	6.28E+06	5.69E+06
Cement		
Density (kg/m^3)	2400	
Young's Modulus (N/m^2)	3.50E+09	
Poisson ratio	0.1	

4.3 Soil Model

Presently, many software tools that are available for the global analysis of riser-conductor systems make use of the Winkler Springs to model soil behavior. This section attempts to investigate the accuracy of the different soil models in wellhead fatigue analysis. A literature review has been conducted to review the basis for the API springs, and alternative P-y curves as proposed by

Jeanjean (2009) and Zakeri et al (2015). Other soil models, namely original Matlock and Gmax (Gregersen et al, 2017), were reviewed and implemented in the global analysis to demonstrate the effect of soil stiffness in wellhead fatigue analysis.

Matlock-API soil model is the industry standard approach used in modelling soil response for piles also known as backbone P-y curves. The P-y curves was originally developed by Matlock for ultimate limit state design of pile foundations for steel jacket subjected to monotonic or cyclic storm or hurricane loading. It has been shown both experimentally and numerically to be too soft at a small displacement required for the estimation of fatigue. Fatigue, however, occur as a result of stress changes and are often well below the elastic yield stress of a typical conductor which corresponds to smaller soil deformation (Russo et al, 2016). As such, a reliable soil P-y model was proposed for accurate conductor fatigue analysis which led to determination of a more appropriate stiffness by considering the unload-reload stiffness (secant stiffness) of the soil once steady state conditions are reached. A vital aspect of developing P-y springs with the FE method is to develop a representative soil model for riser-conductor problems. Monotonic backbone P-y curves were obtained from series of tests at different depths as shown in Figure 4-4. The P-y curves developed with the FE approach are compared with API recommendations.

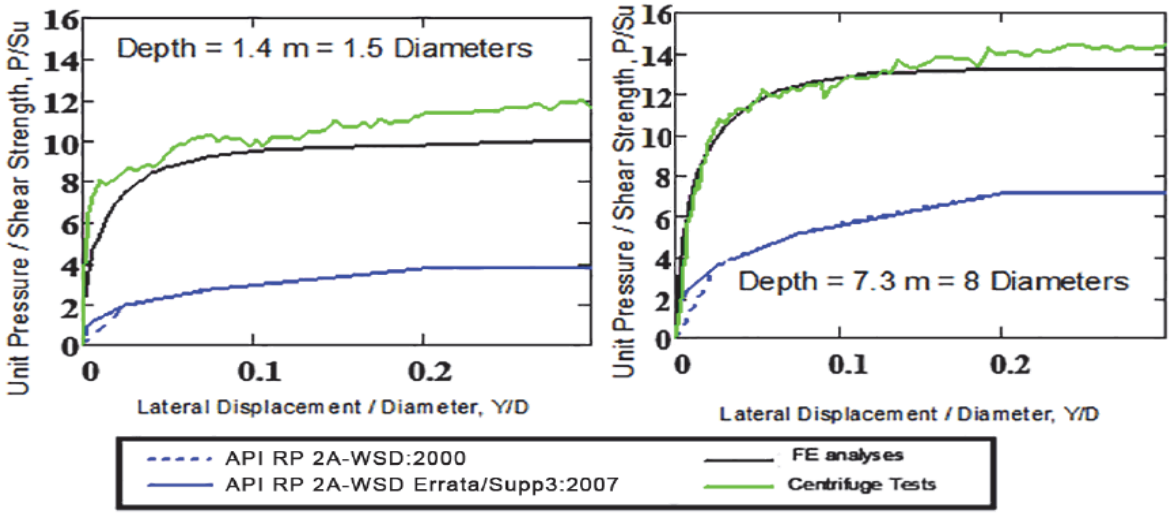

Figure 4-4: Comparison between p-y springs measured in centrifuge tests on kaolinite and computed using the FEA method with API recommendation (API, 2011)

Jeanjean (2009) also conducted some studies and deduced that the application of backbone curves for fatigue analysis is not appropriate. Jeanjean (2009) then developed a more robust soil model for well conductor analysis. This model was developed specifically to improve the initial soil stiffness modelling and its effects on fatigue performance and was verified by extensive physical testing in a geotechnical centrifuge and numerical analyses. It was shown both numerically and experimentally that the API lateral soil springs are too soft at small displacements needed for wellhead fatigue assessment. In addition, the proper characterization fatigue should not be based on the backbone response. Jeanjean's model is stiffer than Matlock API and gives a robust soil model for wellhead fatigue analysis (Gregersen et al, 2017).

According to Jeanjean (2009), the relative soft soil reactions (soil springs) will lead to deeper penetration below the mudline resulting in maximum bending moment range while relative stiffer soil leads to the maximum bending moments range shifting closer to the mud line.

A new empirical equation (Eq. 4.1) was proposed from the equation inspired by O'Neil et al (1990) for P-y curves in stiff clay and the shape of the FEA-generated backbone curve has been fitted as shown in figure 4-5:

$$P = N_p . S_u . \tanh\left[\frac{G_{max}}{100.S_u}\right] . \left(\frac{y}{D}\right)^{0.5} \quad (4.1)$$

where,

P is the soil pressure per unit length of conductor

G_{max} is the maximum soil shear modulus

N_p is the bearing capacity factor

S_u is the shear strength

$\frac{y}{D}$ is the lateral displacement, y, over pile diameter, D

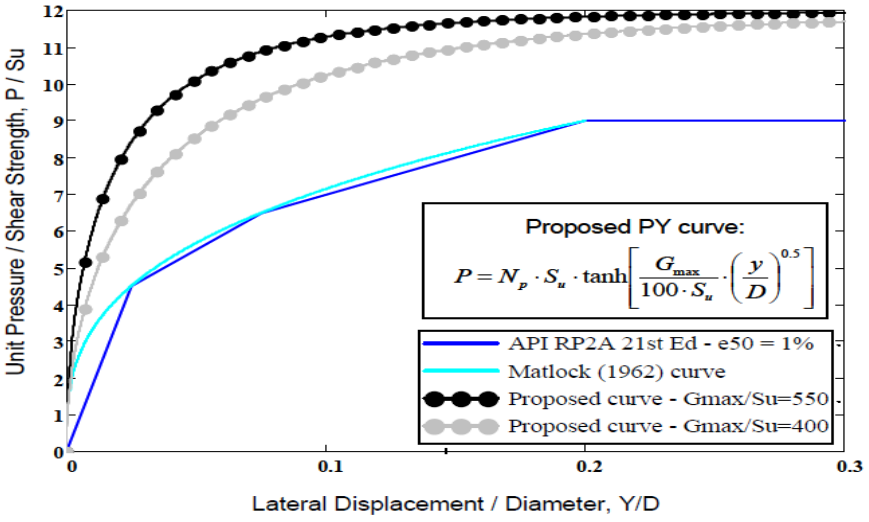

Figure 4-5: P-y curves as per equation 4.1, compared with API and Matlock curves for large embedment depths (Jeanjean, 2009)

The work conducted by Jeanjean (2009) also inspired Zakeri et al. (2015) to develop a model which focuses on the degraded cyclic soil response behavior. Soil degradation occurs during the high sea state affecting the well and BOP response after high loading is finished. The Zakeri et al. (2015) model exhibited stiffer response at small displacement and was validated by extensive centrifuge test and corresponding numerical analyses. The approach outlined by Zakeri et al. is based on the unload-reload stiffness of disturbed soil (degraded soil response) at the steady-state condition and was specifically developed for well conductor fatigue analysis. This model provides a more accurate fatigue life predictions than API soil P-y models since it has a higher initial stiffness and forms the basis for the development of soil constitutive P-y models for implementation into numerical analysis.

A simplified approach was developed based on the degraded soil secant stiffness at the steady-state condition and is recommended for both global and local analyses for normally to lightly over-consolidated clays and for medium-dense sands. The soil pressure per unit length of conductor, P, at each spring location is estimated using the equation below as proposed by Zakeri et al. (2015)

For normally to lightly over-consolidated clays, Eq. (4.2) is used

$$P = 0.5 \times 0.90 \times \tau \times (\frac{y}{D})^{-0.05} \quad (4.2)$$

For medium-dense sands, Eq. (4.3) is used:

$$P = 0.5 \times 730 \times \tau \times (\frac{y}{D})^{0.65} \quad (4.3)$$

The 5Gmax Model has also been considered in this paper and was proposed as a simplified estimate of the initial stiffness corresponding to five times the maximum shear modulus in clay. The minimum displacement has been estimated based on the lateral pressure from Matlock-API

and the displacement has been calculated based on an initial stiffness of 5Gmax (Gregersen et al, 2017).

Based on the laboratory test and field testing with CPT to determine the geotechnical properties of the soil in the well vicinity; soil P-y models were developed for the conductors installed in normally consolidated to lightly overconsolidated clays.

4.3.1 Selection of Soil Parameters

The soil model forms the lower boundary condition and it is an important part of the model since the focus is on the well conductor-soil interaction. The lower boundary condition is considered to be at the wellhead datum. The interaction between the soil and the casing system will have impact on the fatigue performance of the wellhead.

There are a different techniques for modelling the soil-structure interaction as a boundary condition in the global analysis method. These methods are summarized below as per DNV (2015).

In order to describe the lateral soil-structure interaction, P-y curves are used and a series of non-linear springs are created from the curves and attached to the well conductor. This is illustrated in figure 4-6. Each soil layer has distinct properties which are represented with different spring.

The spring stiffness can be defined using the equation below:

$$K = K_{soil}.\Delta z \tag{4.4}$$

where,

K is the spring stiffness

K_{soil} is the stiffness of the soil layer

Δz is the height that the spring support

There are various techniques for modelling the soil-structure interaction as a boundary condition in the global analysis method per DNV (2015):

- set of non-linear lateral springs along the length of the conductor casing
- set of linearized lateral spring along length of the conductor casing
- equivalent wellhead stiffness beam model (as per ISO 13628-7) to represent compliance of soil/conductor interaction
- equivalent lateral and rotational springs applied at a reference elevation (i.e. mudline)
- point of fixity at some depth below mudline

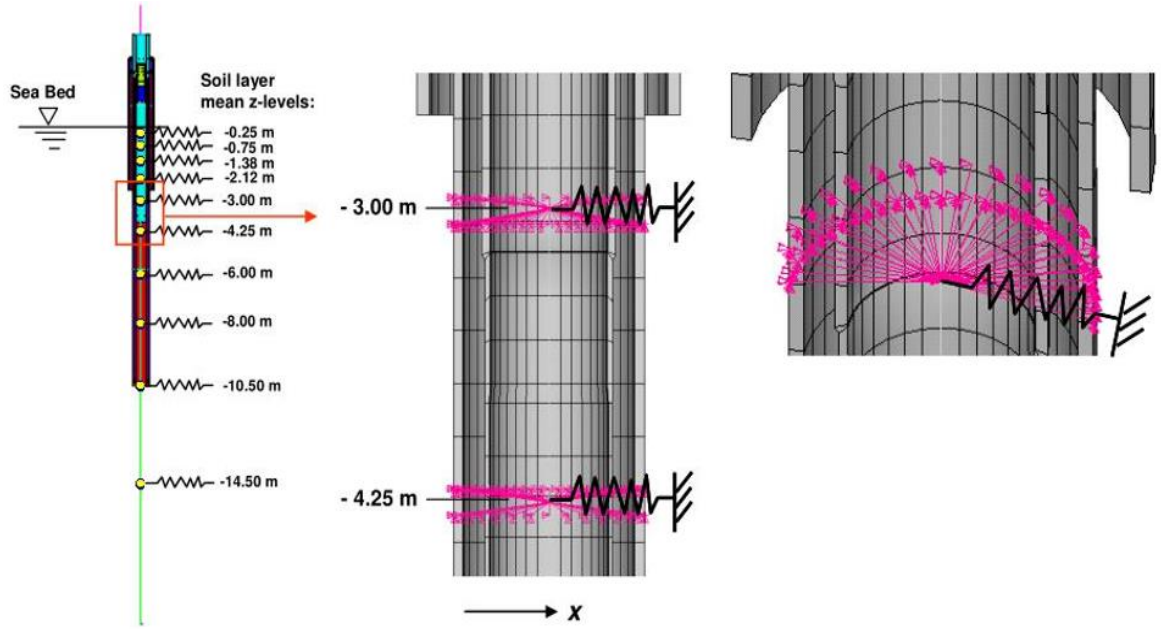

Figure 4-6: Example of non-linear springs that represent the lateral soil support of the well (DNV, 2011).

Gregersen et al. (2017) presented plots of a series of soil model obtained from different authors. The study was carried out to validate the soil models for wellhead fatigue analysis. The P-y curve

plots as obtained by Gregersen et al. (2017) was implemented in the numerical models as non-linear springs attached to discrete locations.

In this analysis, the focus will be on the most popular soil models namely: Matlock API, Jeanjean and Zakeri et al. (2015). The soil model for original Matlock and Gmax will not be compared since their stiffness are very close to that of Matlock API and gives nearly same results with negligible variations.

Figure 4-7 shows the P-y curve stiffness for the different proposed soil models. From Figure 4-7, it can be observed that Matlock API has the lowest lateral stiffness, followed by original Matlock soil model. 5Gmax and Jeanjean (2009) soil formulations have similar stiffness, with slight variation over depth, while Zakeri et al. (2015) has the highest lateral stiffness. Figures 4-8 and 4-9 present the P-y curves for each of the five models for both large and small displacements.

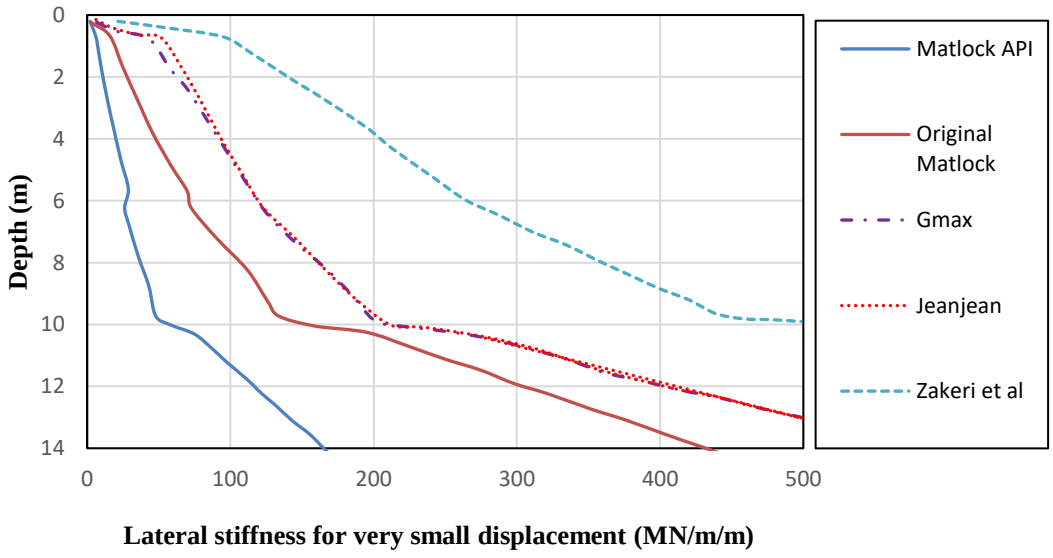

Figure 4-7: P-y curve stiffness (Gregersen et al, 2017)

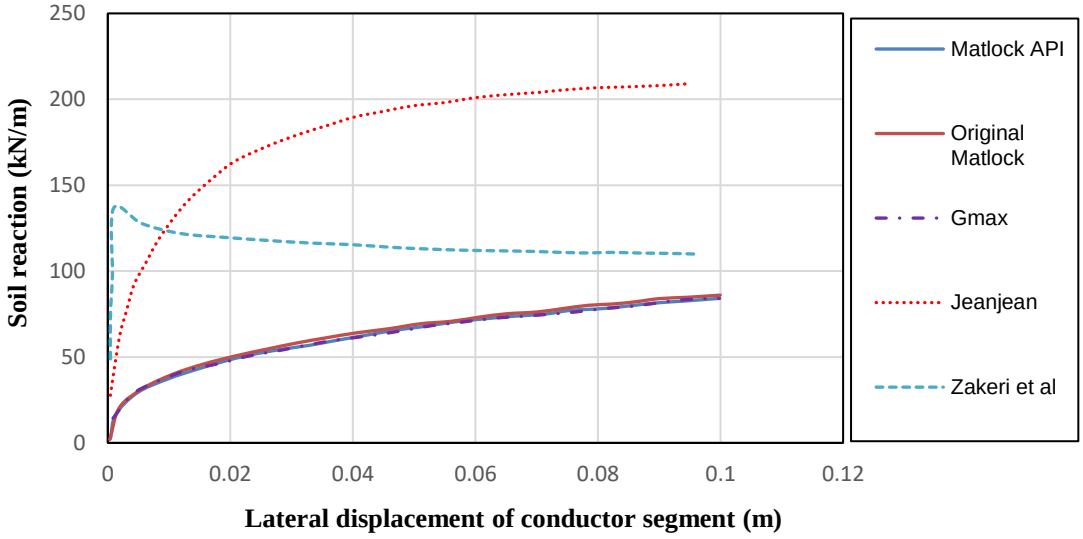

Figure 4-8: P-y curve for large displacement (Gregersen et al, 2017)

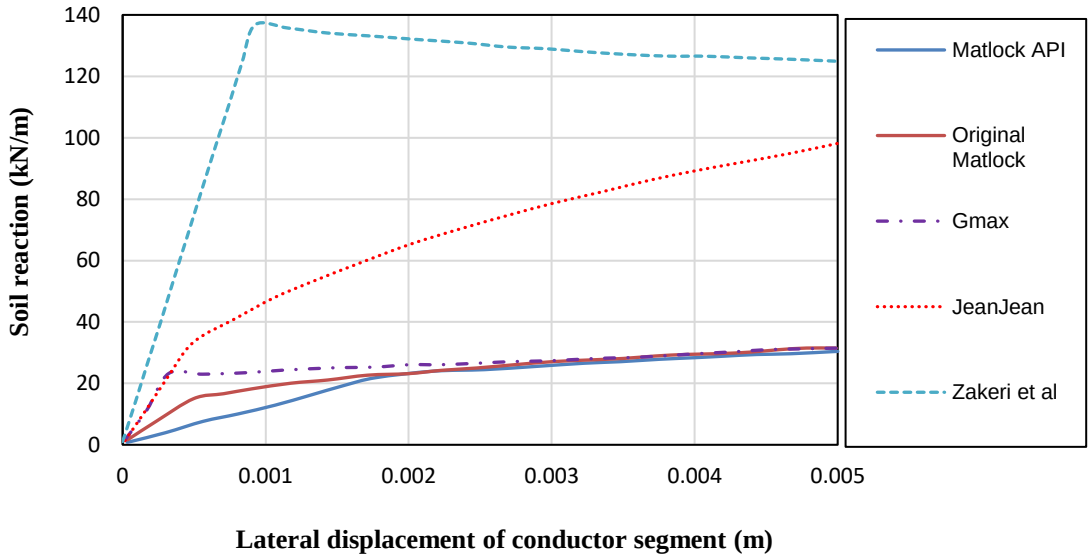

Figure 4-9: P-y Curve for small displacements (Gregersen et al, 2017)

4.4 Verification of Numerical Model

Jaiswal et al. (2016) performed a fatigue analysis for non-rigid locked wellhead using Abaqus software and obtained results for the modal analysis by performing both local and global analyses on the wellhead system. Similar results have been obtained in this thesis for the modal analysis by performing only the global riser analysis using OrcaFlex software. The results of the natural period obtained from OrcaFlex was compared with that obtained by Jaiswal et al. (2016). Table 4-5 shows the results of the natural period for the first two modes. Figure 4-10 and Figure 4-11 show the mode shapes for mode 1 and mode 2 respectively as obtained in the study.

Table 4-5: Natural period for the first two modes

Natural Period (s)		
Mode no	OrcaFlex	Jaiswal et al. (2017)
1	8.61	8.85
2	4.54	4.21

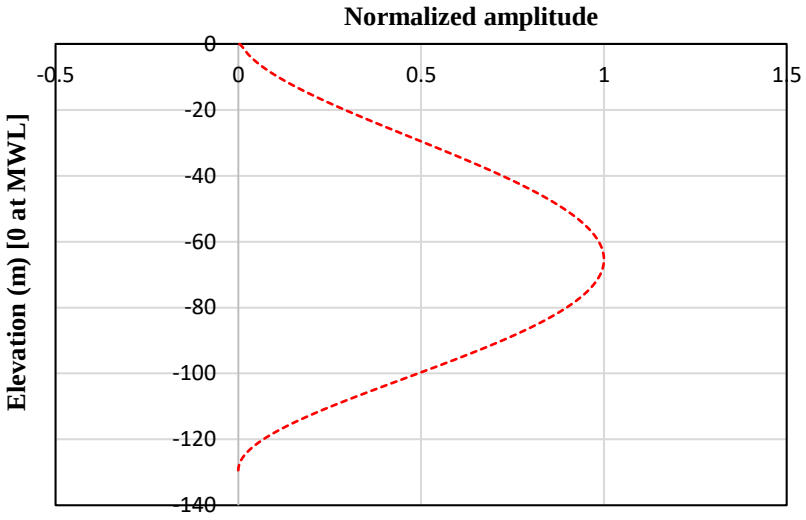

Figure 4-10: First mode shape

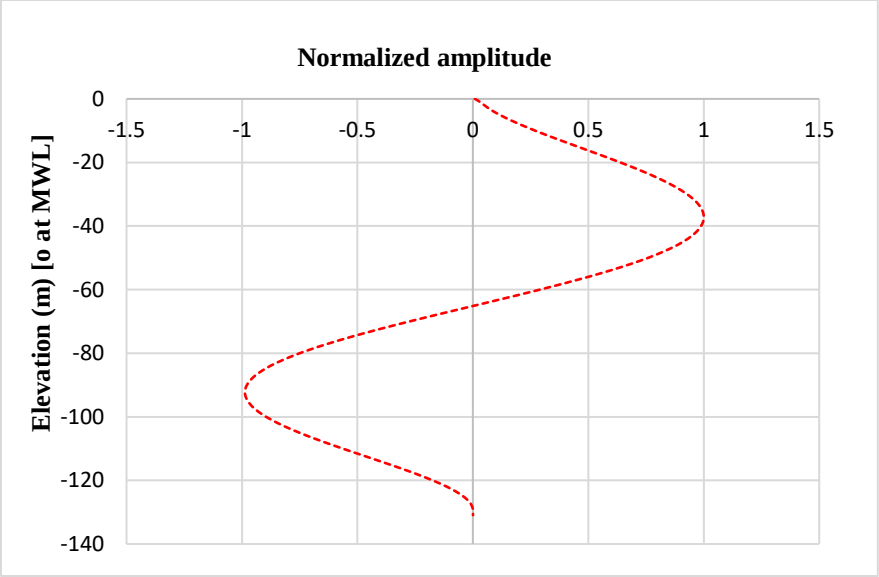

Figure 4-11: Second mode shape

4.5 Environmental Load

The environmental data consist of the sea current, waves and wind in which the drilling riser is subjected during drilling operation. The data used in calculations and as input for the environment are OrcaFlex is presented in this section.

4.5.1 Water Information

The sea data used in this analysis is given in Table 4-6

Table 4-6: Sea data

Parameter	Value
Water density (kg/m^3)	1025
Water depth (m)	140
Water temperature (^{o}C)	10
Kinematic viscosity (m^2/s)	1.35E-06

4.5.2 Waves

The global analysis is run with head sea, significant wave height (*Hs*) and peak spectral period (*Tp*). JONSWAP spectra is used to describe the irregular wave motion. The Pierson-Moskowitz (PM) spectrum and JONSWAP spectrum are frequently applied for wind seas. The PM spectrum was originally proposed for fully-developed sea. The JONSWAP spectrum is an extension of the PM spectrum with other features including fetch limited seas, describing developing sea states. Both spectra describe wind sea conditions that often occur for the most severe sea states (DNV-RP-C205).

The JONSWAP spectrum is expected to be a reasonable model for:

$$3.6 < \frac{T_p}{\sqrt{H_s}} < 5 \qquad (4.5)$$

where,

T_p is the peak spectral period measured in seconds

H_s is the significant wave height measured in meters

The effect of the peak shape parameter, γ for H_s = 4.0 m and T_p = 8.0 s is shown in Figure 4-12 below. In OrcaFlex, the zero crossing period (T_z) if not given is automatically calculated if T_p is known and vice versa.

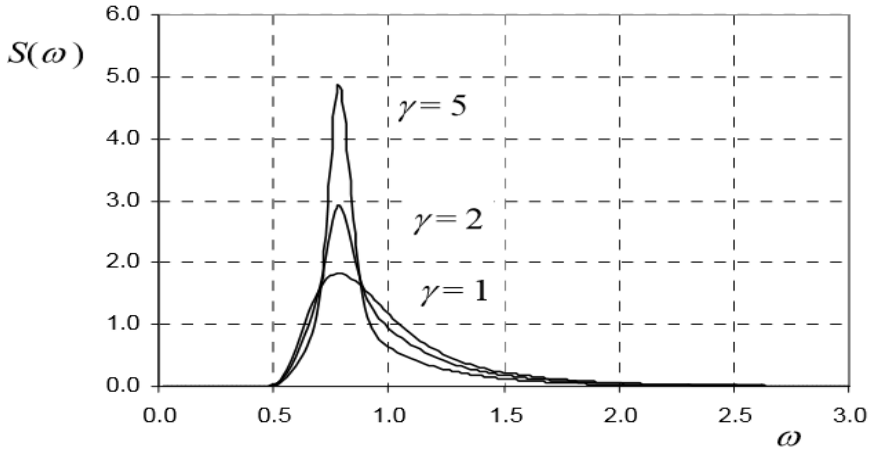

Figure 4-12: JONSWAP spectrum (DNV-RP-C205).

Sea states used in this analysis are within the reasonable JONSWAP model and are shown in Table 4-7. The wave period has a significant effect on the response of the riser and that of the wellhead/casing fatigue damage. However, when the wave period coincides with the natural periods of the vessel there tend to be increase in dynamic response due to possible excitation of resonant response. A typical dynamic response that occurs at different wave periods are summarized below as DNV (2015)

- Rig motion
- Excitation of the riser mode
- Excitation of wellhead/casing-lower package sub-system mode

Table 4-7: Significant wave height and corresponding peak and zero-crossing periods

Sea state	Hs (m)	Tp (s)	Tz (s)
1	6.5	8.5	6.04
2	7	11.2	9.85

4.5.3 Current

The effects of currents have been considered in the wellhead analysis. The current profile is randomly selected in OrcaFlex. Neglecting current may not always overestimate dynamic wellhead loads, as such, careful consideration should be taken in selecting appropriate current profiles (DNV, 2015).

The following vital points are to be noted:

- Currents will give rise to drag and lift forces on submerged structures, hence the amount of drag loading experienced along the length of the riser system may likely affects the fatigue response of the wellhead/casing system
- Current can cause vortex induced vibrations (VIV) on the riser
- Current can create seabed scouring around bottom mounted structures
- The interaction between high currents and waves will cause change in wave height and wave period
- Current can cause slow drift motions of moored platforms

4.6 Modal Analysis

The dynamic structure of the riser is determined using eigenfrequencies and mode shapes. The goal of modal analysis is to determine the natural mode shapes and frequencies of the structure

during free vibration. The physical interpretations of the eigenvalues and eigenvectors which come from solving the system are that they represent the frequencies and corresponding mode shapes. Sometimes, the only desired modes tend to be the lowest frequencies because they can appear to be the most prominent modes at which the object will vibrate, dominating all the higher frequency mode. Hence, the higher the mode, the higher the frequency resulting in higher damage and vice versa.

Modal analyses are computed for the different soil models and the results of the first five natural mode shapes and natural periods are presented below:

Table 4-8: Natural periods

Natural Period (s)					
Mode #	**Matlock-API**	**Original Matlock**	**5Gmax**	**Jeanjean (2009)**	**Zakeri et al. (2015)**
1	8.766	8.765	8.766	8.768	8.768
2	3.263	3.264	3.263	3.266	3.267
3	1.671	1.672	1.671	1.678	1.677
4	1.002	1.003	1.002	1.005	1.005
5	0.69	0.69	0.69	0.693	0.692

4.7 Modelling Program (Parametric and Sensitivity Studies)

4.7.1 Effects of Waves

Subsea wellhead are generally exposed to fatigue due to environmental loading such as waves which implies cyclic loading to the wellhead. A set of simulation files that model the riser system under different load conditions that the system will experience in its lifetime was conducted. The Regular motion analysis is useful for parametric studies but is not as realistic as the irregular wave

environment. To simulate the effect of wave, a sinusoidal horizontal displacement of constant amplitude and period at upper end of the drilling riser was applied. In this analysis, three load cases were considered as shown in Table 4-9.

Table 4-9: Regular sea parameter

Load Case	Hs (m)	Tp (s)
1	0.6	2.7
2	0.6	4.7
3	0.6	9.1

The wave used is Airy wave and are specified in terms of height, period and direction of propagation. A wave direction of 180 degree has been considered in the analysis meaning that the wave is travelling in the negative x-direction. All calculations are performed in the time domain.

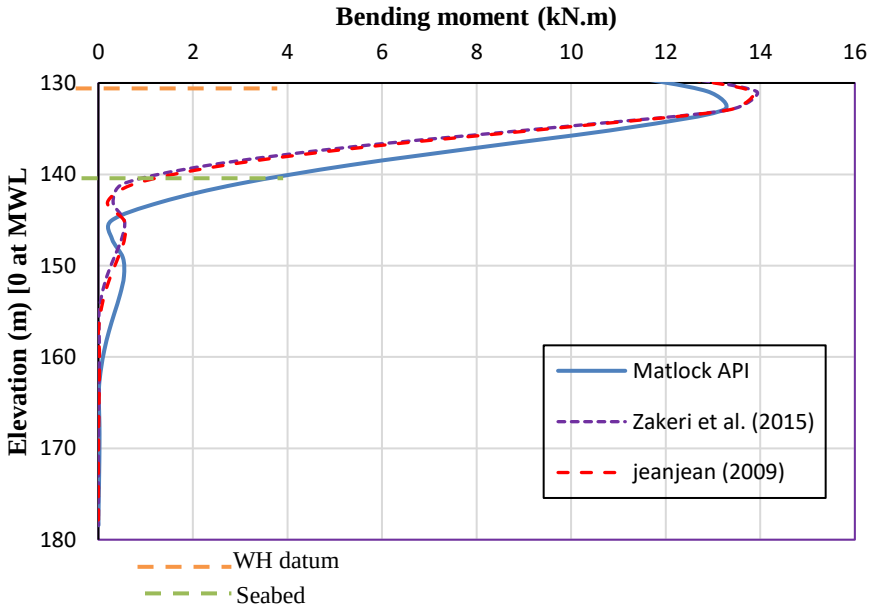

Figure 4-13: Wellhead bending moment at sea state 1 (Hs = 0.6m, Tp = 2.7s)

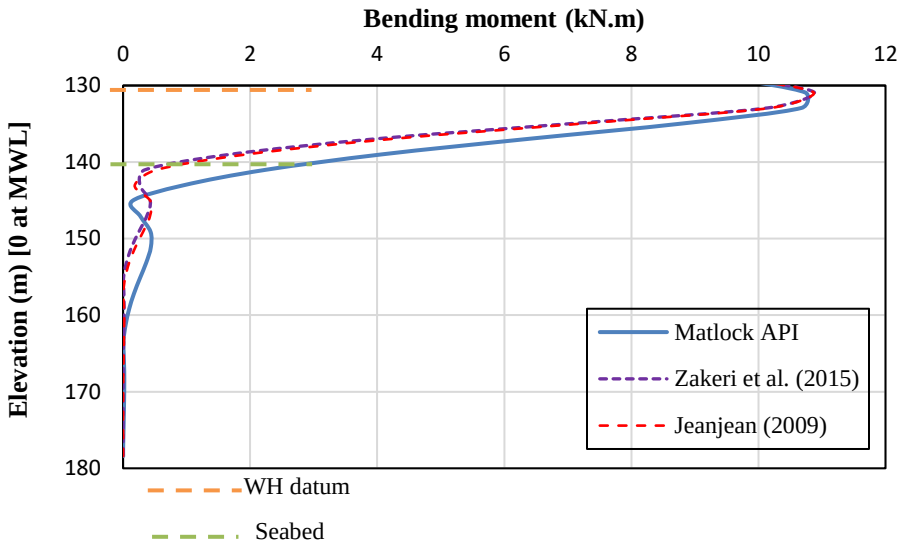

Figure 4-14: Wellhead bending moment at sea state 2 (Hs = 0.6m, Tp = 4.7s)

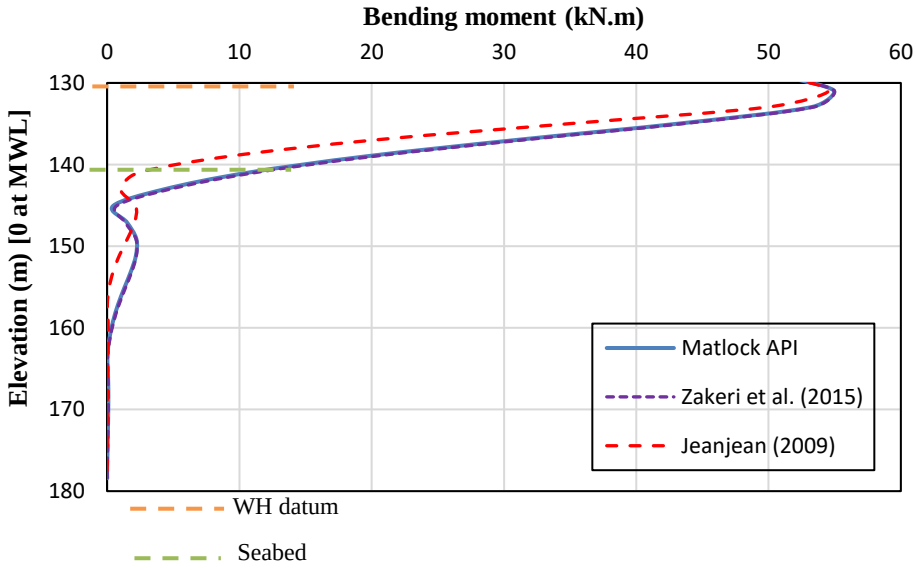

Figure 4-15: Wellhead bending moment at sea state 3 (Hs = 0.6 m, Tp = 9.1 s)

4.7.2 Effects of Current

The estimated wellhead fatigue life is also influenced by the current. The effects of the current was carried out as part of the parametric studies and was simulated for the different soil models in order to assess the relative difference in terms of estimated fatigue damage for the different soil models. It is worthy of note that currents in deep-waters are in general more strong than in shallow-water areas. These studies considered shallow water of depth 140m. Apparently, the current also generated load on the entire riser systems which in turn will impact on the wellhead. The currents influence the drag force and the drilling riser must be able to withstand the impact of large currents. Three different current speeds were considered in this thesis. The data used for this analysis are consistent with the extreme values for one year Omni-directional distributions at the Troll field taken from the metocean report for the StatoilHydro, 2009 Field (Stokvik, 2010). These numbers are said to be high and may not correspond with the reality. In this case, a smaller constant current can also be applied as presented in this work. A current direction of 180 degree was considered. The direction implies that the current is travelling in the negative x-direction.

Global response analysis was conducted to investigate the effects of current. Three cases were considered as shown in Table 4-10.

Figure 4-16 to 4-18 showed the shear forces of the wellhead at different current speed.

Table 4-10: Load Case for Current

Load Case	Speed (m/s)
1	0.72
2	1.25
3	1.55

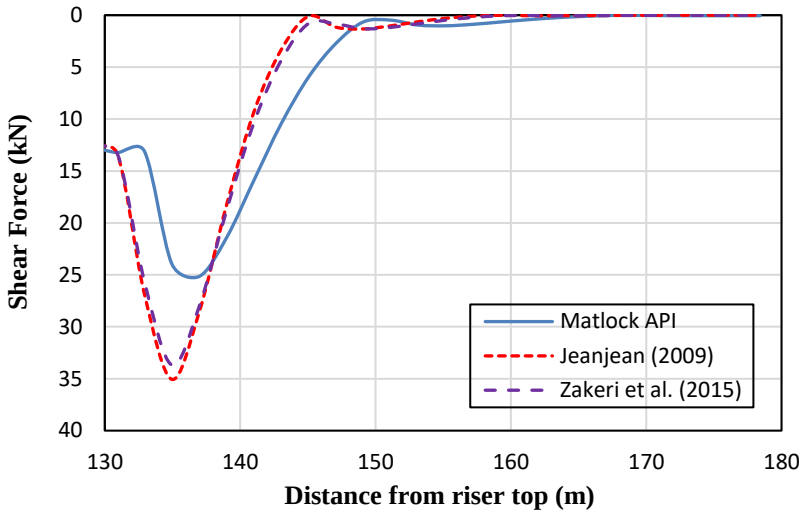

Figure 4-16: Wellhead shear force at current speed = 0.72m/s

The shear force generated from the different speeds for the three different soil models have been compared. The results showed that the current affects the riser response as shown in the shear force diagram. In Figure 4-16, it can be seen that the shear force at location of the wellhead for Matlock API is 14.5 kN and that of Jeanjean (2009) and Zakeri et al. (2015) models are found to be 13.3 kN and 12.7 kN, respectively. Hence, a higher shear force is obtained when using Matlock API while a lower shear force is obtained using Jeanjean (2009) and Zakeri et al. (2015).

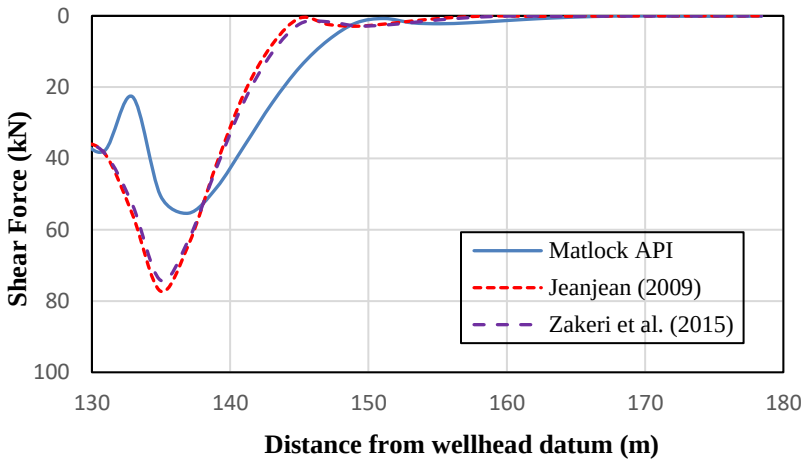

Figure 4-17: Wellhead shear force at current speed = 1.25m/s

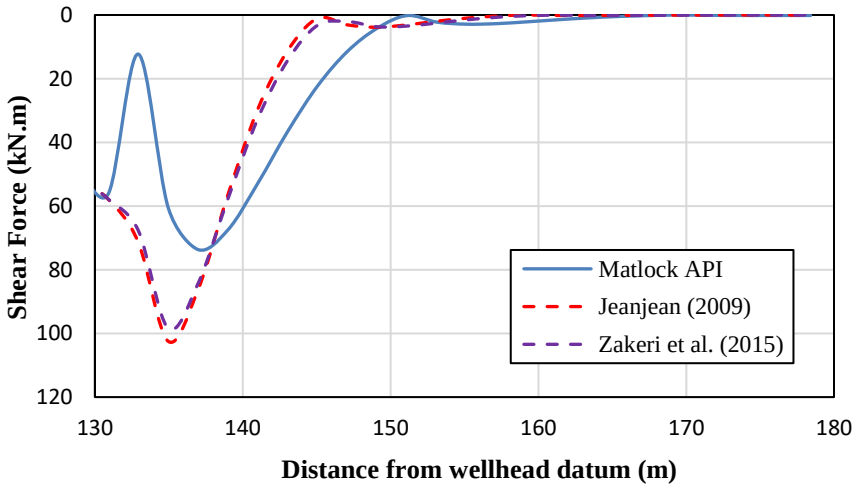

Figure 4-18: Wellhead shear force at current Speed = 1.55m/s

High current also affects the wellhead shear force as observed in Figure 4-18. The higher the current the higher the shear force and vice versa. Current will normally have impact on the subsea wellhead which will also contribute to fatigue failure of the wellhead.

4.7.3 Water Depth Sensitivity Analysis

Water depth sensitivity was performed in order to calculate the fatigue life for a 25 years period for varying water depth. The objective of this studies is to quantify the relative change in fatigue damage in the subsea wellhead over a range of water depths and proposed soil models. The minimum fatigue lives at the wellhead region for varying water depths are also summarized as shown in Table 4-11.

Table 4-11: Fatigue life for varying water depths

Soil Models	**Life (years)**		
	100m	200m	300m
Matlock API	15.9	22.8	29.7
Jeanjean (2009)	18.7	25.2	33.5
Zakeri et al. (2015)	20.8	24.9	33.1

The results of the analysis showed that, the fatigue damage in the wellhead decreases as the water depth increases. The plots of the fatigue damage per 25 years and fatigue life for the varying depths for the different soil models are presented in the Figure 4-19, Figure 4-20 and Figure 4-21.

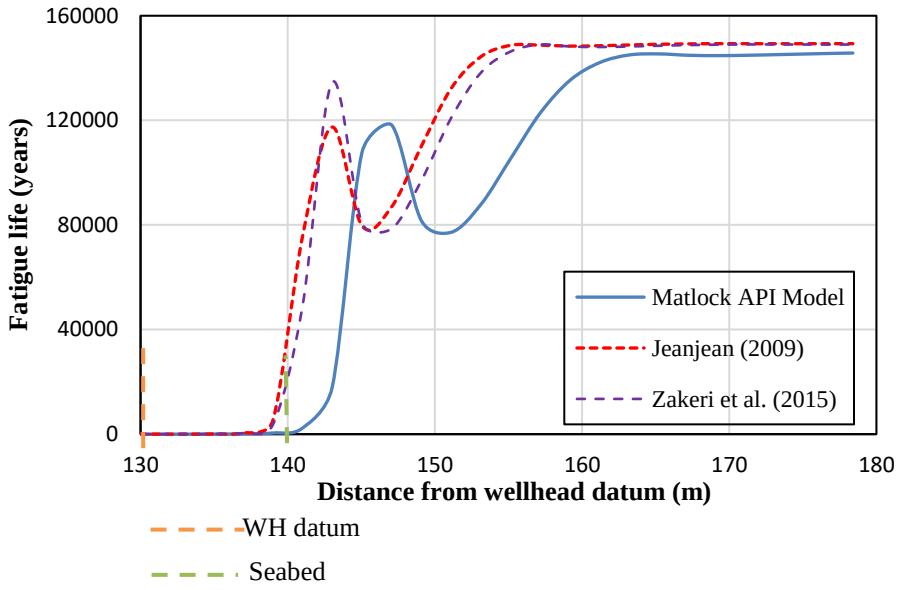

Figure 4-19: Fatigue life for water depth of 100m

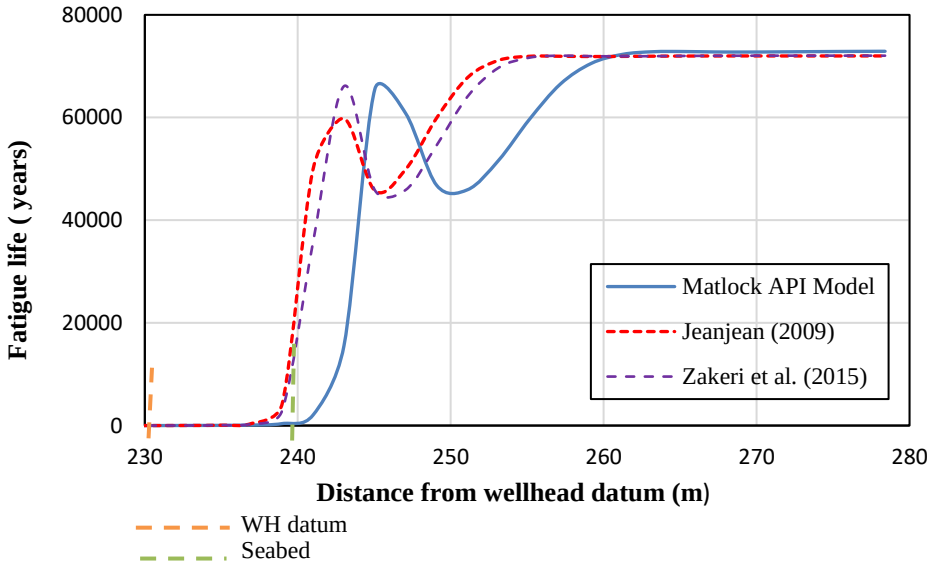

Figure 4-20: Fatigue life for water depth of 200m

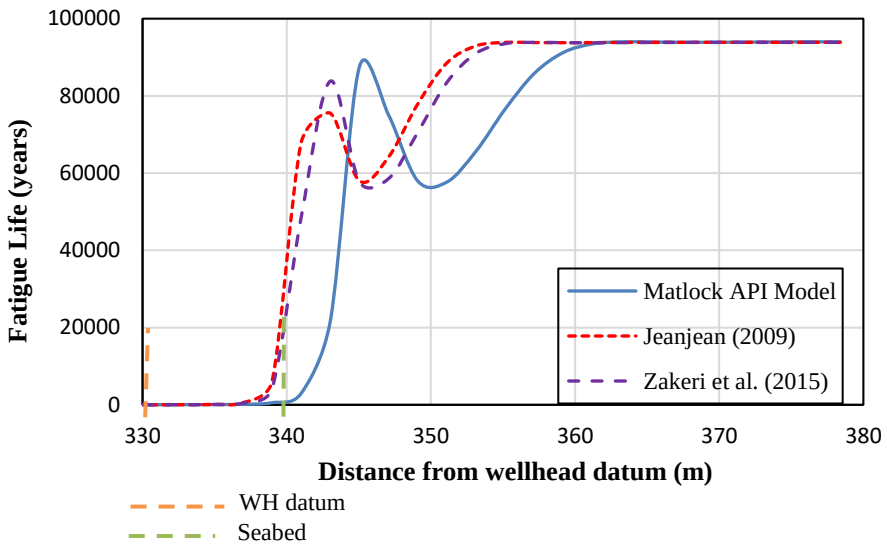

Figure 4-21: Fatigue life for water depth of 300m

The trend for increased levels of fatigue damage in the wellhead and conductor system for the proposed soil models is consistent over the range of water depths considered. Hence, the deeper the water, the lesser the fatigue damage and the higher the fatigue life are and vice versa.

Chapter 5

Effect of Soil Models on Riser Performance

In this section, three soil models, Matlock API (2011), Jeanjean (2009) and Zakeri et al. (2015) models have been used as input to a global riser analysis.

5.1 Modal Analysis Results of Riser

The modal analysis has been performed to identify the natural mode periods or frequencies and mode shapes for each of the proposed soil models. The results of the natural periods and mode shapes for the first five modes are presented and compared in Table 4-8. The mode shapes are plotted and presented in Appendix A.1.

Based on these plots, it can be observed that the natural periods for the Matlock API is slightly different from the Jeanjean (2009) and Zakeri et al. (2015) models. As it can be seen, the higher mode gives higher frequency thereby resulting in greater damage. In addition, the soft soil gives higher frequency when compared to the stiffer soil models.

5.2 Soil-Models Investigation

Global riser analysis is performed for the three additional soil models: Original Matlock, Jeanjean (2009) and Zakeri et al. (2015) The results of the bending moment for the Zakeri et al. (2015) and Jeanjean (2009) models at different sea states were compared with the result obtained from the global analysis using API recommendation soil model (Matlock-API) which served as the base case soil model. The results showed that the wellhead bending moment is affected by the soil stiffness.

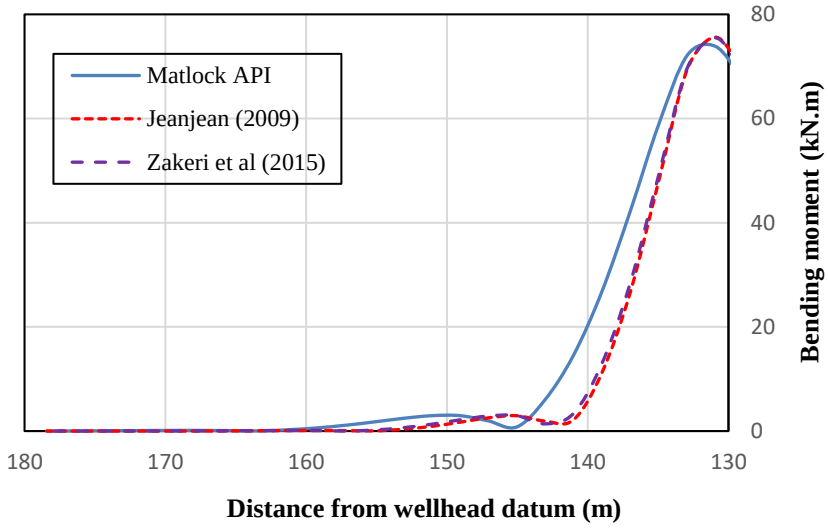

Figure 5-1: Wellhead bending moment for sea state 1 (Hs = 3.6m, Tp = 11s)

It can be seen in Figure 5-1, the bending moments are significantly influenced by the soil formulations. The softer the soil model the larger the bending moment is. Similarly, the stiffer the soil model the smaller the bending moment is. The bending moment at the wellhead region is 72.13 kNm for the Matlock API model, 69.42 kNm for Jeanjean (2009) model and 69.68 kNm for Zakeri et al. (2015) model for the lowest sea state.

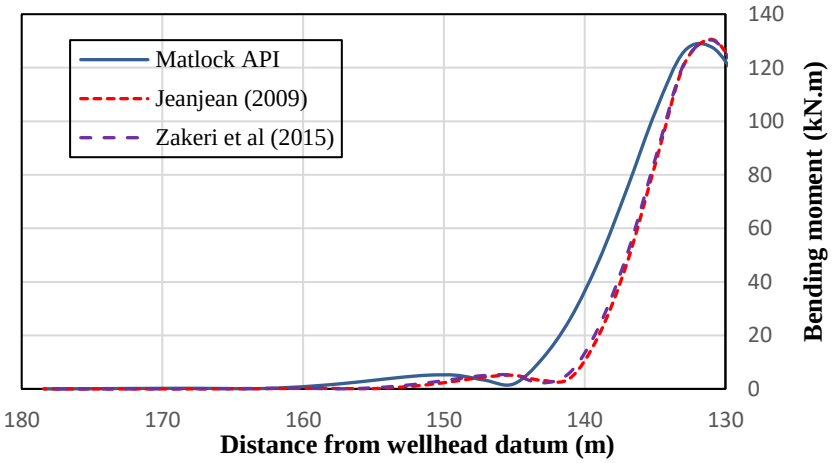

Figure 5-2: Wellhead bending moment for sea state 2 (Hs = 6.5m, Tp = 8.5s)

The bending moments acting on the wellhead were also extracted from the FE model for the high sea state as shown in Figure 5-2. As can be seen in the figure, the bending moments are significantly influenced by the high sea state. This is expected since larger waves typically excite larger forces. The bending moment at the wellhead region varies from 126kNm for the Matlock API model and 121kNm for Jeanjean (2006) and Zakeri et al. (2015) models.

5.2.1 Comparison of Results

Gregersen et al. (2017) performed analysis to validate soil models for wellhead fatigue and presented the results for the bending moment for two different sea states. The results obtained by Gregersen et al. (2017) were compared with the results obtained from this research using OrcaFlex for three different soil models: Matlock API, Jeanjean (2009) and Zakeri et al. (2015).

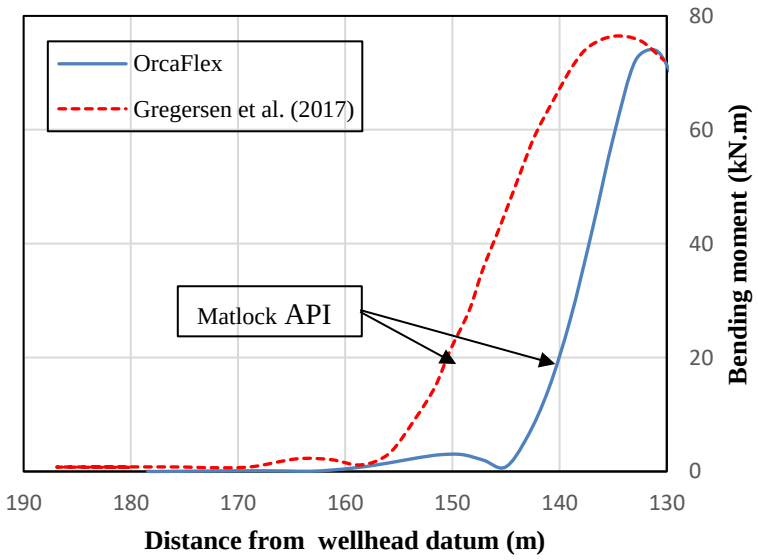

Figure 5-3: Bending moment for Matlock API model (sea state 1: Hs =3.6m, Tp = 11s)

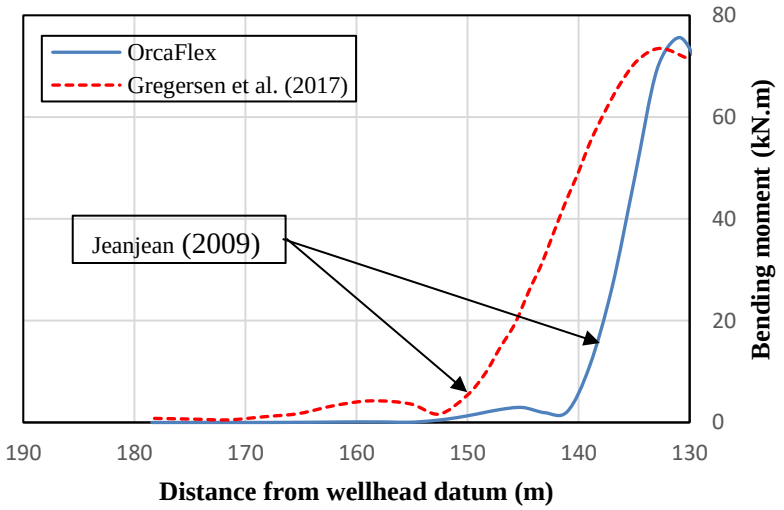

Figure 5-4: Bending moment for Jeanjean (2009) model (sea state 1: Hs =3.6m, Tp = 11s)

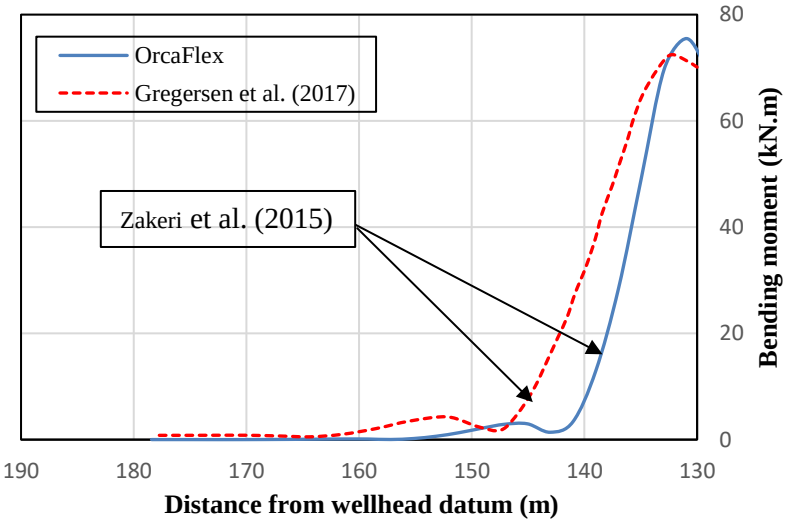

Figure 5-5: Bending moment for Zakeri et al. (2015) model (sea state 1: Hs =3.6m, Tp = 11s)

The results from Gregersen et al. (2017) may not quite agree with that obtained from OrcaFlex due to variation in environmental data and geometric properties selected for this studies. The present

studies considered a water depth of 140m while Gregersen et al. (2017) considered a water depth of 400m. The plots for the wellhead bending moment for the high sea state are shown below.

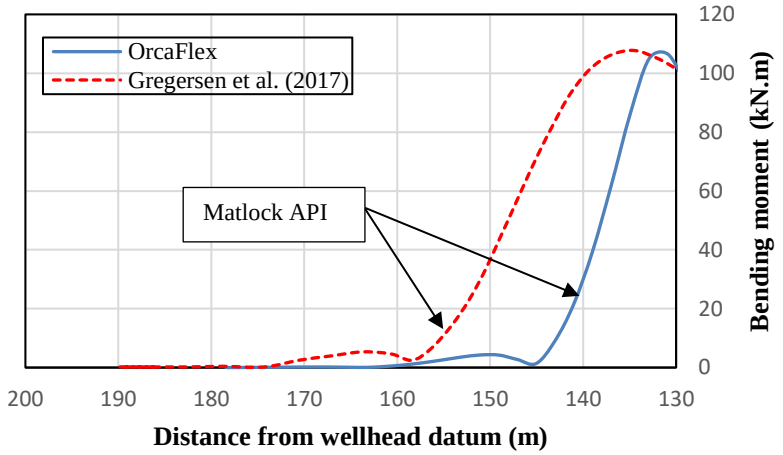

Figure 5-6: Bending moment for Matlock API model (sea state 2: Hs =7.3m, Tp = 12.5s)

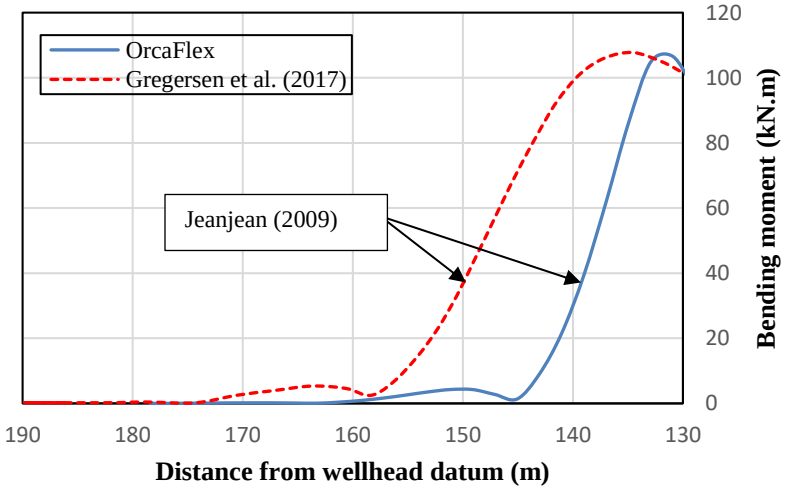

Figure 5-7: Bending moment for Jeanjean (2009) model (sea state 2: Hs =7.3m, Tp = 12.5s)

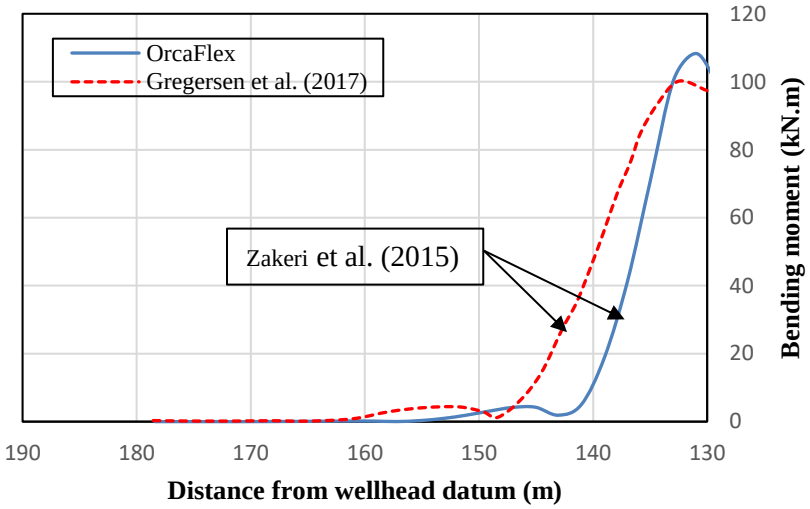

Figure 5-8: Bending moment for Zakeri et al. (2015) model (sea state 2: Hs =7.3m, Tp = 12.5s)

Chapter 6

Wellhead Fatigue Performance on Proposed Soil Models

6.1 Introduction

In this chapter, a general wellhead fatigue analysis method proposed by DNV (2011) during the Joint Industry Project (JIP) is presented. The current study focuses only on the global load response analysis of the wellhead.

6.2 Fatigue Damage Assessment

The most common damage model used in wellhead fatigue analysis is the stress-cycle (S-N) curve method and the Miner-Palmgren summation which is based on constant amplitude stress cycles, high cycle fatigue and the linear damage accumulation hypothesis (DNV, 2015). Another method for assessing fatigue damage is the fracture mechanics which is also termed an Engineering Criticality Assessment (ECA) (DNV, 2015). The ECA is utilized in fit-for-purpose analysis and it is well suited in determination of flaw acceptance criterion of welded structures for fabrication (Zakeri et al., 2015). That is to say that, it is based on the fact that an initial flaw is situated at a region with high stressed.

Accumulation of fatigue stresses results in fatigue damage. The calculation of fatigue damage in subsea wellhead is based on the rainflow cycle counts. Rainflow counting is used to obtain the bending and axial stress distribution along the conductor

A global analysis was performed to calculate the nominal stress range distribution for the riser system in the water column for the conductor and surface casing modeled to a depth of approximately 47m below the mudline to obtain the fatigue life and the overall damage over total

exposure for each of the proposed soil models. A stress concentration factor (SCF) may be applied to the stress time series before rainflow counting is performed based on equation (6.1).

$$\Delta\sigma_{hotspot} = SCF.\Delta\sigma_{nominal} \quad (6.1)$$

Where,

$\Delta\sigma_{hotspot}$ is the hot spot stress range

$\Delta\sigma_{nominal}$ is the nominal stress range

SCF is the stress concentration factor

The fatigue damage calculation is then carried out for each sea state and is then found for each hotspot in the wellhead using the stress histogram and appropriate S-N curve.

In order to determine the total damage, fatigue calculation should combine the effects of all relevant loadings from environments, operations and system configuration.

The fatigue damage increases with the magnitude of the soil resistance force which depends on the soil stiffness.

6.3 Fatigue Analysis Methodology

Wellhead fatigue can be carried out using two methods namely: local and global analyses. A global analysis is the main focus of this thesis and is performed to get a time series of the bending moment at wellhead datum. Different soil P-y curves for the different proposed soil models was implemented in OracaFlex. By using the obtained stresses from the analysis and in combination

with appropriate S-N curves and Miner-Palmgren Summation, a fatigue assessment is carried out. The flowchart in Figure 6-1 describes the procedure for wellhead fatigue analysis

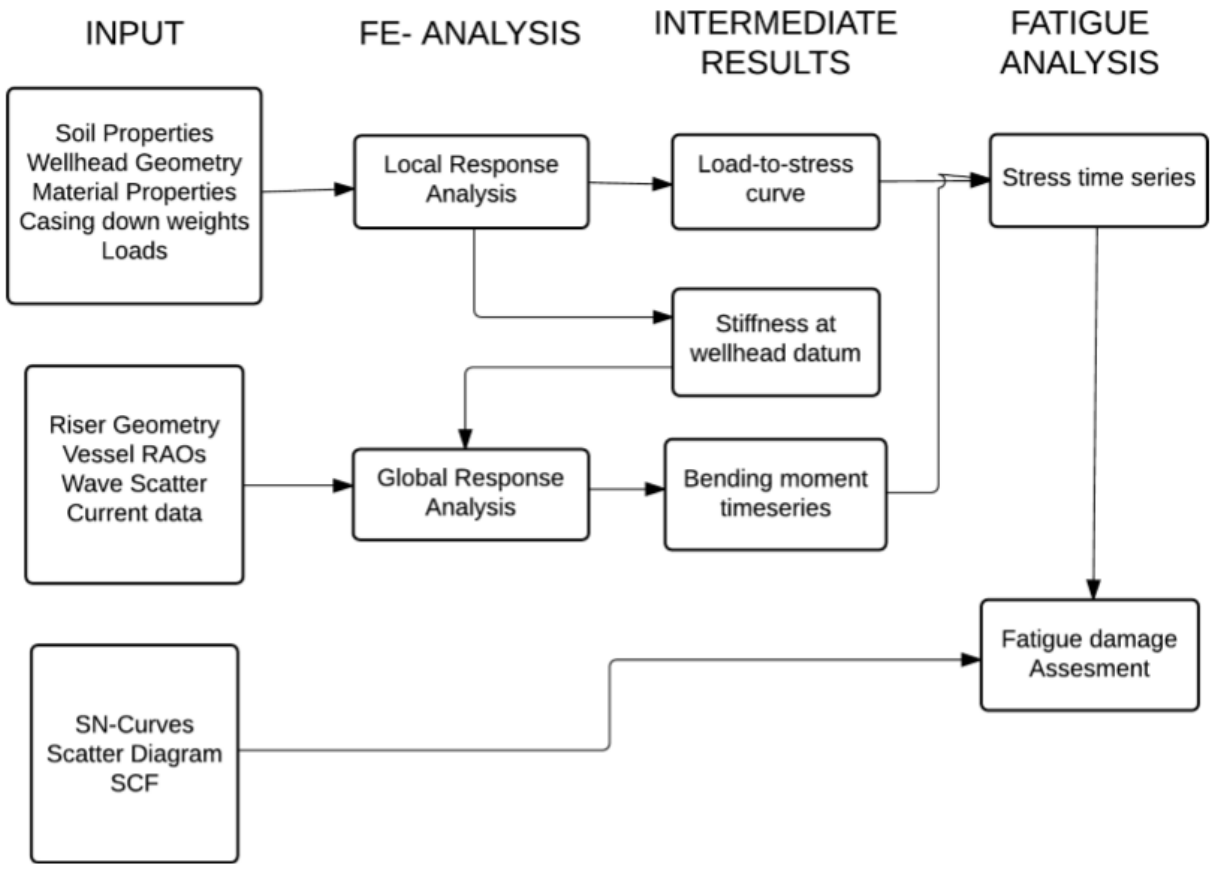

Figure 6-1: Wellhead fatigue methodology flowchart (DNV, 2011)

6.3.1 Global Response Analysis

The global load analysis is performed with the main purpose to get the time series of the bending moment at wellhead datum for all relevant sea states during the operation. The global load analysis, however, is performed in a coupled manner with a lower boundary condition which involves the seabed soil. In the global analysis the entire riser system is modelled using the appropriate FE software (Abaqus, OrcaFlex etc.). To obtain accurate results, the different components and their

behaviour are to be modelled accurately. For a coupled approach as depicted in Figure 4-1, the analysis directly provides sectional loads/stresses at locations of interest within the wellhead/casing system. However, for a decoupled approach as shown in Figure 4-2, the global analysis provides loads imposed to the wellhead/casing system by the riser (DNV, 2015). Global load analysis can be performed using time-domain (TD) or frequency-domain (FD) solutions. A time-domain solution are used to represent non-linear behavior while the frequency-domain is usually intended for linear systems. TD analysis involves accurate simulation of the wave time history and the exact determination of response time histories and statistics.

6.4 Impact of Soil Models on Wellhead Fatigue Performance

The use of an appropriate soil model is crucial for accurate determination of fatigue damage in the subsea wellhead. The stiffness of the soil is the main contributor to the wellhead fatigue damage

A series of fatigue analysis were performed for various P-y models as illustrated in Figures 6-2, 6-3, 6-4 and 6-5. Stiffer P-y curves will produce less cyclic lateral displacement on the wellhead for a given load range than that predicted by API, hence the cyclic stresses in the wellhead will be reduced and the fatigue life will therefore be increased.

In the first analysis, the fatigue damage has been calculated for a period of 25 years for the low sea state by considering each of the proposed soil models. Figure 6-2 and Figure 6-3 show the comparison of the fatigue damage and fatigue life for the low sea state and for each of the different soil models.

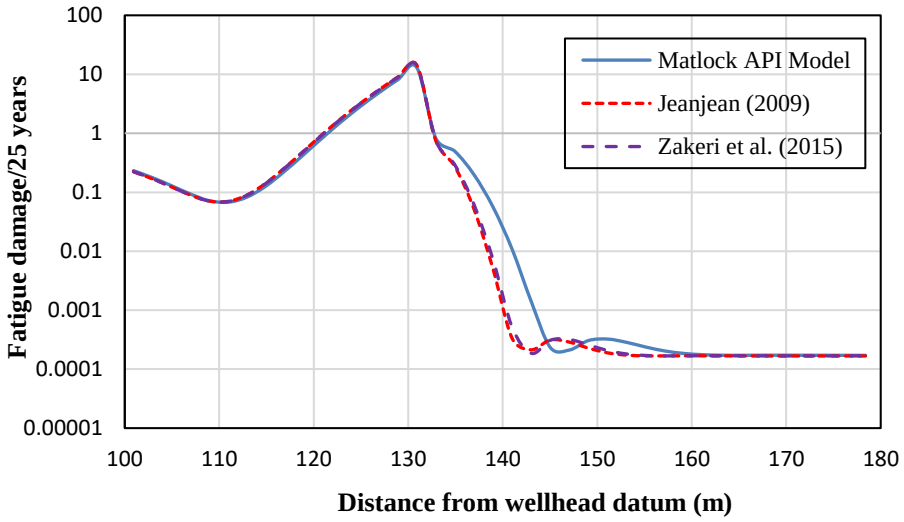

Figure 6-2: WH fatigue damage for load case 1 (Hs = 3.6m, Tp = 11s)

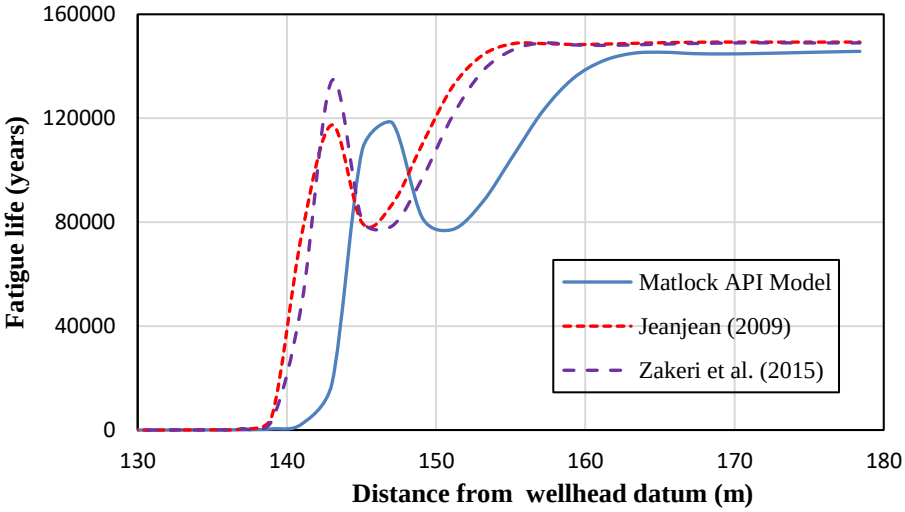

Figure 6-3: WH fatigue life for Load case 1 (Hs = 3.6m, Tp = 11s)

By critically assessing the plots above, it is shown that the Matlock API model has an overall fatigue damage of 0.83 and fatigue life of 30.2 years at the location of the wellhead while the

Jeanjean (2009) model has an overall fatigue damage of 0.75 and fatigue life of 33.3 years and Zakeri et al. (2015) model has an overall fatigue damage of 0.76 and fatigue life of 33 years. The stiffness of the soils have a significant impact on the fatigue damage, this is attributed to the fact that, the lowest soil stiffness (i.e. Matlock API, Original Matlock and Gmax models) leads to larger damage and decreased fatigue life whereas a stiffer soil (i.e. Jeanjean (2009) and Zakeri et al. (2015) models leads to lower damage and increased fatigue life.

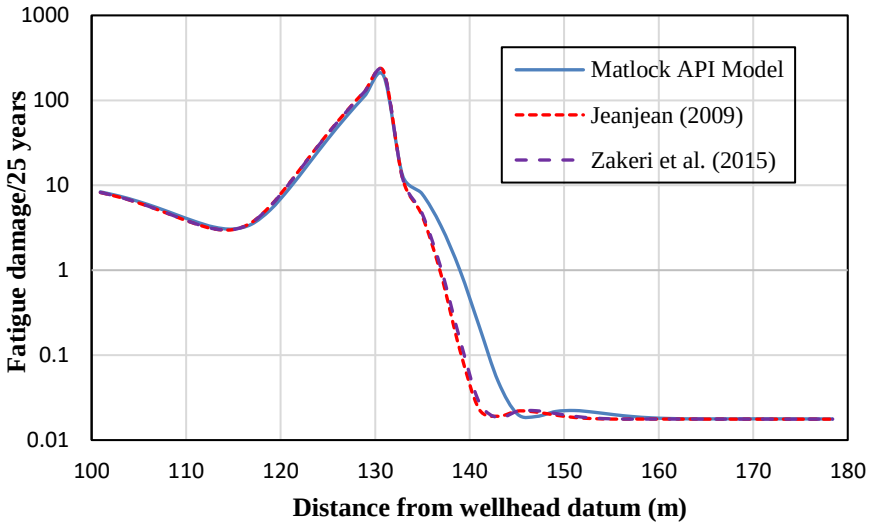

Figure 6-4: WH fatigue damage for load case 2 (Hs = 6.5m, Tp = 8.5s)

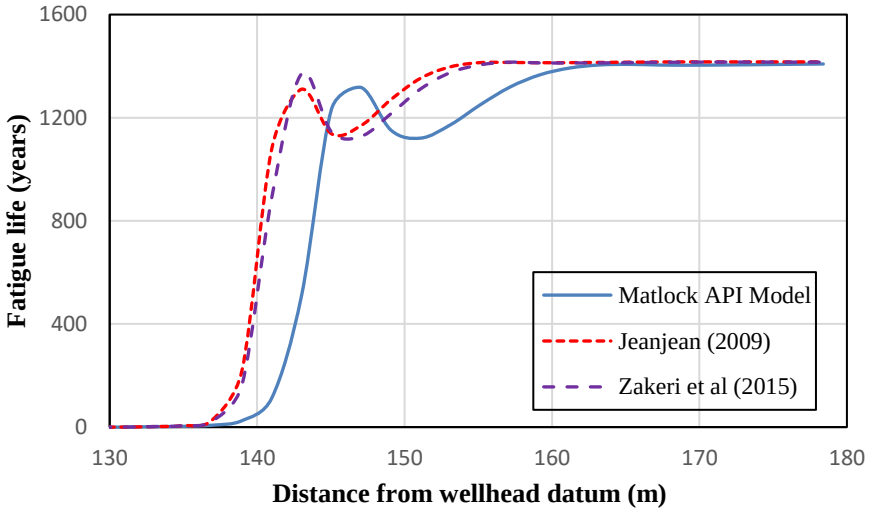

Figure 6-5: WH fatigue life for load case 2 (Hs = 6.5m, Tp = 8.5s)

In the second analysis, a high sea state was simulated over a period of 25 years for each of the soil models. Figures 6-4 and 6-5 show both the overall fatigue damage and fatigue life for the high sea state for each of the proposed soil models. Hence, a higher sea state leads to a more damage and decreases fatigue life.

Chapter 7

Conclusions and Recommendation for future Research

7.1 Conclusions

Essential parts of riser-well integrity are that associated with fatigue and strength. Therefore, understanding the wellhead fatigue response which is affected by seabed interaction plays a significant role in wellhead design in terms of reliability and integrity assessments.

Subsea wellhead fatigue analysis is a critical component of the drilling and production system. It utilizes P-y soil spring which is used to describe the lateral soil-structure interaction. However, there is very little available publications related to soil modelling for wellhead and conductor fatigue analysis. In addition, the computer software packages presently available have limited capability with respect to soil modelling.

Present engineering practice utilizes the P-y curves recommended by API for simulating soil-conductor interaction for fatigue damage assessment. These P-y curves were originally developed based on the work conducted by Matlock specifically for piled foundations which was inappropriate for well fatigue analysis for pile. The pile design is mostly concerned with the limit state of the bending and axial stresses. Recognizing the knowledge gap, researchers such as Zakeri et al. (2015) and Jeanjean (2009) proposed new soil models specific to well fatigue analysis by performing series of centrifuge tests and complementary numerical analysis.

In this study, the influence of seabed soil interaction on wellhead fatigue was investigated. From the results of the analyses, it is evident that the stiffer soil models will greatly reduce the bending moment at the wellhead datum which will further have beneficial impact on the fatigue life of the

subsea wellhead system. Moreover, the softer soil model leads to more damage and decrease in fatigue life on the wellhead.

The global riser analysis performed for the different soil models showed that the Matlock-API soil formulation gives the largest fatigue damage due to the low initial soil stiffness (i.e. stiffness for the first few meters of displacement); secondly, the proper characterization for wellhead fatigue should not be based on the backbone response. The Zakeri et al. (2015) and Jeanjean (2009) soil models have higher initial stiffness and tend to give a low damage and increased fatigue life. Hence, the fatigue response of the wellhead from analysis is affected by the soil models.

7.2 Recommendations for future Research

This study focused on the global load analysis which provides loads imposed to the wellhead/casing system by the riser. The global analysis directly provides sectional loads/stresses at locations of interest within the wellhead/casing system.

Firstly, it is recommended to perform a local analysis model. The local analysis is more suitable for detailed analysis and is used to calculate the exact wellhead fatigue for a given hotspot stresses in the wellhead.

Secondly, a more accurate and reliable method of modelling soil-structure interaction should be studied as the P-y models implemented in the analysis may have some degree of uncertainty. New non-linear hysteretic seabed interaction models should be developed to capture the cyclic degradation of soil stiffness and it effect on overall fatigue performance of wellhead/conductor system.

Further development of the model should be performed to obtain accurate modelling of the flex joint stiffness, BOP and LMRP that correlates better with the full scale measurements for validation of the analyses. The effect of including a non-linear wellhead stiffness model should also be investigated.

The current study considered only the wave-frequency vessel motions. MODU offset can also lead to larger moments on the wellhead. Apparently, during drilling the forces from wind, current, waves and swells will cause the vessel to drift, if this occurs when the drilling riser is connected to the wellhead at the seabed, it will cause cyclic motion of the soil foundation. The riser might get damaged during this extreme event loading conditions which will consequently have impact on the subsea wellhead. It is therefore suggested to incorporate the effect of low-frequency vessel motions as well.

References

API, (2011). “API Recommended Practice 2GEO/ISO 19901-4”, Geotechnical and Foundation Design Considerations. 1st ed. American Petroleum Institute, Washington, DC.

ASTM (2011), ‘E1049-85 Standard Practices for Cycle Counting in Fatigue Analysis

Berge, S. (2006). Fatigue and Fracture Design of Marine Structures II: Fatigue Design of Welded Structures, Institute for Marine Teknikk, NTNU, Trondheim

DNV (2011). Wellhead Fatigue Analysis Method: JIP Structural Well Integrity, number Report no/DNV Reg. No.: 2011-0063/12Q5071-26.

DNV. (2010). Dynamic Risers Fatigue Limit State (Vol. DNV-OS-F201).

DNV. (2012). Fatigue Design of Offshore Steel Structures (Vol. DNV-RP-C203, pp. 178).

DNVGL. (2015). Wellhead fatigue analysis Recommended practice (Vol. DNVGL-RP-0142).

Dong Y. Q. (1994) Vortex-induced nonlinear oscillation of TLP (tension-leg platforms) under combined wave-current. Acta Oceanologica Sinica, 16(3), 121-129 (in Chinese)

Gregersen, K. (2015). Evaluation of Wellhead Fatigue for Drilling Risers - A Study on the Effect of Tension. Master Thesis, Norwegian University of Science and Technology.

Gregersen, K., De Sordi, J., Grytøyr, G., Aronsen, K.H. (2017). “Validation of Soil Models for Wellhead Fatigue Analysis”, OMAE2017-61644, June 2017, Trondheim, Norway.

Gregersen, K., De Sordi, J., Grytøyr, G., Aronsen, K.H. (2017). “Validation of Soil Models for Wellhead Fatigue Analysis”, OMAE2017-61644, June 2017, Trondheim, Norway

Grytøyr, G., Coral, F., Lindstad, H.B., Russo M. (2015)."Wellhead damage based on indirect measurements", OMAE2015-41379, June 2015, St. Johns, Newfoundland, Canada

Guan, Z., Su, K., Su, Y. (2009). "Analysis on lateral load-bearing capacity of conductor and surface casing for deepwater drilling, College of Petroleaum Engineering, China University of Petroleum, Dongying, China.

Harildstad, E., H., Haukanes, Andreas. H., (2013). "Effects of BOP Stack Modelling on Estimated Wellhead Fatigue Damage". Master Thesis, Norwegian University of Science and Technology.

Hegseth J.M. (2014). "Assessment of Uncertainties in Estimated Wellhead Fatigue." Master Thesis, Trondheim Norwegian University of Science and Technology.

Hovland, H. (2014). "Analysis of Global Forces in the Wellhead/Wellhead Connector as a Function of Wellhead Lateral Support and Stiffness". Master Thesis, University of Stavanger.

http://www.dnv.com: DNV.

ISO Standard 10432, 2009 Edition "Petroleum and natural gas industries—Drilling and Production equipment—Wellhead and Christmas Tree Equipment."

ISO Standard 13628-4, 2010 Edition "Petroleum and natural gas industries - Design and operation of subsea production systems" "Part 4: Subsea wellhead and tree equipment"

Jaiswal V; Feng F; Saraswat R; Healy B; Hørte T; Sharma P. (2016). "Fatigue Analysis of Non-rigid Locked Wellhead," Proceedings of the Twenty-sixth International Ocean and Polar Engineering Conference, Rhodes, Greece, June 26-July 1, 2016.

Jeanjean, P. (2009), “Re-Assessment of P-y Curves for Soft Clays from Centrifuge Testing and Finite Element Modeling,” Offshore Technology Conference, Houston, TX, May 4–7, Paper No. 20158

Jin, Y., Caihong L., Hanbin, L., Renjun, X., Shijing C. (2007). “Strength and Stability Analysis of Deep sea Drilling Risers,” Beijing Key Laboratory of Urban Oil and Gas Distribution Technology, China University of Petroleum, Beijing, China.

L.J. Milberger, A. Yu, S. Hosie, and Hines, F. (1991), "Structural requirements for the effective transfer of environmental loadings in a subsea wellhead system," Offshore Technology Conference, Houston, Texas, USA.

Larsen, C. M. (1990). Response Modelling of Marine Risers and Pipelines. Trondheim: NTNU, Division of marine structures.

Lindstad, H.B., Grytøyr, G., Russo, M. (2015). “Direct and Indirect Measurement of Well Head Bending Moments,” OTC-25921-MS, OTC 2015, Houston, Texas.

Lylund, André, L., Bernt J. (2015). Analysis of Riser-induced Loading on Wellhead.” Master Thesis, Trondheim Norwegian University of Science and Technology.

Ma C., Dong Y Q. and Yang L. T. (2000) Comparative Study of Vortex-Induced Nonlinear Oscillation of TLP Tethers Under Two Different Boundary Conditions. Ship Mechanics, 4(1), 56-64 (in Chinese)

Mercan, B., Chandra, Y., Campbell M., Long M. (2017). “Soil Model Assessment for Subsea Wellhead Fatigue Using Monitoring Data.” OTC-27662-MS, OTC 2017, Houston, Texas.

Orcina, OrcaFlex Manual - version 9.8a. Cumbria, UK, 2012.

Reinås, Lorents, R. (2012) "Wellhead Fatigue Analysis: Surface Casing Cement Boundary Condition for Subsea Wellhead Fatigue Analytical Models." PhD Thesis, University of Stavanger.

Russo, M., Zakeri, A., Kuzmichev, S., Grytøyr, G., Clukey, E., Kebadze, E.B. (2016). "Integrity Assessment of Offshore Subsea Wells: Evaluation of Wellhead Finite Element Model against Monitoring Data Using Different Soil Models". Journal of Offshore Mechanics and Arctic Engineering, Dec.2016. Vol 138.

Sparks, C.P. (2007). "Fundamentals of Marine Riser Mechanics: Basic Principles and Simplified Analysis", USA: Penn Well Corporation.

Williams, D., Greene, J. (2012). "The Effects of Modelling Techniques and Data Uncertainty in Wellhead Fatigue Life Calculation," Proceedings of the ASME 2012 31st International Conference on Ocean, Offshore and Arctic Engineering OMAE2012.

Zakeri, A., Clukey E.C., Kebadze, E.B., (2016)." Fatigue Analysis of Offshore Well Conductors: Part I – Study Overview and Evaluation of Series 1 Centrifuge Tests in Normally Consolidated to Lightly Over-Consolidated Kaolin Clay." Applied Ocean Research 57 (2016) 78-95.

Zakeri, A., Clukey E.C., Kebadze, E.B., Jeanjean, P. (2016)." Fatigue Analysis of Offshore Well Conductors: Part II –Development of New Approaches for Conductor Fatigue Analysis in Clays and Sands." Applied Ocean Research 57 (2016) 96-113.

Zakeri, A., Clukey, E., Kebadaze, B., Jeanjean, P., Walker, D., Piercey, G., Templeton, J., Connelly, L., and Aubeny, C. (2015). "Recent Advances in Soil Response Modeling for Well Conductor Fatigue Analysis and Development of New Approaches," Offshore Technology Conference, Houston, TX, May, 4–7, Paper No. OTC-25795-MS.

APPENDICES

Appendix A

Modal Analysis

In this appendix the mode shapes for Matlock API, Jeanjean (2009) and Zakeri et al. (2015) are compared.

A.1 First Five Natural Mode Shapes

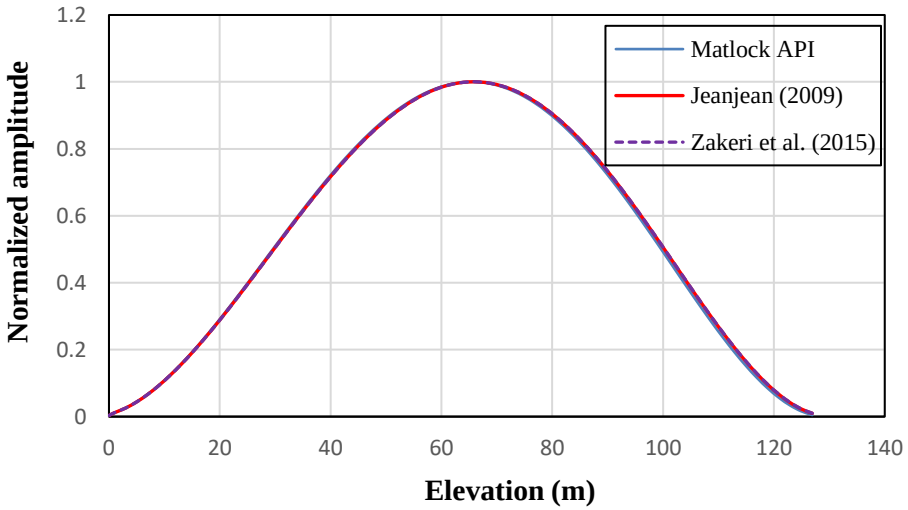

Figure A-1: First mode shape

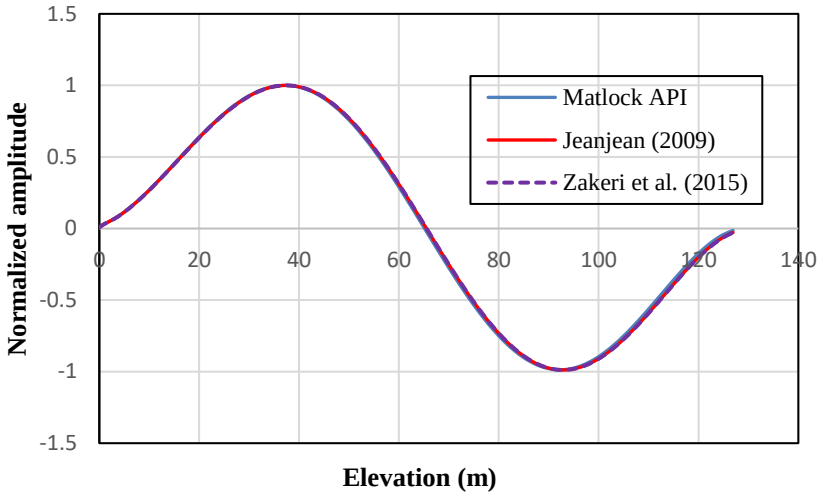

Figure A-2: Second mode shape

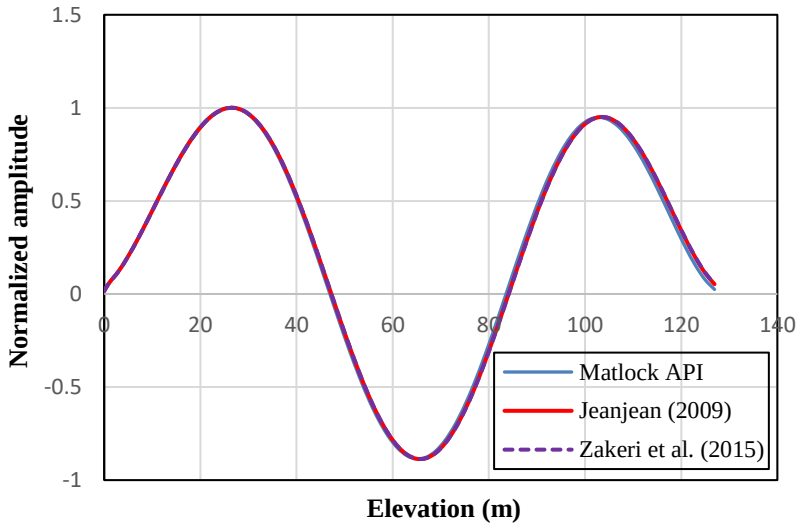

Figure A-3: Third mode shape

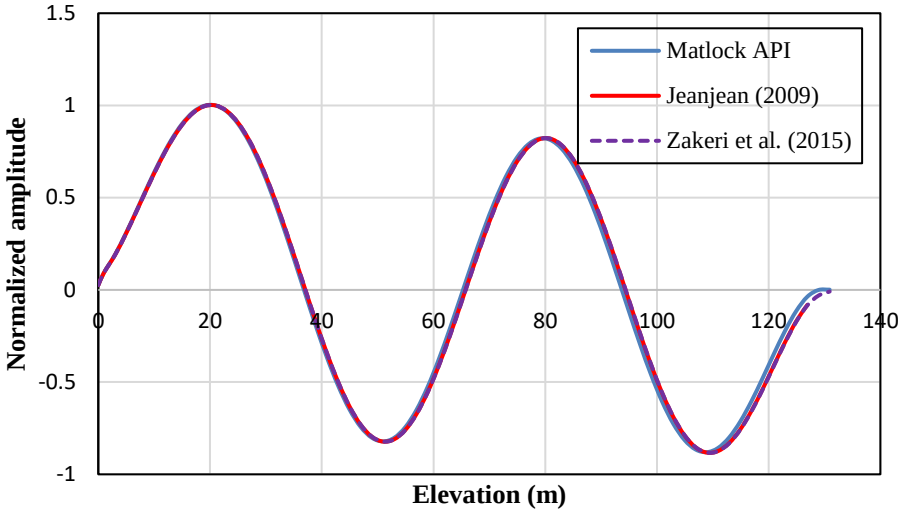

Figure A-4: fourth mode shape

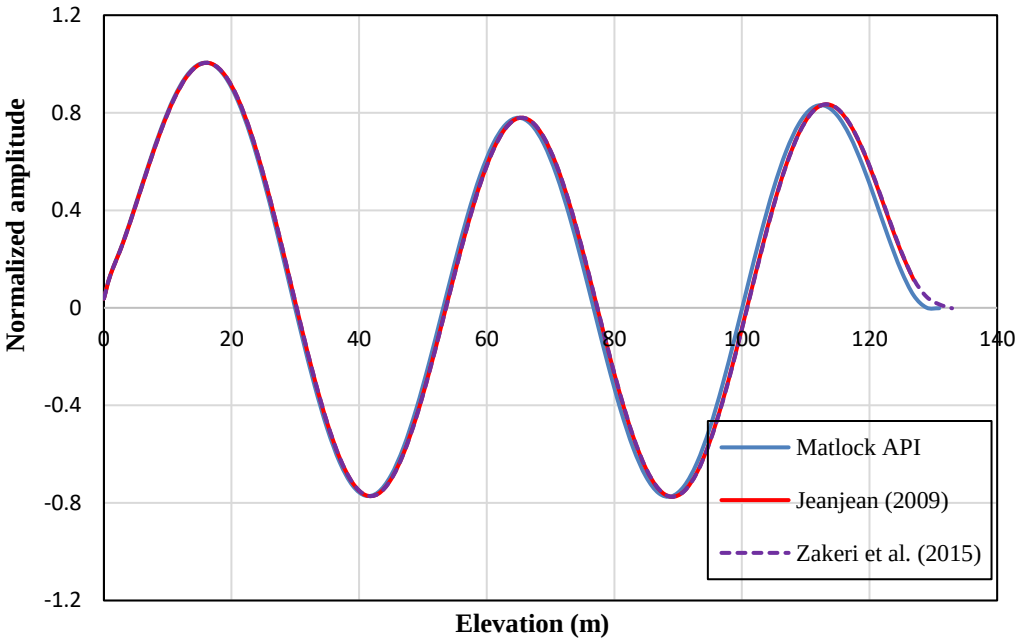

Figure A-5: Fifth mode shape

Appendix B

Irregular Motion Analysis

B.1 Bending Moment Diagram

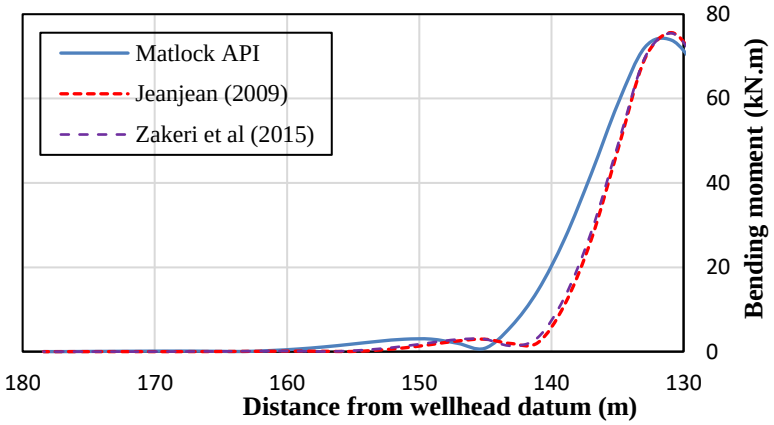

Figure B-1: Wellhead bending moment for sea state 1 (Hs = 3.6m, Tp = 11s)

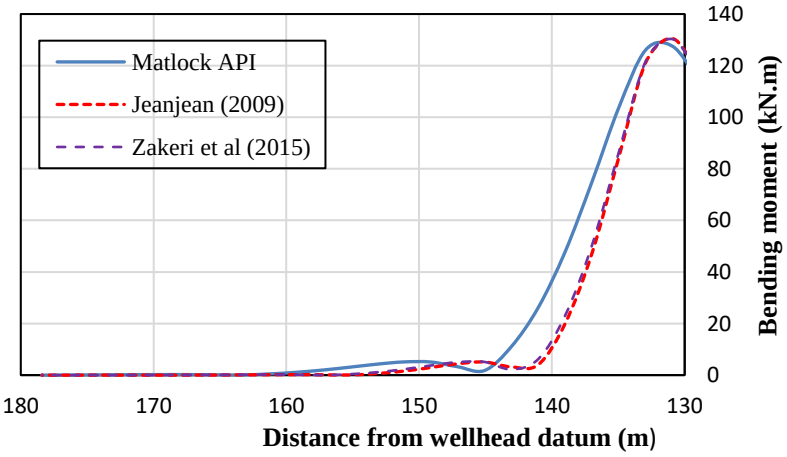

Figure B-2: Wellhead bending moment for sea state 2 (Hs = 6.5m, Tp = 8.5s)

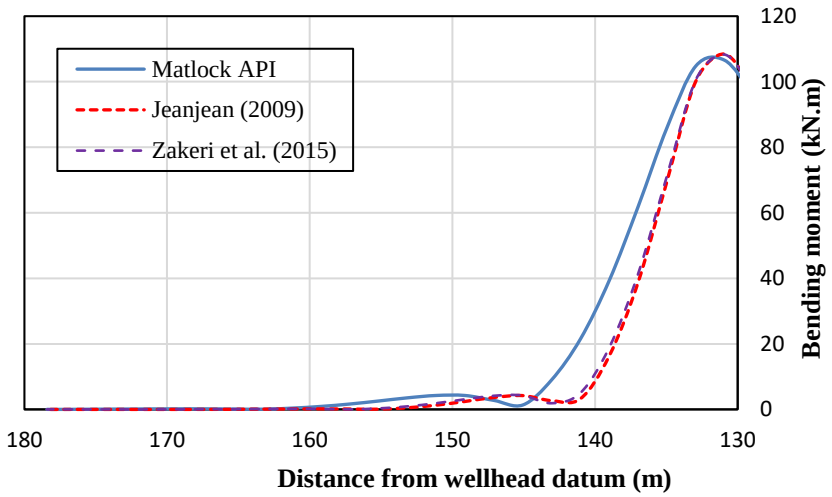

Figure B-3: Wellhead bending moment for sea state 3 (Hs = 7.3m, Tp = 12.5s)

B.2 Shear Force Diagram

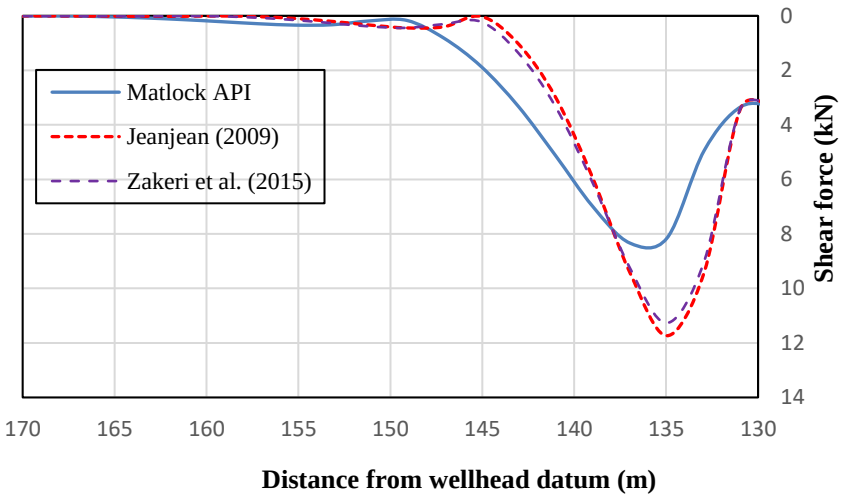

Figure B-4: Wellhead shear force for sea state 1 (Hs = 3.6m, Tp = 11s)

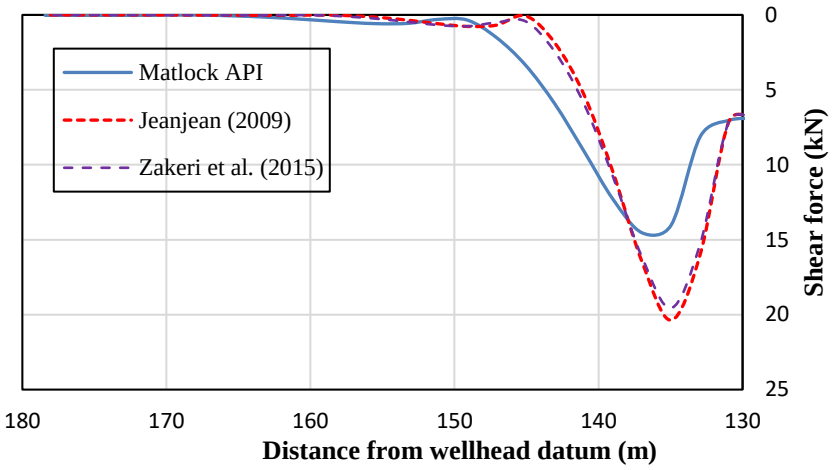

Figure B-5: Wellhead shear force for sea state 2 (Hs = 6.5m, Tp = 8.5s)

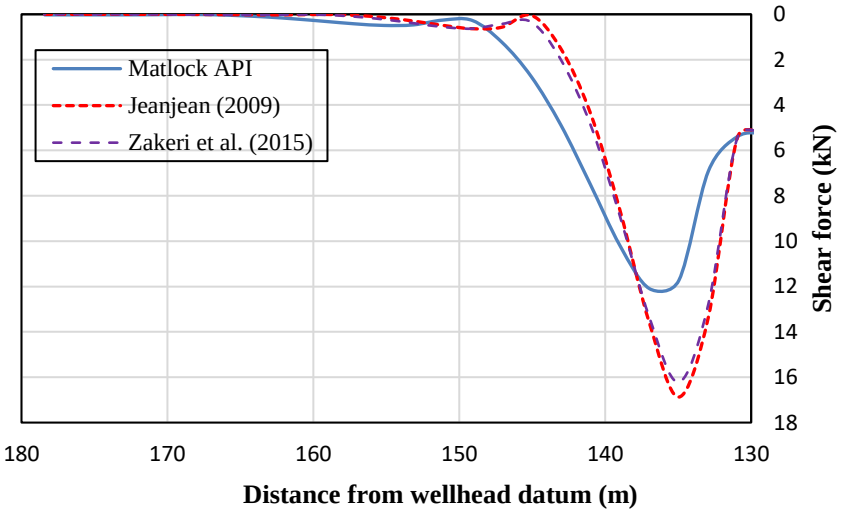

Figure B-6: Wellhead shear force for sea state 3 (Hs = 7.3m, Tp = 12.5s)

Appendix C

Fatigue Damage for Varying Water Depth

C.1 Fatigue Damage for 200m Water Depth

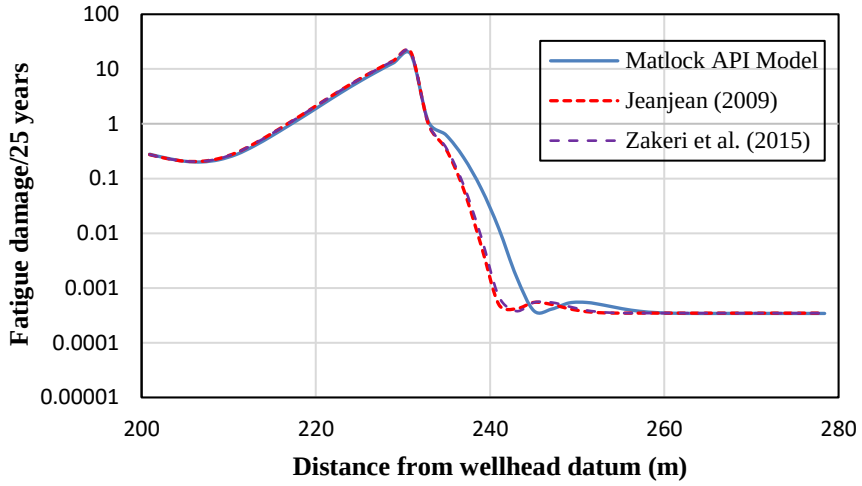

Figure C-1: Fatigue damage for water depth of 200m (Hs = 3.6m, Tp = 11s)

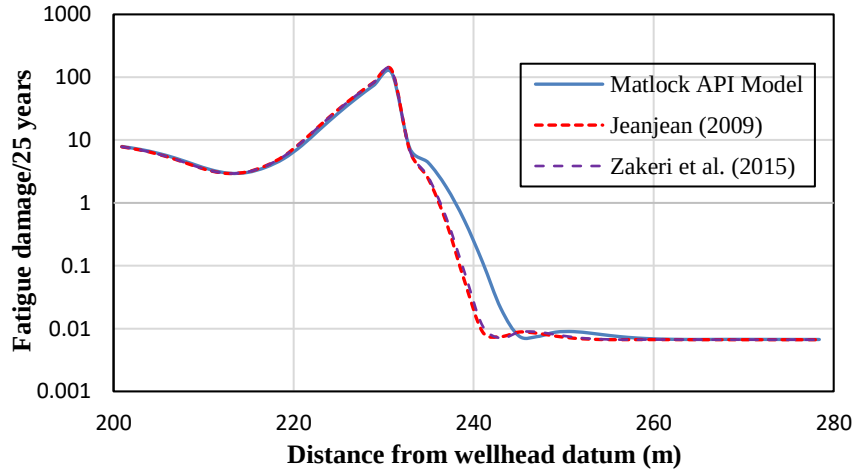

Figure C-2: Fatigue damage for water depth of 200m (Hs = 6.5m, Tp = 8.5s)

C.2 Fatigue Damage for 300m Water Depth

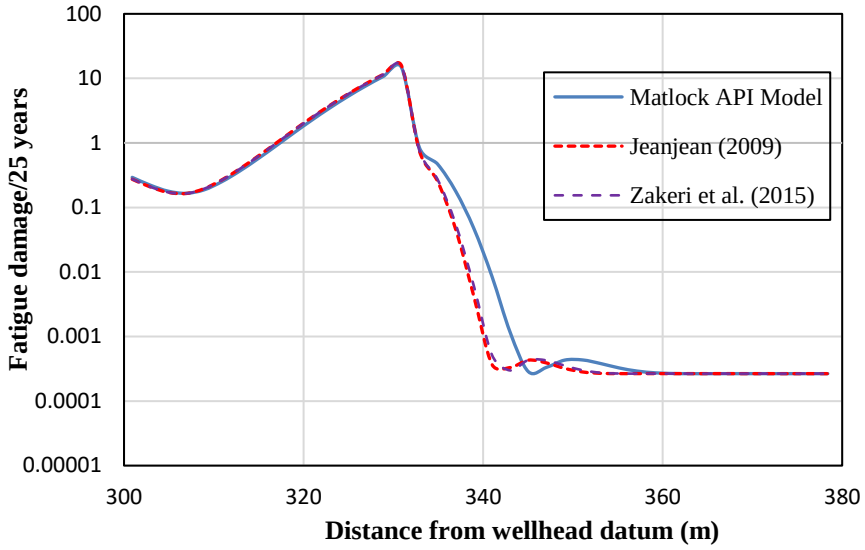

Figure C-3: Fatigue damage for water depth of 300m (Hs = 3.6m, Tp = 11s)

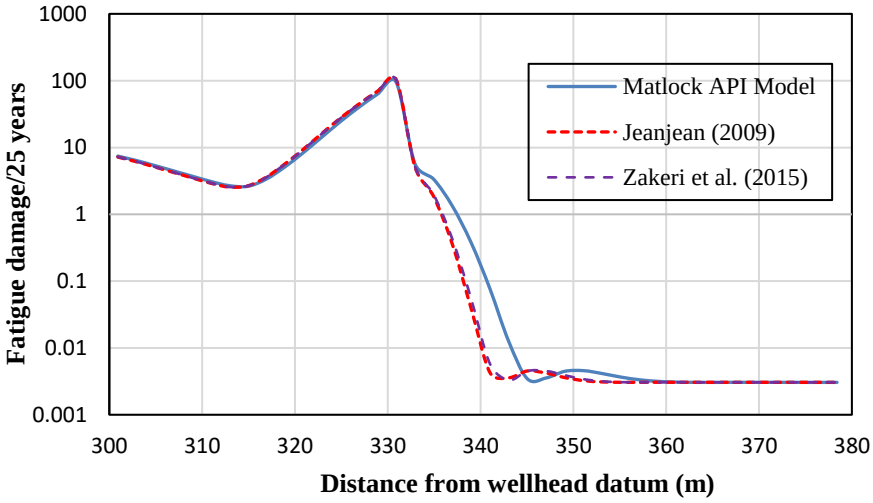

Figure C-4: Fatigue damage for water depth of 300m (Hs = 6.5m, Tp = 8.5s)

C.3 Fatigue Life for 200m Water Depth

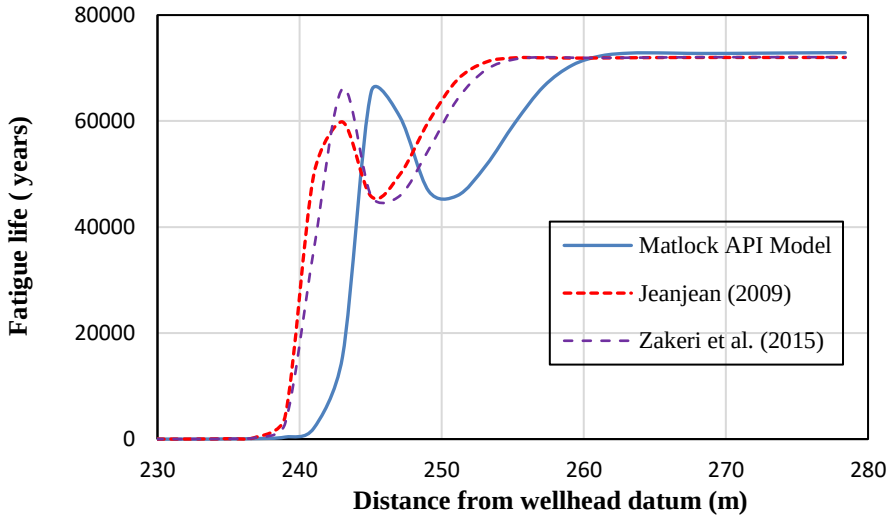

Figure C-5: Fatigue life for water depth of 200m (Hs = 3.6m, Tp = 11s)

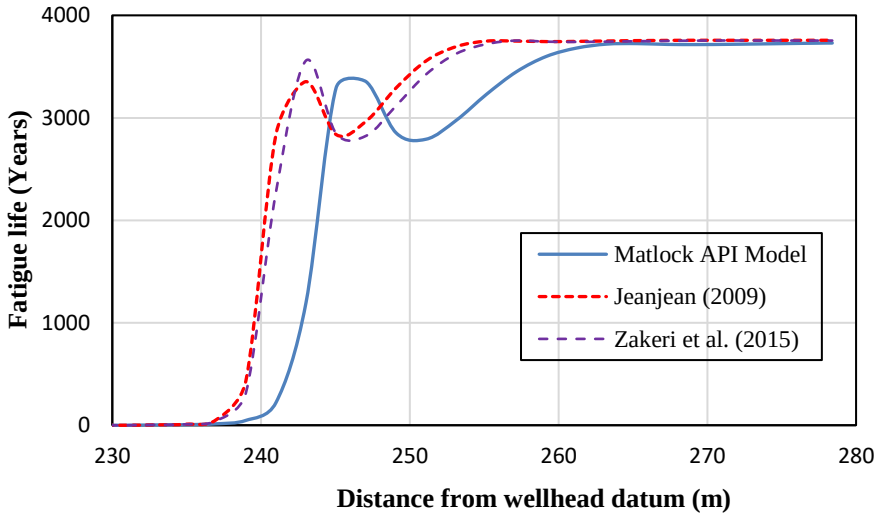

Figure C-6: Fatigue life for water depth of 200m (Hs = 6.5m, Tp = 8.5s)

Appendix D

Damage Summary Table

D.1 100m Water Depth

Matlock API Model @ WD = 100m		
Worst Damage:	**Sea state 1 (Hs = 3.6m, Tp = 11s)**	**Sea state 2 (Hs = 6.5m, Tp = 8.5s)**
Damage per year	0.06396	7.7342
Damage over total exposure	1.5989	193.3549
Life (years)	15.9183	0.1292

Original Matlock Model @ WD = 100m		
Worst Damage:	**Sea state 1 (Hs = 3.6m, Tp = 11s)**	**Sea state 2 (Hs = 6.5m, Tp = 8.5s)**
Damage per year	0.06106	7.6778
Damage over total exposure	1.5266	191.9460
Life (years)	16.9280	0.1301

Gmax Model @ WD = 100m		
Worst Damage:	**Sea state 1 (Hs = 3.6m, Tp = 11s)**	**Sea state 2 (Hs = 6.5m, Tp = 8.5s)**
Damage per year	0.06116	7.7330
Damage over total exposure	1.5289	193.3256
Life (years)	16.6827	0.1292

Jeanjean (2009) Model @ WD = 100m		
Worst Damage:	**Sea state 1 (Hs = 3.6m, Tp = 11s)**	**Sea state 2 (Hs = 6.5m, Tp = 8.5s)**
Damage per year	0.05696	8.7187
Damage over total exposure	1.4240	217.9678
Life (years)	18.7392	0.1146

Zakeri et al. (2015) Model @ WD = 100m		
Worst Damage:	**Sea state 1 (Hs = 3.6m, Tp = 11s)**	**Sea state 2 (Hs = 6.5m, Tp = 8.5s)**
Damage per year	0.05183	8.6416
Damage over total exposure	1.2957	216.03963
Life (years)	20.7525	0.1156

D.2 200m Water Depth

Matlock API Model @ WD = 200m		
Worst Damage:	**Sea state 1 (Hs = 3.6m, Tp = 11s)**	**Sea state 2 (Hs = 6.5m, Tp = 8.5s)**
Damage per year	0.0438	0.2951
Damage over total exposure	1.09595	7.3764
Life (years)	22.8533	3.3869

Original Matlock Model @ WD = 200m		
Worst Damage:	**Sea state 1 (Hs = 3.6m, Tp = 11s)**	**Sea state 2 (Hs = 6.5m, Tp = 8.5s)**
Damage per year	0.0439	0.2955
Damage over total exposure	1.0980	7.3869
Life (years)	22.7535	3.3820

Gmax Model @ WD = 200m		
Worst Damage:	**Sea state 1 (Hs = 3.6m, Tp = 11s)**	**Sea state 2 (Hs = 6.5m, Tp = 8.5s)**
Damage per year	0.0438	0.2951
Damage over total exposure	1.09595	7.3764
Life (years)	22.7957	3.3868

Jeanjean (2009) Model @ WD = 200m		
Worst Damage:	**Sea state 1 (Hs = 3.6m, Tp = 11s)**	**Sea state 2 (Hs = 6.5m, Tp = 8.5s)**
Damage per year	0.0397	0.2695
Damage over total exposure	0.9927	6.7380
Life (years)	25.1655	3.7077

Zakeri et al. (2015) Model @ WD = 200m		
Worst Damage:	**Sea state 1 (Hs = 3.6m, Tp = 11s)**	**Sea state 2 (Hs = 6.5m, Tp = 8.5s)**
Damage per year	0.0401	0.2720
Damage over total exposure	1.00257	6.7990
Life (years)	24.9189	3.6745

D.3 300m Water Depth

Matlock API Model @ WD = 300m		
Worst Damage:	**Sea state 1 (Hs = 3.6m, Tp = 11s)**	**Sea state 2 (Hs = 6.5m, Tp = 8.5s)**
Damage per year	0.0337	0.2309
Damage over total exposure	0.8417	5.7734
Life (years)	29.6803	4.3272

Original Matlock Model @ WD = 300m		
Worst Damage:	**Sea state 1 (Hs = 3.6m, Tp = 11s)**	**Sea state 2 (Hs = 6.5m, Tp = 8.5s)**
Damage per year	0.0338	0.2314
Damage over total exposure	0.8443	5.7850
Life (years)	29.5891	4.3186

Gmax Model @ WD = 300m		
Worst Damage:	**Sea state 1 (Hs = 3.6m, Tp = 11s)**	**Sea state 2 (Hs = 6.5m, Tp = 8.5s)**
Damage per year	0.0337	0.2309
Damage over total exposure	0.8417	5.7734
Life (years)	29.6803	4.3272

Jeanjean (2009) Model @ WD = 300m		
Worst Damage:	**Sea state 1 (Hs = 3.6m, Tp = 11s)**	**Sea state 2 (Hs = 6.5m, Tp = 8.5s)**
Damage per year	0.0298	0.2083
Damage over total exposure	0.7450	5.2074
Life (years)	33.5344	4.7976

Zakeri et al. (2015) Model @ WD = 300m		
Worst Damage:	**Sea state 1 (Hs = 3.6m, Tp = 11s)**	**Sea state 2 (Hs = 6.5m, Tp = 8.5s)**
Damage per year	0.0302	0.2104
Damage over total exposure	0.7538	5.2606
Life (years)	33.1434	4.7491